Available online at www.sciencedirect.com
SCIENCE DIRECT
Progress in Materials Science 51 (2006) 881–981
Progress in Materials Science
www.elsevier.com/locate/pmatsci

Principles of equal-channel angular pressing as a processing tool for grain refinement

Ruslan Z. Valiev [a,1], Terence G. Langdon [b,c,*]

[a] *Institute of Physics of Advanced Materials, Ufa State Aviation Technical University, Ufa 450000, Russian Federation*

[b] *Materials Research Group, School of Engineering Sciences, University of Southampton, Southampton SO17 1BJ, UK*

[c] *Departments of Aerospace & Mechanical Engineering and Materials Science, University of Southern California, Los Angeles, CA 90089-1453, USA*

Received 16 January 2006; accepted 20 February 2006

Abstract

During the last decade, equal-channel angular pressing (ECAP) has emerged as a widely-known procedure for the fabrication of ultrafine-grained metals and alloys. This review examines recent developments related to the use of ECAP for grain refinement including modifying conventional ECAP to increase the process efficiency and techniques for up-scaling the procedure and for the processing of hard-to-deform materials. Special attention is given to the basic principles of ECAP processing including the strain imposed in ECAP, the slip systems and shearing patterns associated with ECAP and the major experimental factors that influence ECAP including the die geometry and pressing regimes. It is demonstrated that all of these fundamental and experimental parameters play an essential role in microstructural refinement during the pressing operation. Attention is directed to the significant features of the microstructures produced by ECAP in single crystals, polycrystalline materials with both a single phase and multi-phases, and metal–matrix composites. It is shown that the formation of ultrafine grains in metals and alloys underlies a very significant enhancement in their mechanical and functional properties. Nevertheless, it is demonstrated also that, in order to achieve advanced properties after processing by ECAP, it is necessary to control a wide range of

* Corresponding author. Address: Departments of Aerospace & Mechanical Engineering and Materials Science, University of Southern California, Los Angeles, CA 90089-1453, USA. Tel.: +44 2380 594772/+1 213 740 0491; fax: +44 2380 593015/+1 213 740 8071.

E-mail addresses: RZValiev@mail.rb.ru (R.Z. Valiev), langdon@soton.ac.uk, langdon@usc.edu (T.G. Langdon).

[1] Tel./fax: +7 3472 733422.

doi:10.1016/j.pmatsci.2006.02.003

microstructural parameters including the grain boundary misorientations, the crystallographic texture and the distributions of any second phases. Significant progress has been made in the development of ECAP in recent years, thereby suggesting there are excellent prospects for the future successful incorporation of the ECAP process into commercial manufacturing operations.

Contents

1. Introduction

Although the mechanical and physical properties of all crystalline materials are determined by several factors, the average grain size of the material generally plays a very significant, and often a dominant, role. Thus, the strength of all polycrystalline materials is related to the grain size, d, through the Hall–Petch equation which states that the yield stress, σ_y, is given by

$$\sigma_y = \sigma_0 + k_y d^{-1/2} \tag{1}$$

where σ_0 is termed the friction stress and k_y is a constant of yielding [1,2]. It follows from Eq. (1) that the strength increases with a reduction in the grain size and this has led to an ever-increasing interest in fabricating materials with extremely small grain sizes.

The grain sizes of commercial alloys are generally tailored for specific applications by making use of pre-determined thermomechanical treatments in which the alloys are subjected to specified regimes of temperature and mechanical testing. However, these procedures cannot be used to produce materials with submicrometer grain sizes because there is invariably a lower limit, of the order of a few micrometers, which represents essentially the minimum grain size readily attained using these procedures. Accordingly, attention has been directed towards the development of new and different techniques that may be used to fabricate ultrafine-grained materials with grain sizes in the submicrometer and the nanometer range.

To place this review in perspective, it is first necessary to provide a formal definition of *ultrafine-grained materials* (UFG). With reference to the characteristics of polycrystalline materials, UFG materials are defined as polycrystals having very small grains with average grain sizes less than $\sim$1 μm. For bulk UFG materials, there are the additional requirements of fairly homogeneous and reasonably equiaxed microstructures and with a majority of grain boundaries having high angles of misorientation. The presence of a high fraction of high-angle grain boundaries is important in order to achieve advanced and unique properties [3].

Two basic and complementary approaches have been developed for the synthesis of UFG materials and these are known as the "bottom-up" and the "top-down" approaches [4].

In the "bottom-up" approach, UFG materials are fabricated by assembling individual atoms or by consolidating nanoparticulate solids. Examples of these techniques include inert gas condensation [5,6], electrodeposition [7], ball milling with subsequent consolidation [8] and cryomilling with hot isostatic pressing [9,10], where cryomilling essentially denotes mechanical milling in a liquid nitrogen environment. In practice, these techniques are often limited to the production of fairly small samples that may be useful for applications in fields such as electronic devices but are generally not appropriate for large-scale structural applications. Furthermore, the finished products from these techniques invariably contain some degree of residual porosity and a low level of contamination which is introduced during the fabrication procedure. Recent research has shown that large bulk solids, in an essentially fully-dense state, may be produced by combining cryomilling and hot isostatic pressing with subsequent extrusion [11] but the operation of this combined procedure is expensive and at present it is not easily adapted for the production and utilization of structural alloys in large-scale industrial applications.

The "top-down" approach is different because it is dependent upon taking a bulk solid with a relatively coarse grain size and processing the solid to produce a UFG microstructure through heavy straining or shock loading. This approach avoids the small product sizes and the contamination which are inherent features of materials produced using the "bottom-up" approach and it has the additional advantage that it can be readily applied to a wide range of pre-selected alloys.

The first observations of the production of UFG microstructures using the "top-down" approach appeared in the scientific literature in the early 1990s in several publications dealing with pure metals and alloys [12–14]. It is important to note these early publications provided a direct demonstration of the ability to employ heavy plastic straining in the production of bulk materials having fairly homogeneous and equiaxed microstructures with grain sizes in the submicrometer range and with a high fraction of high-angle grain boundaries.

In order to convert a coarse-grained solid into a material with ultrafine grains, it is necessary both to impose an exceptionally high strain in order to introduce a high density of dislocations and for these dislocations to subsequently re-arrange to form an array of grain boundaries. In practice, however, conventional metal-working procedures, such as extrusion or rolling, are restricted in their ability to produce UFG structures for two important reasons. First, there is a limitation on the overall strains that may be imposed using these procedures because the processing techniques incorporate corresponding reductions in the cross-sectional dimensions of the work-pieces. Second, the strains imposed in conventional processing are insufficient to introduce UFG structures because of the generally low workability of metallic alloys at ambient and relatively low temperatures. As a consequence of these limitations, attention has been devoted instead to the development of alternative processing techniques, based on the application of severe plastic deformation, where extremely high strains are imposed at relatively low temperatures without incurring any concomitant changes in the cross-sectional dimensions of the samples. An earlier report provided a detailed overview of the use of these processing techniques in the production of bulk nanostructured materials [15].

Formally, *processing by severe plastic deformation* (SPD) may be defined as those metal forming procedures in which a very high strain is imposed on a bulk solid without the introduction of any significant change in the overall dimensions of the solid and leading to the production of exceptional grain refinement so that, typically, the processed bulk solids have 1000 or more grains in any section.

In principle at least, the use of heavy deformation in metal processing, with the objective of producing metal alloys with superior properties, has a long history which may be traced back to the early metal-working of ancient China [16], the blacksmith's production of high-quality Damascus steel in the Middle East [17] and the fabrication of the legendary Wootz steel in ancient India [18]. However, from a modern scientific perspective, developments in processing by SPD were first stimulated over fifty years ago through the extensive and meticulous work of Bridgman in the United States. In these experiments, metals were subjected to large deformation under high applied pressures in attempts to improve the mechanical properties of materials that were inherently fairly brittle. For example, in a series of detailed experiments, subsequently described in a classic text [19], Bridgman subjected metal disks to differing high pressures and to concurrent torsional straining using a methodology that would now be regarded as a classic SPD procedure. However, although Bridgman demonstrated the potential for achieving improved deformability through the application of high pressures, the maximum applied pressure of 0.2 GPa proved to be insufficient to achieve exceptional properties. Accordingly, despite the evidence for successful potential trends in this early work, the principles of processing by SPD received little further attention either in academic circles or in any attempts to make use of this new technology in industrial operations.

Since this early work, many different SPD processing techniques have been proposed, developed and evaluated. These techniques include equal-channel angular pressing (ECAP) [13,20–22], high-pressure torsion (HPT) [23–25], multi-directional forging [26–28], twist extrusion [29,30], cyclic-extrusion–compression [31,32], reciprocating extrusion [33,34], repetitive corrugation and straightening (RCS) [35,36], constrained groove pressing (CGP) [37], cylinder covered compression (CCC) [38], accumulative roll-bonding (ARB) [39,40], friction stir processing (FSP) [41,42] and submerged friction stir processing (SFSP) [43]. All of these procedures are capable of introducing large plastic straining and significant microstructural refinement in bulk crystalline solids. Some of these techniques, such as ECAP, HPT, multi-directional forging and ARB, are already well-established methods for producing UFG materials where, depending upon the crystal structure, the processed microstructures have grain sizes lying typically within the range of $\sim$70–500 nm. The other techniques are currently under development for this purpose.

Of these various procedures, equal-channel angular pressing is an especially attractive processing technique for several reasons. First, it can be applied to fairly large billets so that there is the potential for producing materials that may be used in a wide range of structural applications. Second, it is a relatively simple procedure that is easily performed on a wide range of alloys and, except only for the construction of the die, processing by ECAP uses equipment that is readily available in most laboratories. Third, ECAP may be developed and applied to materials with different crystal structures and to many materials ranging from precipitation-hardened alloys to intermetallics and metal–matrix composites. Fourth, reasonable homogeneity is attained through most of the as-pressed billet provided the pressings are continued to a sufficiently high strain. Fifth, the process may be scaled-up for the pressing of relatively large samples and, as described later in Section 8, there is a potential for developing ECAP for use in commercial metal-processing procedures. These various attractive features have led to many experimental studies and new developments in ECAP processing over the last decade. This review is therefore designed to present a detailed overview of these various developments and to provide information on the current status of ECAP as a processing tool in the fabrication of bulk solids with UFG structures.

2. The development of processing using equal-channel angular pressing

The process of equal-channel angular pressing (ECAP), known also as equal-channel angular extrusion (ECAE), was first introduced by Segal and his co-workers in the 1970s and 1980s at an institute in Minsk in the former Soviet Union [20,44].[2] The basic objective at that time was to develop a metal forming process where high strains may be introduced into metal billets by simple shear. However, although the objective was successfully achieved, the early development of the pressing operation received only limited attention in the scientific community. This situation changed in the 1990s when reports and overviews began to appear documenting the potential for using ECAP to produce ultrafine-grained and submicrometer metals with new and unique properties [13,46–48] and these reports initiated an intense and ongoing interest in scientifically investigating, developing and ultimately utilizing the ECAP process in industrial applications.

This section describes the various types of ECAP that have been developed and applied in the production of ultrafine-grained structures.

2.1. Conventional ECAP with rods and bars

There are a number of reports describing the fundamental process of metal flow during ECAP [21,49–53] and in practice the principle of ECAP is illustrated schematically in Fig. 1 [54]. For the die shown in the illustration, the internal channel is bent through an abrupt angle, Φ, equal to 90° and there is an additional angle, Ψ, equal to 0° in Fig. 1, which represents the outer arc of curvature where the two channels intersect. The sample, in the form of a rod or bar, is machined to fit within the channel and the die is placed in some form of press so that the sample can be pressed through the die using a plunger. The nature of the imposed deformation is simple shear which occurs as the sample passes through the die as shown schematically in Fig. 2: for simplicity, the die angle in Fig. 2 is 90°, the theoretical shear plane is shown between two adjacent elements within the sample numbered 1 and 2, and these elements are transposed by shear as depicted in the lower part of the diagram [55]. Despite the introduction of a very intense strain as the sample passes through the shear plane, the sample ultimately emerges from the die without experiencing any change in the cross-sectional dimensions. This is illustrated by the pressed sample in Fig. 1. Three separate orthogonal planes are also defined in Fig. 1 where these planes are the X or transverse plane perpendicular to the flow direction, the Y or flow plane parallel to the side face at the point of exit from the die and the Z or longitudinal plane parallel to the top surface at the point of exit from the die, respectively. As noted in

[2] The terms ECAP and ECAE are used interchangeably in the scientific literature. However, since the billets used in this process are not extruded through a confining aperture, and thus there is no reduction in the cross-sectional dimensions of the work-piece, this report follows the recommendation proposed at the NATO Advanced Research Workshop on Investigations and Applications of Severe Plastic Deformation (Moscow, Russia, August 1999) and refers exclusively to ECAP [45]. It should be noted also that ECAE® is a registered trademark of Honeywell International, Inc.

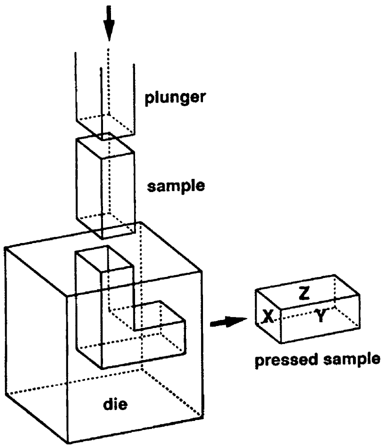

Fig. 1. Schematic illustration of a typical ECAP facility: the X, Y and Z planes denote the transverse plane, the flow plane and the longitudinal plane, respectively [54].

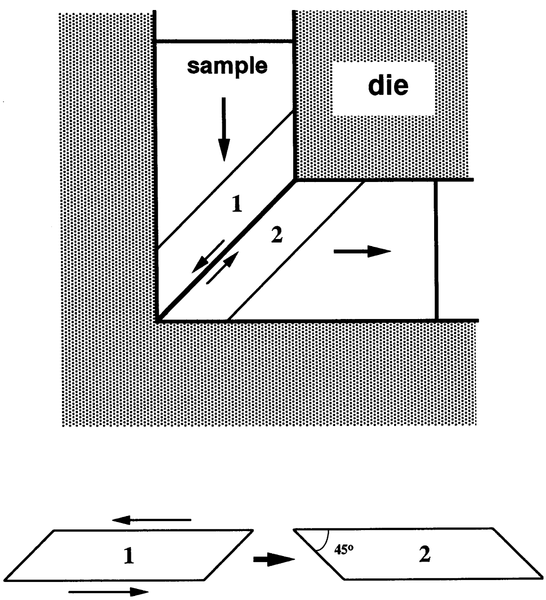

Fig. 2. The principle of ECAP showing the shearing plane within the die: the elements numbered 1 and 2 are transposed by shear as indicated in the lower part of the illustration [55].

Section 1, the retention of the same cross-sectional area when processing by ECAP, despite the introduction of very large strains, is the important characteristic of SPD processing and it is a characteristic which distinguishes this type of processing from conventional metal-working operations such as rolling, extrusion and drawing.

Since the cross-sectional area remains unchanged, the same sample may be pressed repetitively to attain exceptionally high strains. For example, the use of repetitive pressings provides an opportunity to invoke different slip systems on each consecutive pass by simply rotating the samples in different ways between the various passes [21]. In practice, many of the investigations of ECAP involve the use of bars with square cross-sections and dies having square channels. For these samples, it is convenient to develop processing routes in which the billets are rotated by increments of 90° between each separate pass. The same processing routes are also easily applied when the samples are in the form of rods with circular cross-sections. As discussed in detail in Section 3.2, four fundamental processing routes have been identified in ECAP: these are route A where the sample is pressed repetitively without any rotation, route B_A where the sample is rotated by 90° in alternate directions between consecutive passes, route B_C where the sample is rotated in the same sense by 90° between each pass and route C where the sample is rotated by 180° between passes [56].

2.2. The application of ECAP to plate samples

For some industrial applications, such as the use of the ultrafine-grained materials produced by ECAP in superplastic forming operations, it is necessary that the as-pressed samples are in the form of thin metallic sheets. This requirement has prompted an interest in the possibility of applying ECAP to plate samples where the as-pressed materials can be readily prepared for use in conventional metal forming facilities. A limited number of reports are now available on the application of ECAP to plate samples [57–61].

When pressing plate samples, it is necessary to first recognize that there are two distinct pressing configurations. These configurations are illustrated in Fig. 3 where the plate is oriented either (a) in a vertical configuration or (b) in a horizontal configuration [57]: the X, Y and Z axes are indicated in Fig. 3 and they follow the same convention introduced in Fig. 1. Thus, these two configurations correspond to plates having their major axes either in the X and Z directions or in the X and Y directions, respectively.

Inspection of Fig. 3 shows that, unlike the bars and rods described in the preceding section, the number of possible rotations between passes is now limited. Thus, considering the vertical configuration, the sample may be rotated in several different ways. First, by rotation by 180° around the X axis, where this is equivalent to route C and it is designated route C_X where C denotes a rotation by 180° and the subscript X denotes a rotation about the X axis. Second, by rotation by 180° degrees around the Z axis in route C_Z. In practice,

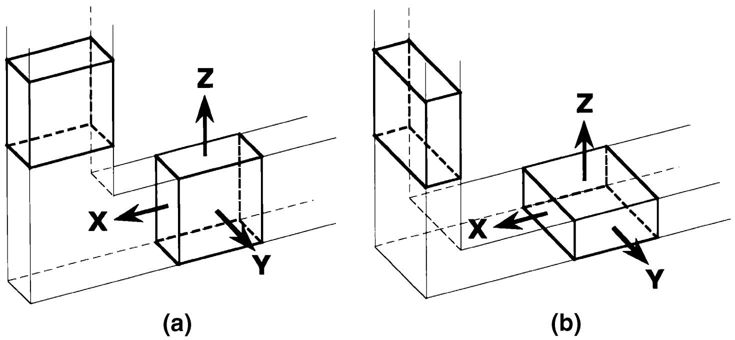

Fig. 3. Application of ECAP to plate samples: (a) vertical configuration and (b) horizontal configuration [57].

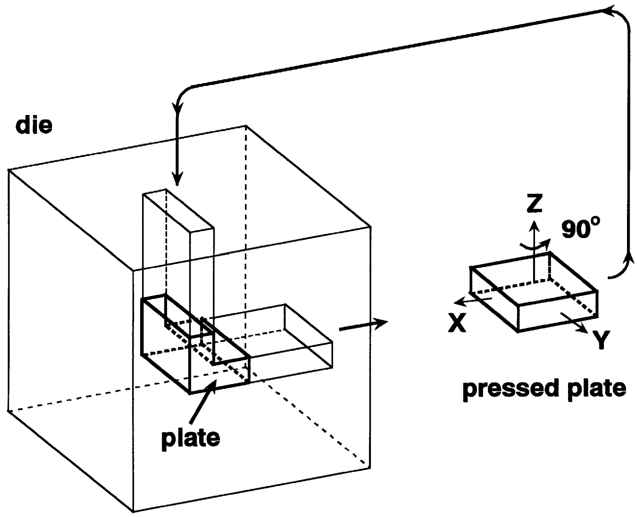

Fig. 4. The procedure adopted for pressing a plate in a horizontal configuration using processing route B_{CZ} [57].

an examination of the shearing patterns associated with these two routes shows that they are identical to the conventional route C available for bar and rod samples. However, there are two additional possibilities not available for bars and rods and these are routes B_{AY} and B_{CY} where the sample is rotated by 90° around the Y axis after each pass either alternately in different directions or in the same sense, respectively. Routes B_{AY} and B_{CY} are not easily executed in practical situations because the plate is sheared into a parallelogram on the first and all subsequent passes so that machining must be undertaken to restore the square sections after every pass.

The horizontal orientation shown in Fig. 3(b) is a more practical situation and it has been used in all experiments conducted to date [57–61]. This orientation provides several potential processing routes including 180° around the X axis in route C_X which is equivalent to route C in bars and rods and 180° around the Y axis in route C_Y which is equivalent to route A. There are also two additional processing routes which are not available with rod samples or when using plates oriented in a vertical configuration as in Fig. 3(a). These new routes involve rotating the horizontal plate by 90° around the Z axis, either in route B_{AZ} or in route B_{CZ} where there are rotations by 90° after each pass in alternate directions or in the same sense, respectively. Detailed experiments on plates of high-purity aluminum have demonstrated that route B_{CZ} is an excellent processing route for plate samples leading to excellent properties with the presence of only minor inhomogeneity after 4 passes through the die [57]. The principles of this processing route are illustrated schematically in more detail in Fig. 4 [57].

2.3. Alternative procedures for achieving ECAP: rotary dies, side-extrusion and multi-pass dies

An important limitation in conventional ECAP, as described in the preceding sections, is that the sample must be removed from the die and reinserted, with or without an intermediate rotation, in order to achieve large numbers of passes and a high imposed strain. These operations are both labor-intensive and time-consuming and, accordingly, several procedures are under development to avoid these limitations.

A simple procedure that effectively eliminates the need for removing specimens from the die between each pass is to make use of rotary-die ECAP [62–71]: this approach is illustrated schematically in Fig. 5 [64]. The facility consists of a die containing two channels, having the same cross-section, intersecting at the center of the die at an angle of 90°. Three punches of equal length are inserted in the lower section of the vertical channel and in the horizontal channel as shown in Fig. 5(a). The sample is inserted in the vertical channel so that it rests on the lower punch and an upper punch is inserted to press the sample with a plunger. The configuration after a single pressing is shown in Fig. 5(b) and the die is then rotated by 90° so that the sample may be pressed again as shown in Fig. 5(c). A careful inspection of the procedure shows that this type of processing is equivalent to route A where the specimen is pressed without any rotation. However, a significant advantage of this type of pressing is the simplicity of operation. For example, rotary-die ECAP has been used effectively for consecutive pressings up to a maximum of 32 passes [66,67]. However, a disadvantage of the process illustrated in Fig. 5 is that the aspect ratios of the sample are small so that end effects may lead to significant inhomogeneities [69].

An alternative but physically similar approach is the side-extrusion process illustrated schematically in Fig. 6 [72]. This process uses four punch-pull cams which are capable of generating high forces during operation. A sample is shown in place in Fig. 6 and it is pressed by punch A under a lateral pressure exerted by punch B. Repetitive pressings may be performed and, as with rotary-die ECAP, this process is equivalent to route A. This procedure has been used effectively for pressing up to 10 passes [72].

An alternative procedure, which does not require the acquisition of a complex pressing facility, is to construct a die having multiple passes. An example of a multi-pass die is shown in Fig. 7 where the die contains a channel bent through five separate angles of 90° [55]. Inspection shows this is equivalent to route C since the second and subsequent passes occur after effectively rotating the sample by 180°. This type of die is useful in order to compare the microstructural characteristics in the same specimen after different numbers of passes. For example, the positions labeled 1, 2, 3, 4 and 5 in Fig. 7 correspond to pressing through 1, 2, 3, 4 and 5 passes of ECAP, respectively. In experiments using a multi-pass facility with a two-piece die that was easily separated to permit access to

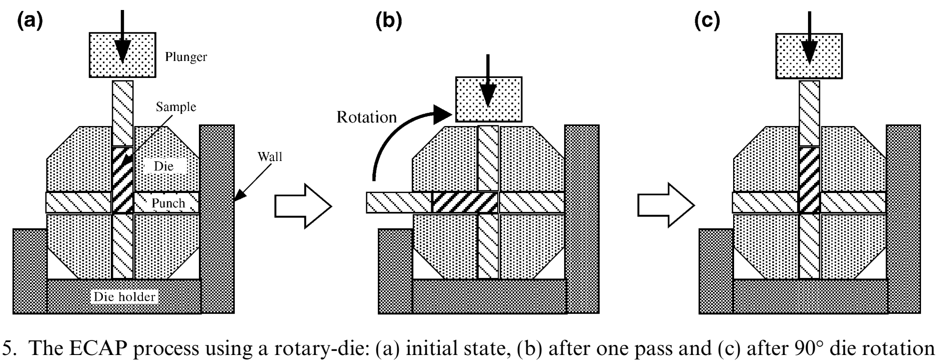

Fig. 5. The ECAP process using a rotary-die: (a) initial state, (b) after one pass and (c) after 90° die rotation [64].

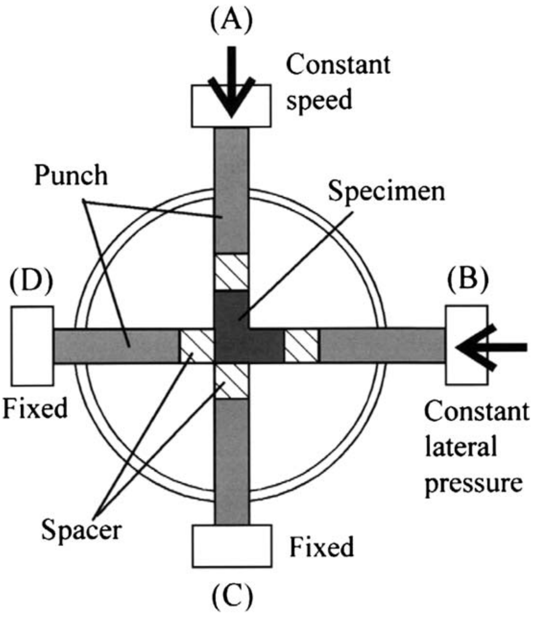

Fig. 6. A schematic illustration of the side-extrusion process for ECAP [72].

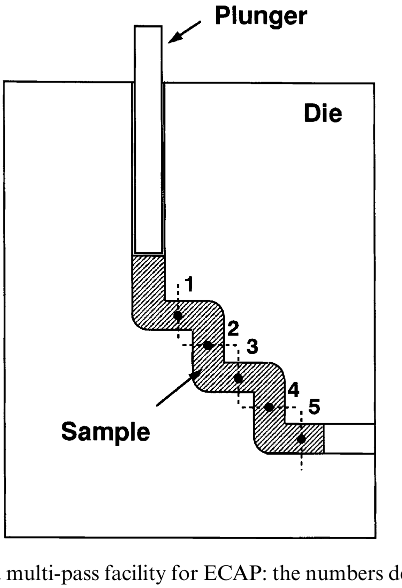

Fig. 7. A schematic illustration of a multi-pass facility for ECAP: the numbers denote positions for examining the sample after the equivalent of 1, 2, 3, 4 and 5 passes, respectively [55].

the specimen, it was shown that the microstructural evolution and the values of the local hardness were identical after the same numbers of passes whether using a multi-pass die or a conventional die containing a single shearing plane [55].

2.4. Developing ECAP with parallel channels

There is an important new development showing the potential for conducting ECAP using a facility containing two parallel channels. Some early results made use of this approach [73–76] but the most recent approach, combining a two-dimensional finite element method (2-D FEM) simulation and direct experiments, provides a very clear demonstration of the advantage of pressing with two parallel channels. The principles of this procedure are illustrated schematically in Fig. 8 [77] where ϕ is the angle of intersection between the parallel channels and K is the channel displacement.

A distinctive feature of ECAP with parallel channels is that, during a single processing pass, two distinct shearing events take place [75,76]. This means in practice that there is a considerable reduction in the number of passes required for the formation of an ultrafine-grained structure. The values for the displacement between the two channels, K, and the angle of intersection of the channels, ϕ, are the main parameters of the die geometry which influence both the flow pattern and the strain–stress state of the ECAP process.

The influence of the ϕ and K parameters on the flow pattern and strain homogeneity of a copper specimen was investigated using 2-D FEM simulation during ECAP with parallel channels [77]. It has been established that the optimal values of these parameters, leading to the largest strain homogeneity in the cross-section of the pressed billet, are $\phi = 100°$ and a displacement value of $K \approx d_c$, where d_c is the channel diameter. This means in practice that the optimum condition is achieved when the measured lateral displacement between the two channels is approximately equal to the dimension of the channel. Under these conditions, the accumulated strain for one pass is approximately equal to 2. It is important to note also that the simulation results have been confirmed experimentally using a grid method.

An important feature has been revealed concerning the nature of metal flow during ECAP in parallel channels. After one full pass, a mesh on the sample appears undistorted

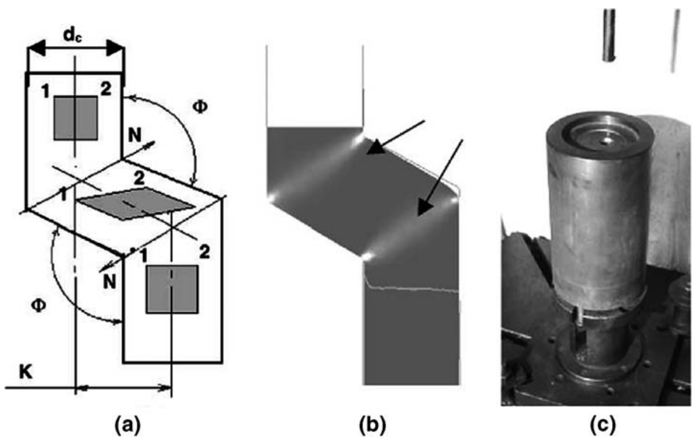

Fig. 8. The principle of ECAP with parallel channels: (a) a schematic illustration where N is in the shear direction, K is the displacement between the two channels, ϕ is the angle of intersection between the two parts of the channel and the internal shaded areas depict the shearing as the sample traverses the shearing zone, (b) a view of the deformation zones obtained by 2-D FEM simulation for ECAP with parallel channels and (c) a general view of the experimental ECAP die-set where $\phi = 100°$ and K is equal to the channel diameter of 18 mm [77].

[77], thereby demonstrating that a uniform strain distribution is achieved including in the tail-pieces. Thus, unlike conventional ECAP, the sample shape after pressing remains identical to the initial sample.

The calculations obtained with parallel channels were used for the fabrication of an ECAP die-set for operation at temperatures up to 500 °C as shown in Fig. 8(c). Samples of Cu and Ti were produced by pressing through 4 passes and observations by transmission electron microscopy (TEM) showed that the structural refinement in these samples corresponded to the formation of an ultrafine-grained structure observed after conventional ECAP when pressing through 8 passes. Furthermore, the UFG structure was rather homogeneous along the length of the bulk sample including up to the ends. Such a high microstructural uniformity is of much practical importance because of the increasing potential for utilizing the material after ECAP [75].

2.5. Continuous processing by ECAP

2.5.1. Continuous confined strip shearing, equal-channel angular drawing and conshearing

Processing by ECAP has attracted considerable attention because it produces ultrafine-grained materials with unique physical and mechanical properties and these materials may have important applications in industry. Nevertheless, the ECAP process as currently used in the laboratory is labor-intensive because it requires much manual effort to add and remove the billets from conventional dies. Accordingly, it is now recognized that any extensive industrial application will require the development of some form of continuous processing technique that can be used efficiently in the production of relatively large volumes of material. Some initial progress has been made in developing continuous ECAP procedures for the processing of long metal strips.

First, a process was developed using a rolling facility combined with the principles of ECAP [78–84]. This process was variously designated continuous confined strip shearing (C2S2) [78,79], dissimilar-channel angular pressing (DCAP) [80,82,83] and equal-channel angular rolling (ECAR) [81,84] and the principles of the process are illustrated schematically in Fig. 9 [82]. Thus, the material is in the form of a thin strip and it is fed into the facility between two rolls, extruded slightly to reduce the thickness from 1.55 to 1.45 mm, and then it flows into the outlet channel where the original thickness of

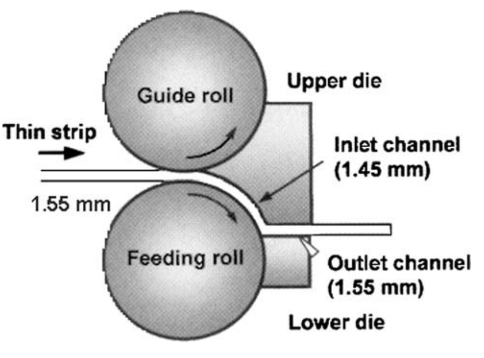

Fig. 9. The principle of the DCAP process for use in continuous production [82].

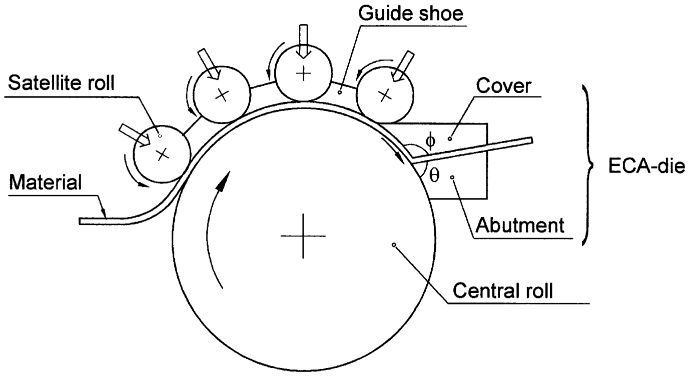

Fig. 10. The principle of the conshearing process [90].

1.55 mm is restored. The terminology DSAP arises therefore because of the small difference in the thickness associated with the passage into the outlet channel.

Second, equal-channel angular drawing (ECAD) was proposed as a potential route for the processing of rod samples [85,86] but subsequent calculations, combined with experiments, demonstrated that ECAD entails a reduction in the cross-sectional area of the sample by >15% so that it cannot be used effectively for multi-pass processing [87].

Third, the conshearing method was proposed for use with metal strips [88–90] and this process, which employs a continuous rolling mill, is illustrated schematically in Fig. 10 [90]. In this procedure, the material is fed into the mill between satellite rollers and a large central roller and all of these rollers rotate at the same peripheral speed in order to generate a large extrusion force. The strip passes between the rollers and ultimately passes from the mill through an abutment where it is displaced through an angle ϕ. Detailed experiments using commercial purity aluminum strips showed that optimum conditions were achieved for ECAP when the angle within the abutment was given by $\phi = 65°$ [90].

Despite the apparent success associated with these various procedures, the results obtained to date cover only a very limited range of materials and they deal also with the processing of very small batches of each alloy. More work is now needed to provide a detailed assessment of the potential for using these techniques to produce large quantities of materials in a continuous process that is both fast and economically viable.

2.5.2. The ECAP–Conform process

The conform extrusion process was developed over 30 years ago for the continuous extrusion of wire products [91,92] but very recently it has been conveniently combined with ECAP in the ECAP–Conform process [93].

In this process, the principle used to generate the frictional force to push a work-piece through an ECAP die is similar to the Conform process [91] while a modified ECAP die design is used so that the work-piece can be repetitively processed to produce UFG structures.

The designed and constructed ECAP–Conform set-up is illustrated schematically in Fig. 11 [93]. As shown in the diagram, a rotating shaft in the center contains a groove and the work-piece is fed into this groove. The work-piece is driven forward by frictional forces on the three contact interfaces with the groove so that the work-piece rotates with

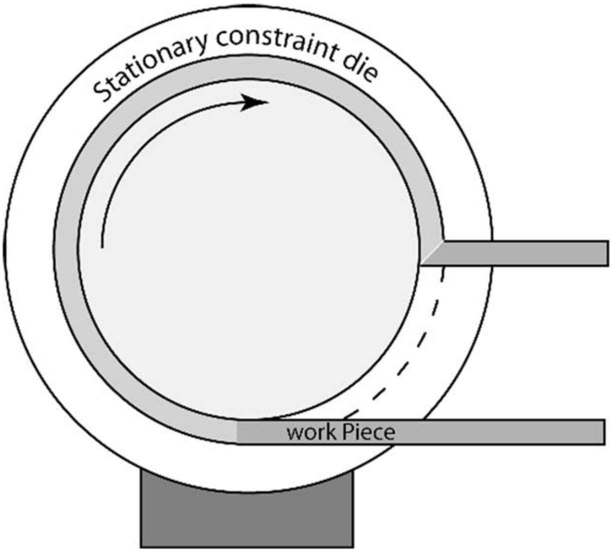

Fig. 11. A schematic illustration of the ECAP–Conform process [93].

the shaft. However, the work-piece is constrained within the groove by a stationary constraint die and this die also stops the work-piece and forces it to turn at an angle by shear as in a regular ECAP process. In the current set-up, the angle is close to 90° which is the most commonly used channel intersection angle in ECAP. This set-up effectively makes the ECAP process continuous. Other ECAP parameters, such as the die angle and the strain rate, can also be incorporated into the facility.

In recent work [93], a commercially-pure (99.95%) coarse-grained long Al wire with a diameter of 3.4 mm and more than 1 m in length was used for processing at room temperature with 1–4 passes using ECAP via route C in which the sample was rotated by 180° between the ECAP passes. The initial grain size of the Al wire was ~5–7 μm. Fig. 12 shows an Al work-piece at each stage of the ECAP–Conform process, from the initial round

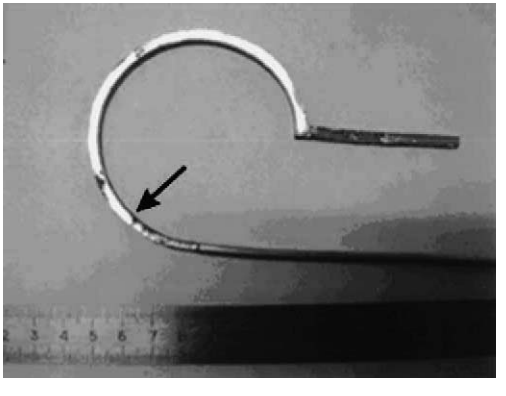

Fig. 12. An Al work-piece undergoing processing by ECAP–Conform: the arrow marks the transition to a rectangular cross-section [93].

feeding stock to the rectangular Al rod after the first ECAP pass [93]. As indicated, the rectangular cross-section was formed shortly after the wire entered the groove (marked by an arrow in Fig. 12). The change was driven by the frictional force between the groove wall and the Al work-piece. Thus, the frictional force pushed the wire forward and deformed the wire to make it conform to the groove shape. After the wire cross-section changed to the square shape, the frictional force per unit of wire length became larger because of the larger contact area between the groove and the wire. The total frictional force pushed the wire forward from the groove into the stationary die channel which intersected the groove at an angle of 90°. This latter part of the straining process is therefore similar to the conventional ECAP process. Observations by TEM have shown that the ECAP–Conform process leads to a microstructural evolution that is typical of the ECAP process and thus this new technique can effectively refine grains and produce UFG microstructures.

2.6. Consolidation by ECAP

Although ECAP is generally associated with the processing of solid metals, it may be used also for the consolidation of metallic powders [94–100].

Fig. 13 shows an ECAP facility used effectively for the pressing of an aluminum powder of the Al-2024 alloy [95]. The powder had an initial size of <45 μm and it was cold isostatically pressed to a billet size with a diameter of 20 mm and length of 70 mm. As illustrated in Fig. 13, the channels within the die met at an angle of 105° and there was an outer arc of curvature of 75°. Repetitive pressings of the billet were undertaken at a temperature of 573 K up to a maximum of 3 passes through the die. An important difference in the

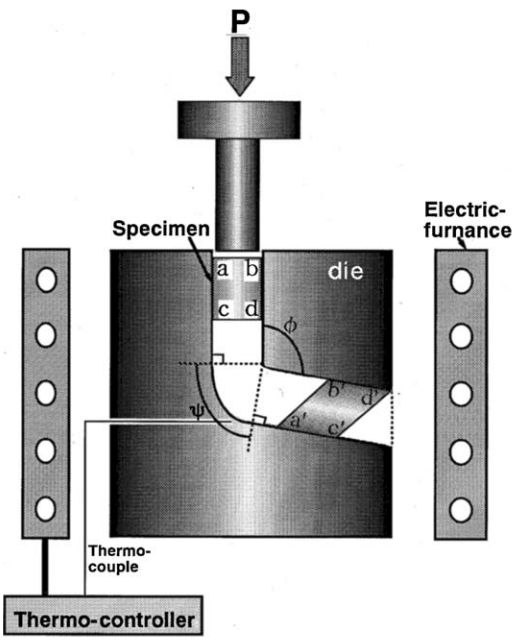

Fig. 13. The ECAP principle used for the consolidation of aluminum alloy powder: the powder is inserted into a tight-fitting outer jacket labeled *abcd* [95].

pressing of powders is that cracking occurs readily on the surface of the pressed samples. To avoid cracking during ECAP consolidation, the Al-2024 powder was machined and inserted into a tight-fitting outer jacket of the Al-2024 alloy and the pressing was conducted at a temperature of 573 K: the jacketed specimen is marked as *abcd* in Fig. 13. The results from this research demonstrated the production of a fully-dense alloy without the presence of any surface cracking [95]. It was shown recently that the propensity for cracking may be significantly reduced, or even eliminated, by pressing under a confining back-pressure and, in addition, a grain size of ~1 μm was achieved when consolidating pure aluminum powder [100]. These and other similar results confirm, therefore, the potential for using ECAP as a tool in powder consolidation for the production of UFG microstructures.

2.7. Construction of an ECAP facility

It is a relatively simple task to establish a facility for conventional ECAP by machining a two-piece split die consisting of a highly polished smooth plate bolted to a second polished plate containing a square-sided channel. This type of die works well in the laboratory and can be used for multiple passes provided care is taken to manually tighten the bolts between each separate pass. A suitable lubricant such as MoS_2 is generally used to minimize frictional effects at the die walls. However, an alternative approach for minimizing friction is to make use of more complex configurations incorporating moving die walls [52,53,101–103]. Two examples of movable die walls are shown in Fig. 14 where there is a movable wall shown shaded (a) in the entrance channel and (b) in the exit channel: as illustrated, these two configurations lead to different slip line solutions at the theoretical shear plane [53].

An alternative approach is to construct a solid die from tool steel. Solid dies have an advantage because they avoid any problems associated with the extrusion of slivers of material between the separate parts of a die. However, solid dies require the use of a channel having a circular cross-section and, in addition, the die must be constructed with a

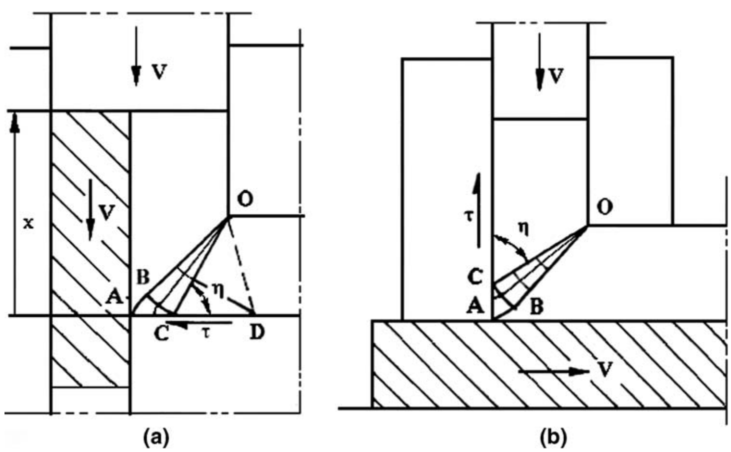

Fig. 14. The principle of ECAP with movable die walls (shown shaded): (a) in the entrance channel and (b) in the exit channel [53].

finite outer arc of curvature at the point of intersection of the two parts of the channel so that $\Psi \neq 0°$. In practice, experiments have shown that little or no inhomogeneity is introduced into the pressed samples by using solid dies having arcs of curvature of $\Psi \approx 20°$ [104]. Furthermore, model experiments with billets made of plasticine have revealed no significant differences when using samples with either square or circular cross-sections [105]. When working with solid dies, it is important to note that it is necessary to remove each specimen from the die by pressing the next specimen into the die. In practice, therefore, the final specimen is generally removed using a dummy specimen which then remains within the die.

The scaling of ECAP processing to incorporate large billets and the pressing of hard-to-deform materials require more complex construction of the ECAP facilities in order to maintain enhanced loading during the pressing operation. This is true also for the development of ECAP processing for commercial use as discussed in Section 8 and for these conditions the construction of an optimal die requires special technical solutions.

3. Fundamental parameters in ECAP

The ECAP procedure is a metal flow process operating in simple shear and characterized by several fundamental parameters such as the strain imposed in each separate passage through the die, the slip systems operating during the pressing operation and the consequent shearing patterns present within the as-pressed billets. Taken together, these various processes define uniquely the precise nature of the pressing operation. As will be demonstrated in Section 4, all of these parameters play a critical role in determining the nature of the UFG structure introduced by ECAP.

3.1. The strain imposed in ECAP

An abrupt strain is imposed on a sample in every passage through an ECAP die. The magnitude of this strain may be estimated using an analytical approach based on the various die configurations illustrated schematically in the two-dimensional representation shown in Fig. 15 [106], where Φ is the channel angle and the angle Ψ represents the angle associated with the arc of curvature where the two parts of the channel intersect. Three conditions are shown in Fig. 15: thus, Fig. 15(a) corresponds to a limiting situation where $\Psi = 0°$, Fig. 15(b) corresponds to a second limiting situation where $\Psi = (\pi - \Phi)°$ and Fig. 15(c) represents an intermediate condition where $0° < \Psi < (\pi - \Phi)°$. The strain is estimated by assuming a fully-lubricated specimen so that any frictional effects may be neglected.

For the situation where $\Psi = 0°$ in Fig. 15(a), a small square element in the entrance channel, labeled *abcd*, passes through the theoretical shear plane and becomes distorted into the parallelogram labeled $a'b'c'd'$. It can be shown from first principles that the shear strain, γ, is given by

$$\gamma = 2\cot\left(\frac{\Phi}{2}\right) \tag{2}$$

Using the same approach for Fig. 15(b), it follows that

$$\gamma = \Psi \tag{3}$$

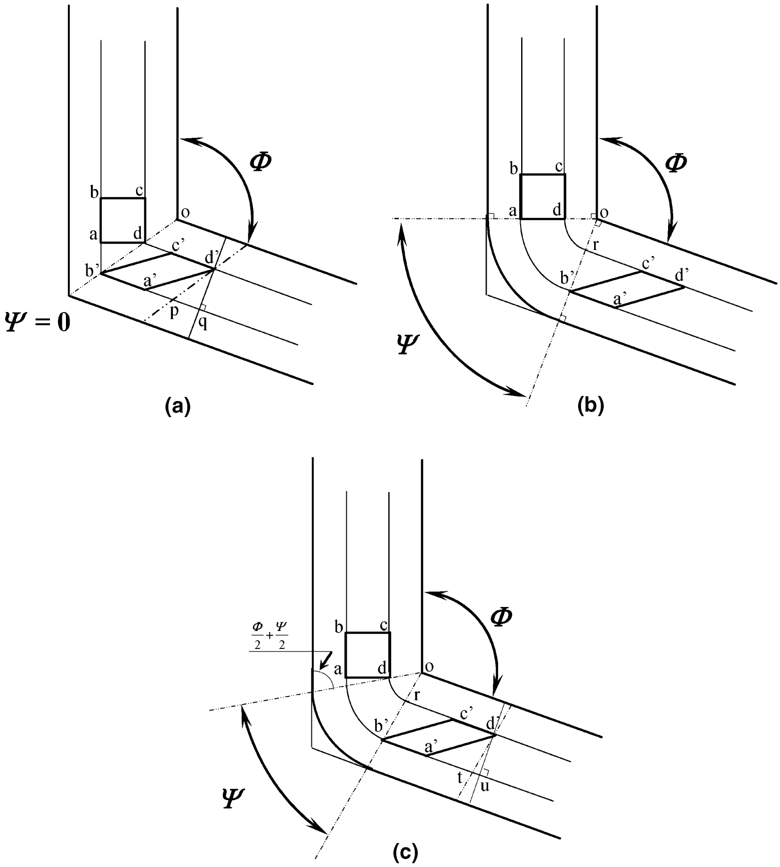

Fig. 15. Principle of ECAP where Φ is the angle of intersection of the two channels and Ψ is the angle subtended by the arc of curvature at the point of intersection: (a) $\Psi = 0$, (b) $\Psi = \pi - \Phi$, (c) an arbitrary value of Ψ lying between $\Psi = 0$ and $\Psi = \pi - \Phi$ [106].

and a similar analysis for Fig. 15(c) leads to the general solution

$$\gamma = 2\cot\left(\frac{\Phi}{2} + \frac{\Psi}{2}\right) + \Psi \operatorname{cosec}\left(\frac{\Phi}{2} + \frac{\Psi}{2}\right) \tag{4}$$

It follows from inspection that the general solution in Eq. (4) reduces to Eq. (2) when $\Psi = 0°$ and to Eq. (3) when $\Psi = (\pi - \Phi)°$. Finally, the equivalent strain after N passes, ε_N, may be expressed in a general form by the relationship [106]

$$\varepsilon_N = \frac{N}{\sqrt{3}}\left[2\cot\left(\frac{\Phi}{2} + \frac{\Psi}{2}\right) + \Psi \operatorname{cosec}\left(\frac{\Phi}{2} + \frac{\Psi}{2}\right)\right] \tag{5}$$

Eq. (5) is consistent with an earlier estimate of the strain where a die was analyzed with $\Psi = 0°$, the channel angle Φ was taken as 2φ and the strain after N passes was estimated as [21]

$$\varepsilon_N = \frac{2N}{\sqrt{3}} \cot \varphi \tag{6}$$

Eq. (6) is also identical to the relationship derived in an alternative analysis [107]. Thus, all of these approaches lead to similar relationships for the equivalent strain but Eq. (5) has the advantage that it incorporates the angle associated with the arc of curvature, Ψ. Eq. (5) is also reasonably consistent with alternative approaches [108–110] and it provides a simple and direct procedure for estimating the strain for any selected die having different values for Φ and Ψ.

There is experimental evidence supporting the use of Eq. (5) in experiments on ECAP. First, model experiments were conducted where layers of colored plasticine were pressed through a plexiglass die and measurements of the strain in these experiments revealed excellent agreement with Eq. (5) in the central regions of the billets although there were deviations near the cell walls because of frictional effects [111]. Second, model experiments were conducted in which two half-billets of pure aluminum, with a regular rectangular grid drawn on one of their common interfaces, were pressed through a die having $\Phi = 90°$ and $\Psi = 0°$ and the strain was measured directly after pressing [112]. The result showed excellent agreement with Eq. (5) throughout 85% of the billet although there was an area of non-uniform deformation occurring in the vicinity of the lower surface of the billet where the material passed through the outer corner of the die. The experiment showed this region of non-uniformity occupied only ~15% of the total area.

It is convenient to prepare a graphical representation of Eq. (5) because this provides a simple visual understanding of the significance of the die angles Ψ and Φ. This type of plot was initially constructed for die angles at and above $\Phi = 90°$ [113] but subsequently the approach was extended to include die angles as small as 45° [114]: the latter approach is

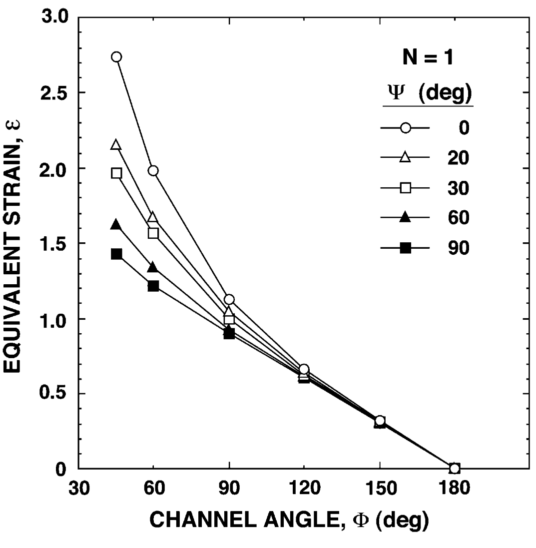

Fig. 16. Variation of the equivalent strain, ε, with the channel angle, Φ, over an angular range of Φ from 45° to 180° for values of the angle of the arc of curvature, Ψ, from 0° to 90°: the strains are shown for a single pass where $N = 1$ [114].

shown in Fig. 16 for a single pass with $N = 1$ where the channel angle Φ ranges from 45° to 180° and the arc of curvature varies from 0° to 90° [114].

Several conclusions may be reached from inspection of Fig. 16. First, the angle at the arc of curvature, Ψ, has a relatively minor effect on the equivalent strain except only for channel angles less than 90°. Second, exceptionally high strains may be achieved in a single pass by constructing a die with very low values of Φ and Ψ. Third, for conventional dies where the channel angle is generally equal to 90°, the equivalent strain is close to ~1 for a single pass and this strain is essentially independent of the angle representing the arc of curvature, Ψ.

3.2. The processing routes in ECAP

As noted briefly in Section 2.1, there are four basic processing routes in ECAP and these routes introduce different slip systems during the pressing operation so that they lead to significant differences in the microstructures produced by ECAP [115–117]. The four different processing routes are summarized schematically in Fig. 17 [55]: thus, in route A the sample is pressed without rotation, in route B_A the sample is rotated by 90° in alternate directions between consecutive passes, in route B_C the sample is rotated by 90° in the same sense (either clockwise or counterclockwise) between each pass and in route C the sample is rotated by 180° between passes. Various combinations of these routes are also possible, such as combining routes B_C and C by alternating rotations through 90° and 180° after every pass, but in practice the experimental evidence obtained to date suggests that these more complex combinations lead to no additional improvement in the mechanical properties of the as-pressed materials [118]. Accordingly, for the simple processing of bars or rods, attention is generally devoted exclusively to the four processing routes delineated in Fig. 17.

3.3. Slip systems for the different processing routes

The different slip systems associated with these various processing routes are depicted schematically in Fig. 18 where the X, Y and Z planes correspond to the three orthogonal planes shown in Fig. 1 and slip is shown for different passes in each processing route: thus, the planes labeled 1 through 4 correspond to the first 4 passes of ECAP [115]. In route C, the shearings continue on the same plane in each consecutive passage through the die but

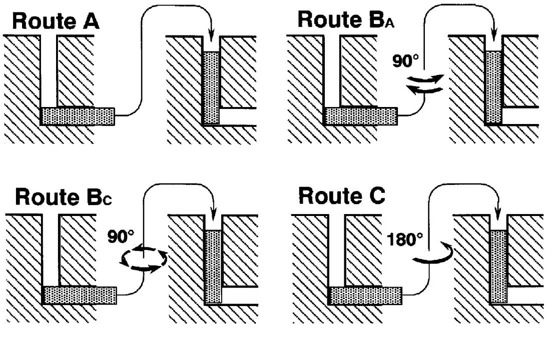

Fig. 17. The four fundamental processing routes in ECAP [55].

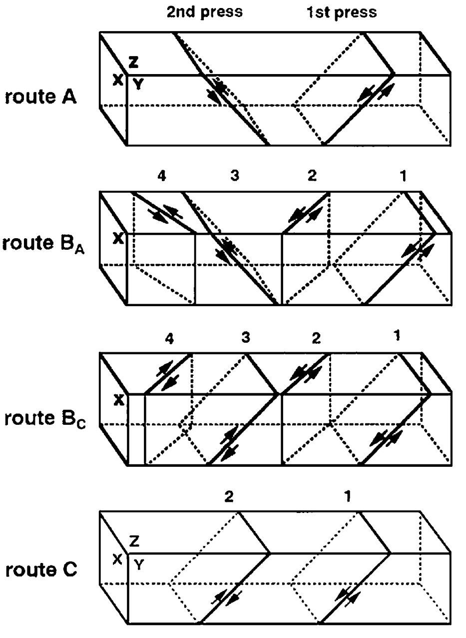

Fig. 18. The slip systems viewed on the X, Y and Z planes for consecutive passes using processing routes A, B_A, B_C and C [118].

the direction of shear is reversed on each pass: thus, route C is termed a redundant strain process and the strain is restored after every even number of passes. It is apparent that route B_C is also a redundant strain process because slip in the first pass is cancelled by slip in the third pass and slip in the second pass is cancelled by slip in the fourth pass. By contrast, routes A and B_A are not redundant strain processes and there are two separate shearing planes intersecting at an angle of 90° in route A and four distinct shearing planes intersecting at angles of 120° in route B_A. In routes A and B_A, there is a cumulative build-up of additional strain on each separate pass through the die.

The implications of these shearing systems is illustrated in Fig. 19 where the four major rows correspond to the four different processing routes and the illustrations depict the macroscopic distortions introduced into a cubic element, as viewed on the X, Y and Z planes, for up to a maximum of 8 passes through the die [56]. Thus, for each plane of sectioning and each processing route, Fig. 19 documents the distortions visible in the faces of the cubic element. It is apparent from Fig. 19 that the cubic element is restored every 2 passes using route C and every 4 passes using route B_C whereas the distortions become more acute when using routes A and B_A. Furthermore, there is no deformation of the cubic element on the Z plane when using routes A and C. The implications of these distortions are considered later when examining the influence of the processing route on the development of an ultrafine-grained microstructure.

3.4. The shearing patterns associated with ECAP

A valuable approach in examining the implications of ECAP is to consider the shearing patterns that develop on each orthogonal plane for each processing route. This informa-

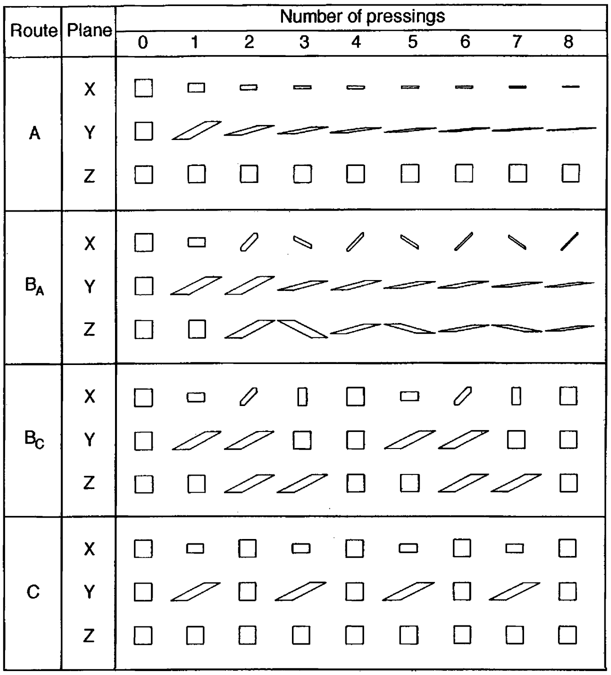

Fig. 19. The distortions introduced into cubic elements when viewed on the X, Y and Z planes for processing routes A, B_A, B_C and C when pressing through 1–8 passes [56].

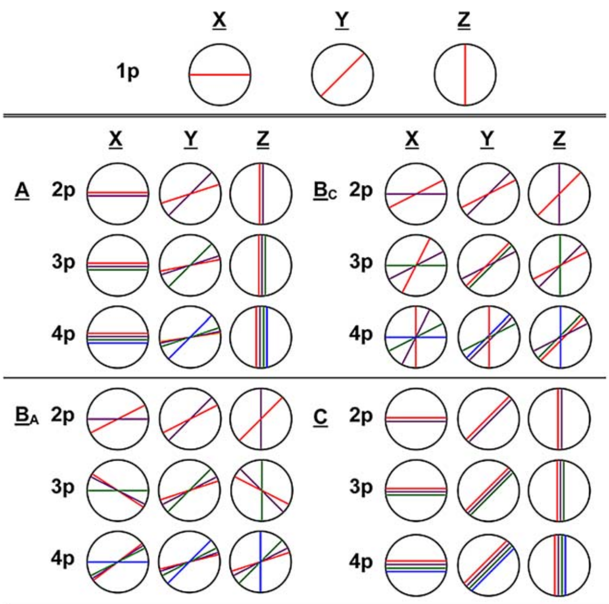

Fig. 20. The shearing patterns on the X, Y and Z planes for processing routes A, B_A, B_C and C when pressing through 1, 2, 3, and 4 passes: the colors red, mauve, green and blue correspond to the first, second, third and fourth pass, respectively [119].

Table 1
Angular ranges for slip using different processing routes [119]

Processing route	Number of passes	Total angular range, η		
		X	Y	Z
A	2p	0°	27°	0°
	3p	0°	34°	0°
	4p	0°	37°	0°
B_A	2p	27°	18°	45°
	3p	33°	27°	63°
	4p	37°	31°	72°
B_C	2p	27°	18°	45°
	3p	63°	18°	63°
	4p	90°	63°	63°
C	2p	0°	0°	0°
	3p	0°	0°	0°
	4p	0°	0°	0°

tion is now available both for the processing routes in conventional ECAP when using 90° and 120° dies and for the pressing of plate samples where rotation occurs about the Y or Z axes [119].

Fig. 20 shows the shearing patterns for conventional ECAP using a 90° die with rotation about the X axis as viewed in the four separate processing routes [119]. The top line in Fig. 20 shows the slip visible on the X, Y and Z planes after 1 pass (1p) and the remaining lines show the patterns for routes A, B_A, B_C and C after 2 (2p), 3 (3p) and 4 (4p) passes, respectively: it should be noted that the lines are color-coded so that the colors red, mauve, green and blue correspond to the first, second, third and fourth pass, respectively. These drawings demonstrate there is a considerable variation in the total angular range of slip viewed on any selected plane during ECAP. For simplicity, this angular range is denoted by η and the individual values of η for each plane and each set of passes is summarized in Table 1. Thus, the angular range is zero on all planes when using route C or when viewing the X or Z planes in route A. It is also apparent from Table 1 that route B_C yields the largest angular range with values of η of 90°, 63° and 63° after 4 passes on the X, Y and Z planes, respectively. These angular ranges are re-examined later when considering the preferred route for developing an equiaxed and homogeneous microstructure.

4. Experimental factors influencing ECAP

When materials are processed using ECAP, several different factors influence the workability and the microstructural characteristics of the as-pressed billets. These factors fall into three distinct categories. First, there are factors associated directly with the experimental ECAP facility, such as the values of the angles within the die between the two parts of the channel and at the outer arc of curvature where the channels intersect. Second, there are experimental factors related to the processing regimes where some control may be exercised by the experimentalist including, for example, the speed of pressing, the temperature of the pressing operation and the presence or absence of any back-pressure. These two sets of experimental factors are considered in this section. Third, there are also other processing factors which may play a role in influencing the extent of the grain refinement and the homogeneity of the as-pressed microstructure including the nature of the crystallographic texture and the distribution of grain misorientations in the unpressed material. It follows therefore that it is important for the experimentalist to conduct a detailed characterization of the material prior to initiating the pressing operation. These microstructural characteristics and other processing factors determined by the operator, including the processing route (whether A, B_A, B_C or C) and the total number of passes imposed on the sample, are considered separately in Section 5 which specifically delineates the microstructural aspects of ECAP.

4.1. Influence of the channel angle, Φ

The channel angle, Φ, is the most significant experimental factor since it dictates the total strain imposed in each pass, as shown by the plot presented earlier in Fig. 16, and thus it has a direct influences on the nature of the as-pressed microstructure. Nevertheless, despite the critical importance of this angle, most experiments reported to date use values of Φ from 90° to 120° and there is generally little or no attempt to make any significant comparison between the results obtained when using dies having different channel angles.

There are two separate reports describing experimental assessments of the significance of the channel angle. The first report describes experiments on pure aluminum using a series of dies having values of Φ from 90° to 157.5° [120] and the second report describes experiments on OFHC copper pressed using two dies having channel angles of either 90° or 120° [121]. Since the earlier investigation provides a detailed report on the microstructures attained with each channel angle, it is important to examine these results in more detail.

The experiments were conducted using four separate dies having channel angles of 90°, 112.5°, 135° and 157.5°: these four dies are illustrated schematically in Fig. 21 and the diagrams include the values for the arcs of curvature, Ψ [120]. Pure aluminum billets were pressed through these dies at room temperature using route B_C where each sample is rotated by 90° in the same direction between each pass. In order to provide a meaningful

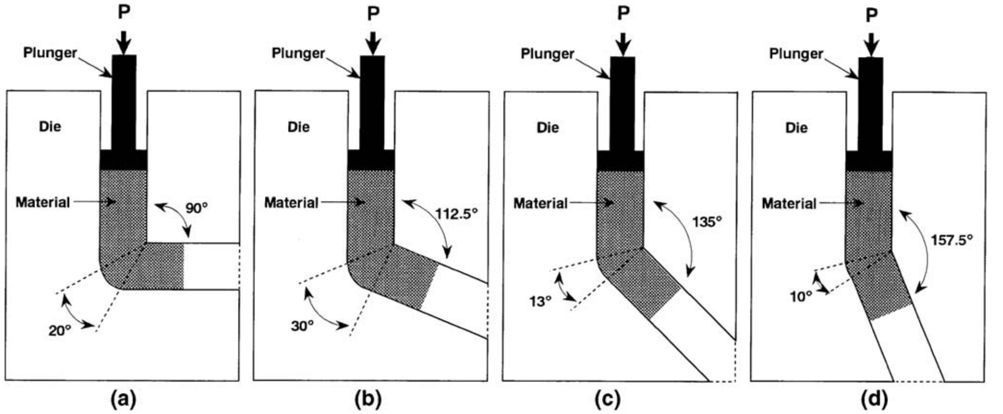

Fig. 21. Schematic illustration of the dies used to evaluate the influence of the channel angle, Φ: the values of Φ are (a) 90°, (b) 112.5°, (c) 135° and (d) 157.5° [120].

comparison between the various channel angles, the numbers of passes through each die were adjusted so that the total imposed strains were ~4 for each sample. Thus, making use of Eq. (5), the samples were pressed for totals of 4, 6, 9 and 19 passes corresponding to total strains of 4.22, 4.27, 4.21 and 4.33 for the dies having angles of 90°, 112.5°, 135° and 157.5°, respectively. The resultant microstructures are shown in Fig. 22 together with selected area electron diffraction (SAED) patterns taken from regions having diameters of 12.3 μm [120]. It is readily apparent from inspection of these photomicrographs that an array of ultrafine equiaxed grains is achieved most easily when the sample is subjected to a very intense plastic strain using a die with a channel angle of 90°. Furthermore, the SAED pattern for a channel angle of $\Phi = 90°$ shows that these boundaries have high angles of misorientation. By contrast, the microstructure becomes less regular, and the SAED patterns show there are higher fractions of boundaries having low angles of misorientation, when the channel angle is increased.

These results demonstrate that, at least for pure aluminum, the total cumulative strain is not the important factor in determining the microstructure in ECAP but rather it is important to ensure that a very high strain is imposed on each separate pass. This means in practice that the ideal ECAP die will have a channel angle close to 90° and it implies also that similar microstructures cannot be attained with other techniques, as in conventional extrusion using multiple passes, where small incremental strains are imposed in each separate pass.

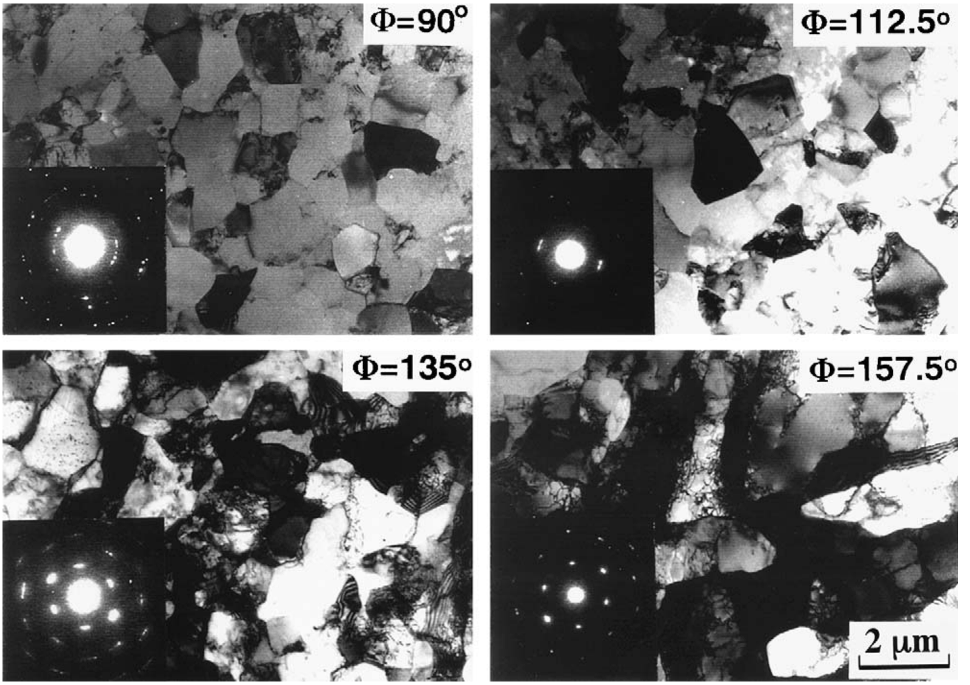

Fig. 22. Microstructures and SAED patterns obtained using the dies shown in Fig. 21 when each sample is pressed to an imposed strain of ~4 [120].

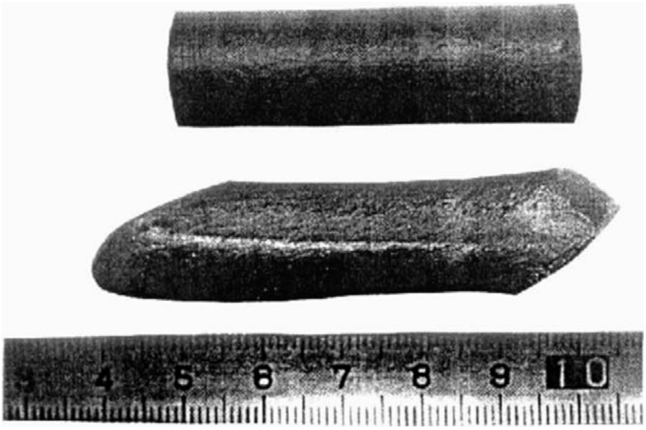

Fig. 23. A view of billets of pure tungsten: before processing by ECAP (above) and after processing by ECAP through 8 passes using route C (below) [122].

Despite the efficiency of ECAP dies with channel angles of $\Phi = 90°$, it is important to recognize that it is experimentally easier to press billets when using dies with angles that are larger than 90°. For some very hard materials or with materials having low ductility, this may be an important consideration. For example, experiments showed that it was not feasible to press commercial purity tungsten through a die with a channel angle of 90° at a temperature of $\sim$1273 K because of cracking in the billets but excellent results were

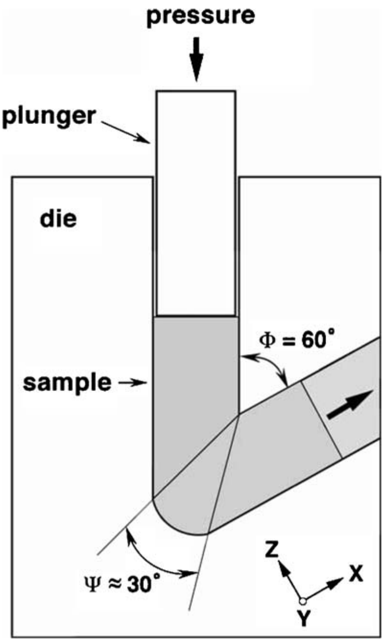

Fig. 24. A schematic illustration of an ECAP die having a channel angle of $\Phi = 60°$ [114].

achieved at the same pressing temperature when the channel angle was increased to 110° [122]. Fig. 23 shows a tungsten billet before (upper) and after (lower) pressing with $\Phi = 110°$ for 8 passes using route C [122].

Since the strain imposed in ECAP increases with decreasing channel angle, it may be advantageous to perform the pressings using channel angles which are <90°. A single report describes the pressing of pure aluminum and an Al–Mg–Sc alloy using a die having a channel angle of 60° as illustrated in Fig. 24 [114]. The results from these experiments showed that it was possible to produce excellent microstructures using a die with $\Phi = 60°$ and the average grain sizes were slightly smaller than with the dies having $\Phi = 90°$: thus, the grain sizes for the 60° and 90° dies were ~1.1 and ~1.2 μm for pure Al and ~0.30 and ~0.36 μm for the Al–Mg–Sc alloy, respectively [114]. Despite the apparent advantage of using a die with $\Phi < 90°$, high pressures are required to successfully produce billets without the introduction of any cracking. Accordingly, it is reasonable to conclude that a channel angle of 90° represents the optimum configuration for an ECAP die.

4.2. Influence of the angle of curvature, Ψ

The angle of curvature, Ψ, denotes the outer arc where the two parts of the channel intersect within the die. This angle plays only a minor role in determining the strain imposed on the sample, as shown by the estimates of equivalent strain given in Fig. 16. Nevertheless, it is important to investigate the influence of this angle in the production of ultrafine-grained materials.

There have been numerous attempts to analyze the deformation occurring in ECAP through the use of finite element modeling and many of these analyses incorporate an evaluation of the significance of the curvature angle Ψ [101,123–137]. The role of this angle is also important because, whereas conventional split two-part dies are easily constructed with $\Psi = 0°$, all solid dies will necessarily incorporate $\Psi > 0°$. The significance of these differences was carefully investigated using samples of pure aluminum and two separate dies: a split die having $\Phi = 90°$ and $\Psi = 0°$ where the billets had a square cross-section with dimensions of 10×10 mm^2 and a solid die having $\Phi = 90°$ and $\Psi = 20°$ where the billets had a circular cross-section with a diameter of 10 mm [103,138]. Samples were pressed through both dies at room temperature for totals of four passes, equivalent to imposed strains of ~4.6 and ~4.2 for the split and solid dies, respectively, and the samples were then sectioned perpendicular to their long axes and the local values of the Vickers microhardness were recorded following a regular grid pattern with a spacing between each point of ~0.5 mm. The results from these measurements showed excellent consistency between these two die configurations. This may be illustrated using a color-coded representation [103] or, for simplicity, by plotting the hardness values on contour maps as shown in Fig. 25 [138]. Thus, the average values of the Vickers microhardness were ~42.1 and ~43.2 for the split and solid dies, respectively, where these values are identical to within the experimental error.

Careful inspection of Fig. 25 shows both samples exhibit very small regions of inhomogeneity which are located in the vicinity of the bottom surfaces of the billets. This is reflected by the contours showing local hardnesses of <35 in these regions and it is consistent both with measurements reported for the local strains when using a sample containing a grid pattern [112] and with predictions from finite element analyses [101,123–

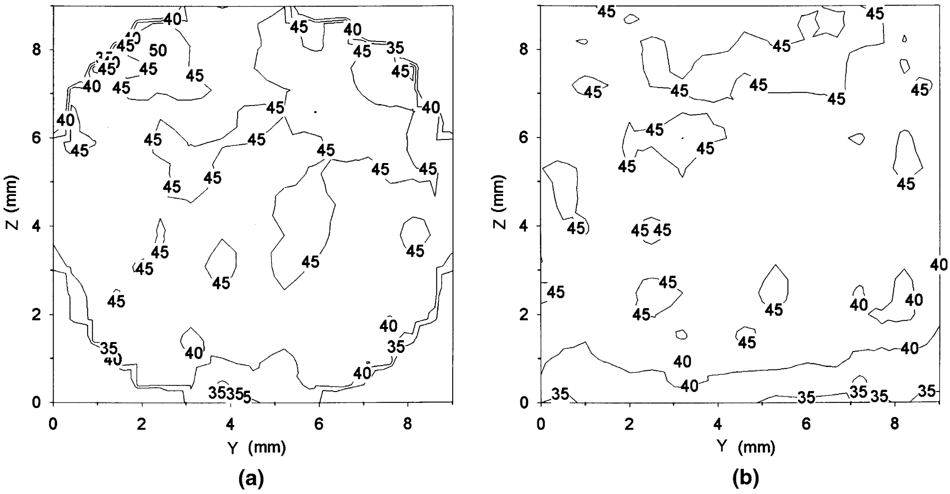

Fig. 25. Contour maps showing the values of the microhardness recorded on the X plane of samples of pure Al pressed through 4 passes using route B_C using an ECAP die with $\Phi = 90°$ and arcs of curvature of (a) $\Psi = 20°$ and (b) $\Psi = 0°$ [138].

129,131,133]. Nevertheless, the results do not support the claims, from finite element considerations, that the use of a die with a round corner will introduce an increase in the extent of inhomogeneities in the as-pressed billets [125,128,129,131,133]. The reason for this apparent disagreement probably lies in the values selected for Ψ in the theoretical calculations. For example, a detailed theoretical analysis was conducted using $\Phi = 90°$ and with the two curvature angles of $\Psi = 0°$ and $90°$ [128] and the latter value of Ψ was used to reach conclusions concerning the validity of pressing with a die having a round corner. By contrast, the experimental data shown in Fig. 25 employed dies with values of Ψ of either 0° or 20° and the results demonstrate that, at least for these two similar curvature angles, the data are in excellent agreement.

The explanation for this agreement lies in the development of the corner gap or "dead zone" which is formed at the outer corner when the billets pass through the die. This means that the billet no longer remains in contact with the die walls at this outer corner and the occurrence of these dead zones has been revealed both in model experiments [111,112] and in finite element calculations [101,123–128,133]. It has been shown that, for a pressing speed of 1 mm s^{-1}, the angle subtended by the corner gap depends upon the rate of strain hardening in the material with the corner gaps varying from ~51° in commercial purity 1100 aluminum to ~22° for an Al-6061 alloy tested in a T6 condition [126]. The presence of this corner gap will therefore negate the significance of the curvature angle, at least for values of Ψ up to ~20°, thereby leading to the similarities in the hardness values recorded in Fig. 25 for values of Ψ of 0° and 20°.

It is possible also to introduce a corner angle on the inner surface where the two parts of the channel intersect, as illustrated schematically in Fig. 26 where R is the fillet radius for both the inner and outer arcs [139]. For this condition, following the same approach developed earlier in the derivation of Eq. (5) where the element $abcd$ is deformed to $a'b'c'd'$ on passing through the shearing zone [106], it can be shown that the shear strain is given by

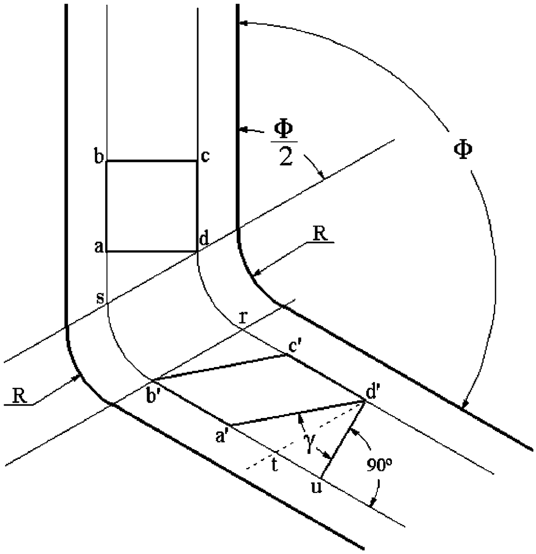

Fig. 26. An ECAP die showing equal values for the fillet radius, R, at the outer and inner arcs of intersection between the two channels [139].

$2\cot(\Phi/2)$ which is consistent with Eq. (5) and identical to Eq. (2) in Section 3.1. Furthermore, it is important to note that this relationship is true for any value of the fillet radius R. The generality of this relationship for all values of R has led to the proposal that the design of the ECAP die may be improved by using a configuration of the type depicted in Fig. 26 [139,140]. From a practical point of view, however, this alternative approach is unrealistic because split dies are easily constructed with no curvature at either the outer or inner points of intersection and in solid dies, where an outer arc of curvature is required, it is difficult to machine a die having equal fillet radii at both the inner and outer intersections.

In view of these difficulties, it is reasonable to conclude that the most promising approach is to construct a die with a channel angle of $\Phi = 90°$, with an outer angle of curvature of $\Psi \approx 20°$ and with no arc of curvature at the inner point of intersection of the two parts of the channel.

4.3. Influence of the pressing speed

Processing by ECAP is usually conducted using high-capacity hydraulic presses that operate with relatively high ram speeds. Typically, the pressing speeds are in the range of $\sim$1–20 mm s^{-1}. Nevertheless, it is feasible to construct dies for use in conventional mechanical testing machines and this provides the capability of extending the pressing speeds over a very wide range.

The first detailed examination of the influence of the pressing speed involved the pressing of pure aluminum and an Al–1%Mg alloy at ram speeds from 10^{-2} to 10 mm s^{-1} [54]. These results demonstrated that the pressing speed has no significant influence on the equilibrium size of the ultrafine grains formed by ECAP but, since recovery occurs more easily

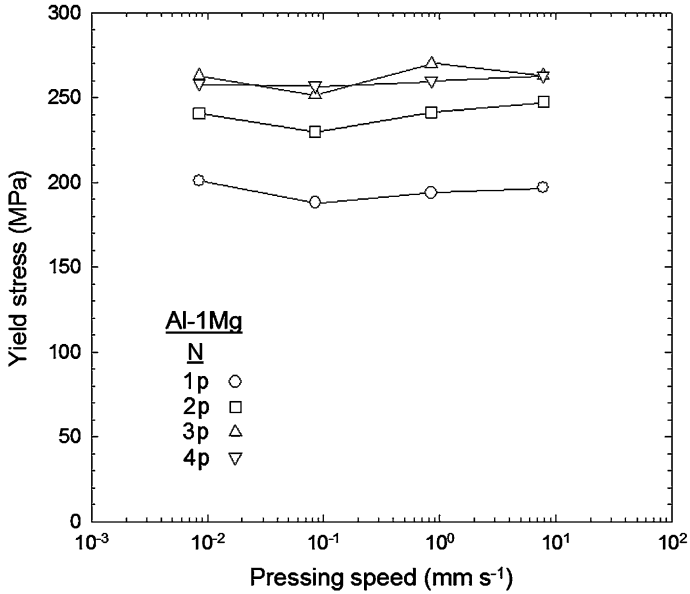

Fig. 27. Variation of the yield stress with the pressing speed for an Al–1%Mg alloy after ECAP through 1, 2, 3 and 4 passes: data recorded at room temperature using a strain rate of 1.0×10^{-1} s^{-1} [54].

when pressing at the slower speeds, these lower speeds produce more equilibrated microstructures. The lack of any significant dependence on the pressing speed is illustrated for the Al–1%Mg alloy in Fig. 27 where the yield stress in subsequent tensile testing at room temperature using a strain rate of 1.0×10^{-1} s^{-1} is plotted against the pressing speed after a number of passes, N, from 1 to 4 using route B_C [54]. These results confirm the increasing strength with increasing numbers of passes through the die, the tendency to saturate after $N \approx 4$ passes and the lack of any dependence on the pressing speed.

A similar conclusion was reached also in tests on pure Al and three Al-based alloys using pressing speeds of 18 and 0.18 mm s^{-1} where it was shown that there is an abrupt heating of the samples when testing at the faster rate but no significant heating at the slower rate [141]. In addition, tests on titanium using pressing speeds of 0.2 and 2.8 mm s^{-1} revealed only minor microstructural differences in these specimens after pressing through only 1 pass [142].

4.4. Influence of the pressing temperature

The pressing temperature is a key factor in any use of ECAP because it can be controlled relatively easily. The first detailed investigation of the influence of temperature involved samples of pure Al, an Al–3%Mg alloy and an Al–3%Mg–0.2%Sc alloy with the pressing conducted from room temperature to 573 K [143]. In order to ensure a careful and correct monitoring of the temperature within the die to within ±5 K during each pressing operation, a solid die was constructed with a thermocouple inserted into a small hole which was drilled horizontally to a position within ~5 mm of the channel wall in the vicinity of the shearing plane. Careful monitoring established that it took approximately

1 h to reach the required temperature within the die and another ~10 min for temperature stabilization. Accordingly, the pressing was undertaken using two separate specimens with the first specimen heated, placed in the die, held at temperature for ~10 min and then pressed and the second specimen held in a separate furnace at the same temperature prior to insertion into the die and pressing. Thus, the operation was undertaken using two specimens and a separate furnace to maintain the specimens at a reasonably constant temperature at all times.

The results from these experiments revealed two important trends. First, there was an increase in the equilibrium grain size with increasing temperature as shown in Fig. 28 [143]. Second, it was concluded from an examination of the SAED patterns that the fraction of low-angle grain boundaries increased with increasing temperature due, it was suggested, to the faster rates of recovery at the higher temperatures which led to an increasing annihilation of dislocations within the grains and a consequent decrease in the numbers of dislocations absorbed into the subgrain walls. However, there was also a significant dependence on material because the transition to a high fraction of low-angle boundaries occurred at pressing temperatures of 473 K in pure Al and at 573 K in the Al–3%Mg alloy. Furthermore, there was no transition to arrays of low-angle boundaries in the Al–3%Mg–0.2%Sc alloy [143].

The tendency for larger grains or subgrains to form at the higher pressing temperatures was confirmed in several subsequent investigations [144–149] and detailed analyses using Kikuchi patterns confirmed also the tendency for a higher fraction of high-angle boundaries to form at the lower temperatures [144,145,148,149]. For the pressing of pure Ti, there was evidence for a change in the deformation mechanism from the formation of parallel shear bands to the formation of deformation twinning bands when the pressing temperature was increased from 473 to 523 K [150]. All of these results demonstrate that, although it is generally experimentally easier to press specimens at high temperatures, optimum ultrafine-grained microstructures will be attained when the pressing is performed at the lowest possible temperature where the pressing operation can be reasonably conducted without the introduction of any significant cracking in the billets. By maintaining a low

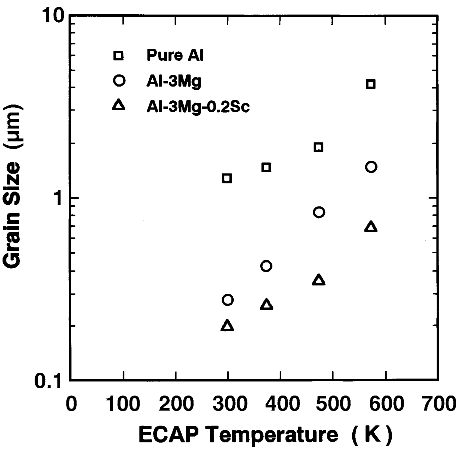

Fig. 28. Grain size after ECAP versus the pressing temperature for pure Al and Al–3%Mg and Al–3%Mg–0.2%Sc alloys [143].

pressing temperature, this ensures the potential for achieving both the smallest possible equilibrium grain size and the highest fraction of high-angle boundaries.

4.5. The role of internal heating during ECAP

The preceding section reviews the significance of the pressing temperature but there is an additional potential thermal effect due to any temperature rise, ΔT, that may occur in the billet during the pressing operation. There have been two experimental measurements to date of the magnitude of ΔT. In the first experiment, the temperature rise was measured for pure Al, a commercial Al-1100 alloy and Al–1%Mg and Al–3%Mg solid solution alloys with the pressing conducted at room temperature and with a thermocouple inserted into a hole drilled parallel to the longitudinal axis to a distance of 30 mm from the rear face of the billet [141]. In the second experiment, ΔT was measured for an Al–Si–Mg alloy,

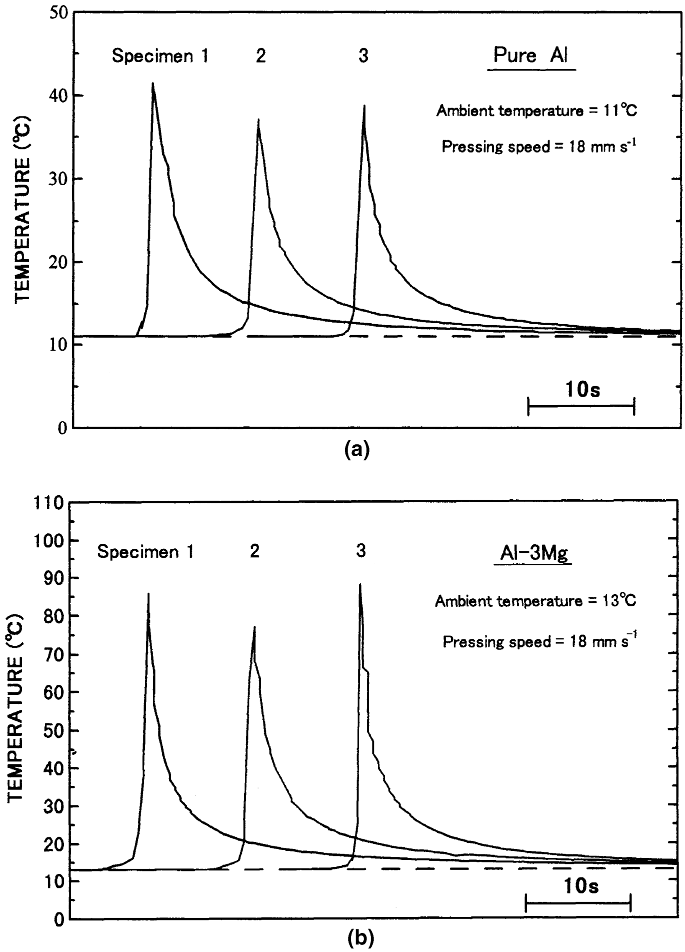

Fig. 29. Local heating during passage through the shearing plane in ECAP at room temperature using a pressing speed of 18 mm s^{-1} for three identical specimens of (a) pure Al and (b) an Al–3%Mg alloy [141].

an Al-7075 alloy and a magnesium AZ91 alloy pressed at 573 K and for an Al-6061 composite with an alumina fiber reinforcement pressed at 673 K with the thermocouples inserted from the front of each billet [151].

Fig. 29 shows representative results for the pressing of pure Al and the Al–3%Mg alloy at room temperature using a pressing speed of 18 mm s^{-1}: the upper plot shows the measured temperature rises for three identical specimens of pure Al and the lower plot shows similar data for three identical specimens of the Al–3%Mg alloy [141]. It is apparent from these plots that there are very abrupt increases in the temperature within each sample at the point where it passes through the shearing plane. For pure Al, the ambient temperature was 11 °C and the temperature increased to ~40 °C on entry into the shearing zone but thereafter the temperature decreased to <15 °C within ~10 s. The results for the Al–3%Mg alloy were similar except that the ambient temperature was 13 °C and the temperature increased to a maximum of ~85 °C but with a subsequent decrease to <20 °C within ~10 s. It is also clear from Fig. 29 that there is excellent reproducibility of these plots for the three identical specimens used in each case. Subsequently, a finite element analysis was undertaken to predict the temperature rise in the ECAP pressing of the Al–1%Mg and Al–3%Mg alloys and the predictions were shown to be in excellent agreement with the experimental data given in Fig. 29 [134].

An examination of the experimental values measured for ΔT showed that these values scaled approximately with the ultimate tensile stress (UTS) of the materials [141]: this correlation is shown in Fig. 30 where the open points were obtained at a pressing speed of 18 mm s^{-1} and the closed point was obtained at a pressing speed of 0.18 mm s^{-1}. This plot demonstrates, therefore, that the temperature rise becomes more important in the pressing of stronger materials. Subsequently, a lumped heat transfer analysis was used to predict the temperature rise when pressing by ECAP while ignoring any temperature inhomoge-

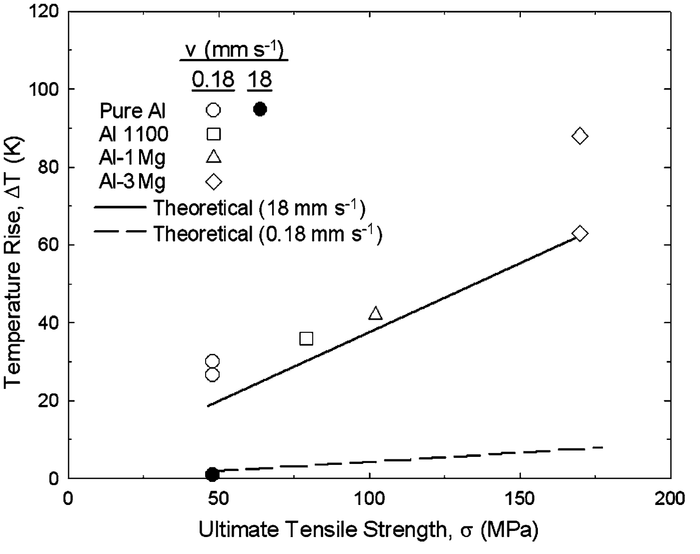

Fig. 30. Experimental values for the temperature rise in pure Al and three aluminum-based alloys as a function of the ultimate tensile strength using pressing speeds, v, of 0.18 and 18 mm s^{-1} [141]: the solid and broken lines are the theoretical predictions using a lumped heat transfer analysis [152].

neities within the billet [152]. The results from this analysis showed that the temperature rise increases with increasing strength of the material and with increasing ram speed in the pressing operation. The calculated predictions from the analysis are given by the two lines in Fig. 30 which correspond to the experimental pressing speeds of 18 and 0.18 mm s^{-1}, respectively [152]. Inspection shows these predictions are in excellent agreement with the experimental data.

4.6. Influence of a back-pressure

The important role of using a back-pressure was first stressed in very early work on the mechanics of ECAP [20]. However, in recent years it has become an area of special interest [153–157] primarily because ECAP die-sets have been designed which may be used to conduct the processing operation with a precise back-pressure which is computer-controlled.

An important advantage in imposing a back-pressure is that it leads to a very considerable improvement in the workability of the processed samples. For example, during the ECAP of Cu in the absence of a back-pressure it is generally found that cracks appear on the billet surface after about 12–13 passes. However, when a back-pressure of only 300 MPa is imposed during ECAP, the same samples remain integral without any perceptible cracking even after 16 or more passes [158]. Similarly, a sample of a quenched aluminum 6061 alloy failed in the first pass during ECAP at room temperature in the absence of a back-pressure but during pressing with a back-pressure of 450 MPa the sample was processed up to 4 passes without any cracking [156].

Another important advantage of back-pressure is the visible enhancement introduced in the uniformity of the metal flow during the ECAP operation. As already noted, during ECAP there is an underfilling of the outer angle of the die due to the formation of a dead zone and, especially in strain-hardenable materials, there is also a change in the shape of the deformation zone from a pure shear line to a fan shape within the die [101]. As a result, the microstructural refinement becomes less uniform, especially in the vicinity of the bottom surface of the billet. By contrast, the application of a back-pressure leads to a filling of this outer corner, and a consequent removal of the dead zone, regardless of the character of the material strengthening. Furthermore, the deformation zone becomes closer to a localized shear band which is typical of a rigid perfectly-plastic body [159].

The influence of back-pressure on the degree of grain refinement was investigated using Cu with an imposed back-pressure of 400 MPa [156]. These experiments showed the grain size was reduced from 0.24 μm without any back-pressure to 0.18 μm in the presence of a back-pressure. More work is now needed to determine whether this additional grain refinement is a consequence of the change in the metal flow pattern during the processing operation or whether the applied pressure directly influences the processes of microstructural evolution. Additional experiments are also needed to evaluate the role of a back-pressure with other materials.

Technically, a back-pressure can be imposed in several different ways. The simplest procedure is to increase the level of friction in the exit channel or to make use of a viscous-ductile medium [153]. However, an improved and more controlled procedure is to use special devices such as the application of a second punch in the output channel [153,157,159]. Fig. 31 shows schematic examples of the use of (a) a second punch exerting a pressure P_2 and (b) a viscous-ductile medium in the exit channel [153]. In practice, an optimum condition may be achieved by using a computer-controlled ECAP die where it is possible to

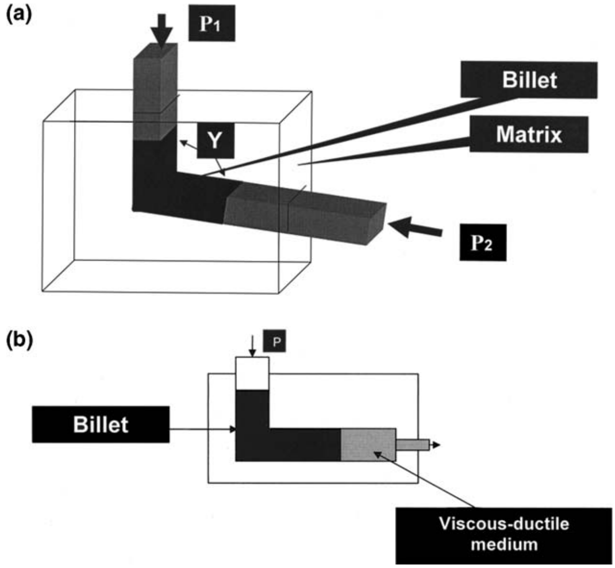

Fig. 31. The principle of ECAP with back-pressure: (a) schematic illustration of the ECAP die where P_1 is the pressing force, P_2 is the back-pressure force and Y is the angle of channel intersection and (b) implementation of this principle using a viscous-ductile medium in the output channel [153].

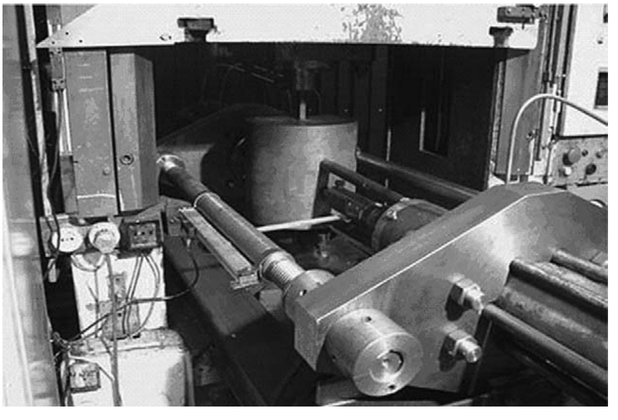

Fig. 32. An experimental die-set for ECAP with a back-pressure incorporating the principle shown in Fig. 31(a) with the use of two punches where the first punch provides the pressure force and the second punch controls the back-pressure [156].

control not only the forward and backward pressures but also the velocities of both punches: an example of this type of facility is shown in Fig. 32 [156].

5. Characteristic features of simple metallic systems processed by ECAP

The most significant feature of ECAP is the ability to achieve very significant and uniform grain refinement in a wide range of materials with the as-pressed grain sizes lying typically within the submicrometer range. However, the characteristics of the as-pressed microstructures are influenced by several variables including the total strain imposed in ECAP processing (and therefore on the number of passes through the ECAP die), the processing route (in terms of routes A, B_A, B_C and C) and the nature of the material (including the crystal structure, the stacking-fault energy and the rate of microstructural recovery). All of these features interact in different ways so that, when combined with experimental factors such as the values of the angles Φ and Ψ within the die, the values of the pressing speed and temperature and the imposition of any back-pressure, there are a multiplicity of permutations which make it difficult to identify the precise requirement in order to achieve an optimum ultrafine-grained microstructure. Nevertheless, there are some basic trends that provide very clear indications of the best procedures that may be undertaken in order to achieve excellent microstructures after ECAP leading to exceptionally high strength and good mechanical properties.

The various factors influencing the as-pressed microstructures of simple systems are examined in this section and the following section examines the pressing of more complex alloys and composites.

5.1. Macroscopic characteristics after ECAP

The characteristics of the microstructures introduced by ECAP have been evaluated in numerous investigations. However, almost all of these investigations employ transmission electron microscopy for determinations of the grain sizes produced by ECAP and the nature of any dislocation interactions occurring within the grains. An alternative approach is to employ optical microscopy to study the shearing of the original grains as they pass through the shearing plane within the die. An initial examination of shearing at the macroscopic level provides an opportunity to make direct comparisons with the theoretical predictions both for the three-dimensional shearing behavior of large solid bodies and for the slip systems visible on orthogonal sections after ECAP processing.

Experiments were conducted at the macroscopic level using pure aluminum as a model material with an initial annealed equiaxed grain size in the range of ~0.5–1.0 mm [160]. The experiments used a split die with a channel having dimensions of $10 \times 10\ \text{mm}^2$, a channel angle of $\Phi = 90°$ and a curvature angle of $\Psi = 20°$ and the pressings were conducted at room temperature using different processing routes.

Fig. 33 shows the macroscopic appearance after one pass of three orthogonal surfaces representing the *X*, *Y* and *Z* planes as defined in Fig. 1, where each plane was electro-polished after pressing and then anodized for ~40 min [160]. Inspection of the *X* plane in Fig. 33 shows that the grains which were initially equiaxed have become elongated along the *Y* direction and flattened in the *Z* direction. In addition, slip is visible within these elongated grains lying approximately parallel to the *Y* direction. On the *Y* plane, the grains are elongated in a direction inclined, in an anti-clockwise rotation, through an angle of ~25–30° to the *X* direction. Within these grains, slip systems operate over a range of angles from ~29° to ~70° but primarily at an angle of ~45° to the *X* direction. Finally, on the *Z* plane the grains remain reasonably equiaxed, they retain essentially the initial size and there is some slip parallel to the *Y* direction.

All of these observations are in excellent agreement with the theoretical predictions as shown in a summary form in Fig. 19 and depicted schematically for a three-dimensional configuration in Fig. 34 for a die with $\Phi = 90°$ and, for simplicity, with $\Psi = 0°$ [160]. Thus,

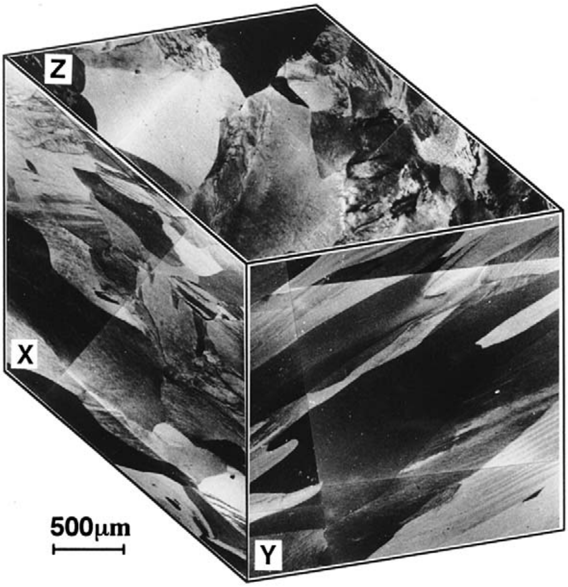

Fig. 33. Macroscopic appearance on the X, Y and Z planes for polycrystalline aluminum after ECAP through one pass [160].

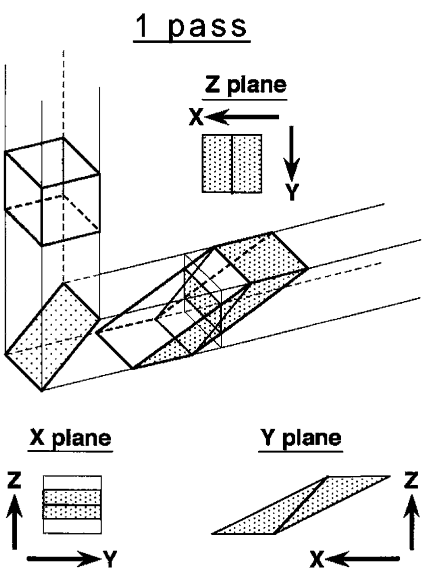

Fig. 34. Schematic illustration of the shearing of a cubic element in a single pass through an ECAP die with $\Phi = 90°$: the inserts show the distortions of the grains and the operative slip systems when viewed on the X, Y and Z planes [160].

the cubic element in the entrance channel in Fig. 34 is pressed through the theoretical shear plane at the intersection of the two parts of the channel and it is then sheared into the rhombohedral shape depicted within the exit channel. Individual inserts are given for the *X*, *Y* and *Z* planes showing the distortions of the grains in the shaded outlines and the operative slip system within each grain. The predicted behavior is in excellent agreement with the experimental observations shown in Fig. 33 in terms of both the macroscopic distortions of the grains and the predominant slip directions. For example, the observations of distorted grains lying at 25–30° to the *X* direction when viewed on the *Y* plane is consistent with Fig. 34 where the grains are elongated at a predicted angle of 27° to the *X* direction. The experimental observation of multiple slip over an angular range of ~20° to ~70° when viewed on the *Y* plane reflects the limitations on the crystallographic shear directions in the face-centered cubic lattice and the influence of the surrounding grains in maintaining a contiguous structure.

Fig. 35 shows similar representations after two passes using (a) route A, (b) route B and (c) route C: it follows that, since the sample was taken through only two passes, routes B_A and B_C are identical for this situation [160]. Again, these experimental observations are in excellent agreement with the theoretical predictions shown in Fig. 36 for the three different

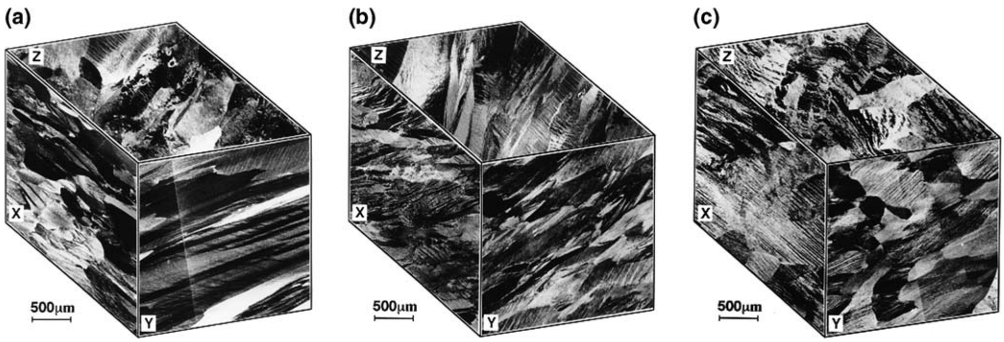

Fig. 35. Macroscopic appearance on the *X*, *Y* and *Z* planes for polycrystalline aluminum after ECAP through two passes using (a) route A, (b) route B and (c) route C [160].

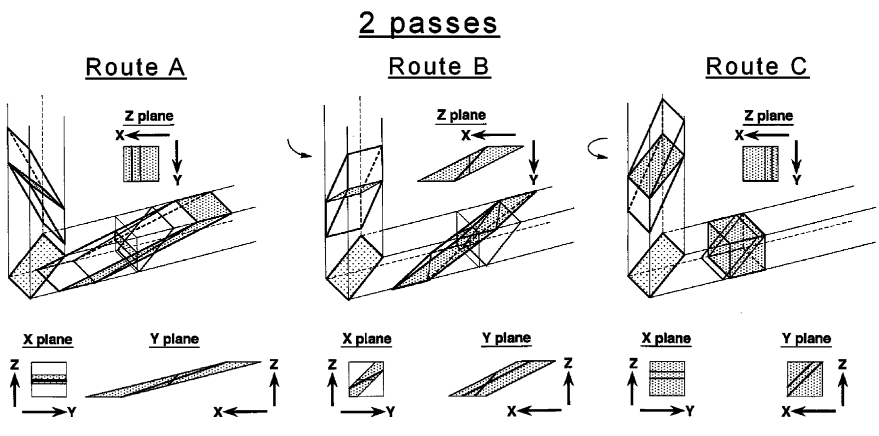

Fig. 36. Schematic illustration of the shearing of a cubic element in the second pass through an ECAP die with $\Phi = 90°$ when using routes A, B and C: the inserts show the distortions of the grains and the operative slip systems when viewed on the *X*, *Y* and *Z* planes [160].

processing routes [160]. It is important to note also that the cubic element is restored after two passes when using route C.

The conclusion from this investigation is that processing by ECAP leads to significant distortions of the large equiaxed grains that are present in the unpressed alloy and the distortions introduced by pressing correlate directly, at least in the initial stages of pressing, with the predictions from simple three-dimensional modeling. This correlation includes both the distortions of the grains at the macroscopic level and the predominant slip systems visible within the grains on three orthogonal planes of sectioning. Additional confirmation of these distortions at the macroscopic level was obtained by incorporating embedded solid inserts into the unpressed billets and then pressing these billets and examining the distortions of the embedded elements after ECAP [161]. For example, this approach was used to confirm the restoration of a cubic element after 2 passes using route C [161].

Although the macroscopic approach using optical microscopy provides very useful information in the earliest stages of deformation in ECAP, the approach is not feasible after large numbers of passes because the grains become extremely distorted and it is difficult if not impossible to clearly differentiate the shapes of the individual grains.

5.2. The development of an ultrafine-grained microstructure

5.2.1. Microstructures in single crystals

The pressing of single crystals has received very little attention to date. However, there is a very significant advantage in making use of single crystals in ECAP processing because it provides a unique opportunity to select the orientation of the crystal with respect to the pressing direction and the theoretical shear plane. There is an early report of the pressing of single crystals of pure Cu but unfortunately there was no attempt to precisely rotate the crystals into different orientations prior to ECAP [162]. More recently, detailed experiments have been conducted on carefully oriented single crystals of aluminum [163–165] and copper [166–169].

For the experiments on single crystals of aluminum, the tests were conducted using a split die with channel and curvature angles of $\Phi = 90°$ and $\Psi \approx 30°$, respectively: the situation is depicted schematically in Fig. 37 where, for simplicity, the curvature angle is shown as $\Psi = 0°$ [163]. Fig. 37 depicts the three orthogonal axes, X, Y and Z, the theoretical shear plane at 45° to the X direction and a single crystal within the die oriented such that the $\{1\,1\,1\}$ slip plane lies parallel to the theoretical shear plane within the ECAP die, the $\langle 1\,1\,0\rangle$ slip direction lies parallel to the direction of shear and the $\langle 1\,1\,2\rangle$ direction corresponds to the Y direction: for simplicity, this is termed the 0° orientation. A series of experiments was conducted using single crystals of high-purity aluminum in the 0° orientation shown in Fig. 37 [163] and in orientations where the $\{1\,1\,1\}$ slip plane and $\langle 1\,1\,0\rangle$ slip direction were rotated about the Y direction either in a counter-clockwise sense by $-20°$ [164] or in a clockwise sense by $+20°$ [165] to give the $-20°$ and 20° orientations, respectively.

It is especially useful to consider a single crystal lying initially in the 20° orientation because, due to the arc of curvature of $\Psi \approx 30°$ within the die at the outer point of intersection of the two parts of the channel, the operative slip system in this crystal experiences almost a maximum shear factor on entering the shear zone in the vicinity of the arc of cur-

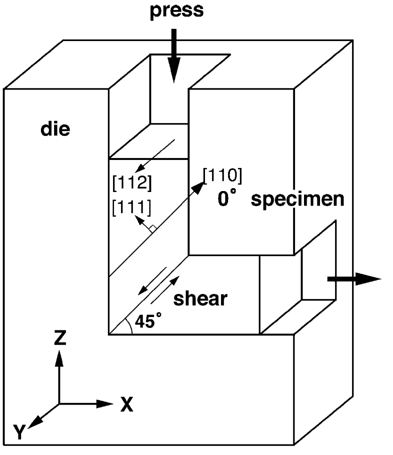

Fig. 37. Schematic illustration of a cross-section through an ECAP die showing the three orthogonal axes and the initial orientation of a single crystal: this is designated the 0° orientation [163].

vature. After pressing a single crystal through the ECAP die for a single pass using the initial 20° orientation, Fig. 38 shows the microstructure visible in the center of the billet on the Y plane where the X and Z directions lie parallel to the bottom and side edges of the photomicrograph, respectively, and the SAED pattern was taken with a beam diameter of 12.3 μm [165]. It is apparent from the SAED pattern that the boundaries visible in Fig. 38 have low angles of misorientation and thus the microstructure consists of a regular and well-defined array of elongated subgrains lying in the form of parallel bands which are inclined at a measured angle of 65° with the horizontal or X axis. Careful measurements showed the average width of these subgrains was ~1.3 μm. Since the single crystal lay initially in a 20° orientation, it follows that the crystal experienced a maximum shearing on entering the ECAP die and, as the crystal moved through the shear zone defined by the arc of curvature at the outer corner of the die, there was a rotation of the crystal to an angle close to ~65° which is consistent with the subgrain structure visible in Fig. 38. Furthermore, careful analysis of the microstructure showed that the longer axes of these subgrains lay parallel to the slip traces of the $(\bar{1}\,\bar{1}\,\bar{1})[\bar{1}\,1\,0]$ slip system so that these elongated subgrains are formed in ECAP with their longer sides aligned parallel to the primary slip plane. Similar results were reported also for crystals initially in the 0° orientation [163].

Investigations performed on copper single crystals subjected to ECAP for one pass showed that macroscopic heterogeneity and the dislocation structures after ECAP depend critically on the initial crystal orientation, with their characteristic features varying from banded structures with a considerable orientation splitting and layered dislocation boundaries to equiaxed cells [166,167].

Thus, by incorporating a very careful analysis of the crystallographic orientations before and after passing through the die, these results demonstrate that the pressing of single crystals through a single pass in ECAP provides a very useful tool for obtaining fundamental information on the nature of the microstructures produced by ECAP processing. Further work is now needed to extend this same approach to higher numbers of passes.

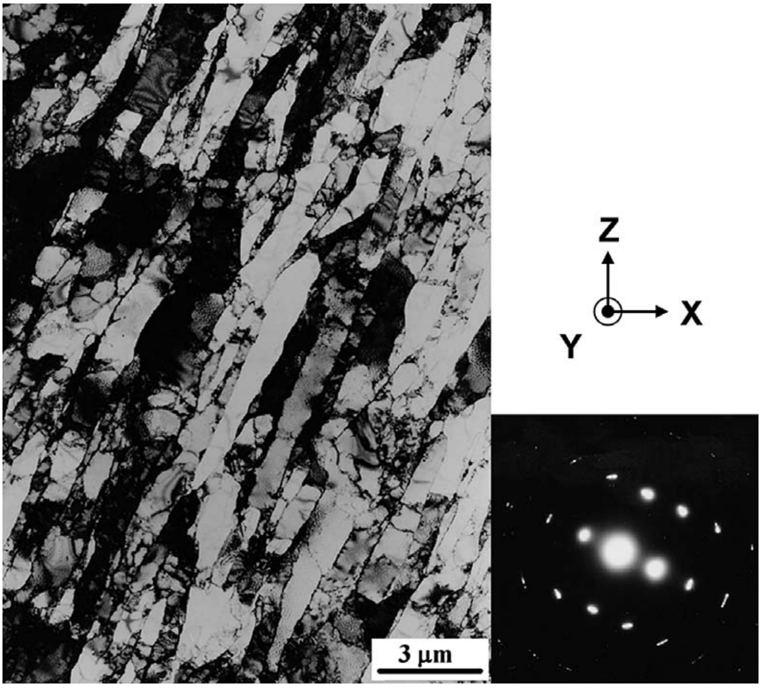

Fig. 38. Microstructure on the Y plane for an aluminum single crystal in the 20° orientation after one pass through an ECAP die with $\Phi = 90°$: the X and Z directions lie parallel to the lower edge and parallel to the side edge of the photomicrograph, respectively [165].

5.2.2. Microstructures in polycrystalline materials

Any critical evaluation of the microstructures developed in ECAP processing requires that separate observations are taken on the X, Y and Z planes as a function of the numbers of passes through the ECAP die and the effect of the processing route. Detailed results of this type are available for pure polycrystalline aluminum having an initial grain size in the unpressed condition of ~1.0 mm [113,170].

The microstructures formed in pure aluminum on the X, Y and Z planes are shown in Fig. 39 after a single pass through a die having $\Phi = 90°$ and $\Psi = 20°$ together with the appropriate SAED patterns taken using a beam diameter of 12.3 μm [170]. Several important trends are visible from careful inspection of Fig. 39. First, the SAED patterns show the boundaries have low angles of misorientation and, as in the single crystal shown in Fig. 38, the microstructures on each plane consist of bands of subgrains with these bands oriented either horizontally and parallel to the Y direction when viewed on the X plane, at approximately 45° to the X direction in a counter-clockwise sense when viewed on the Y plane or perpendicular to the direction of flow and thus to the X direction when viewed on the Z plane. Reference to the theoretical predictions given in the upper row for one pass in Fig. 20 shows that these experimental observations are in excellent agreement with the anticipated behavior after a single pass based solely on a consideration of the shearing patterns in ECAP [119].

Fig. 40 provides similar representations after 2 passes through the die for processing using (a) route A, (b) route B and (c) route C: it is noted again that routes B_A and B_C

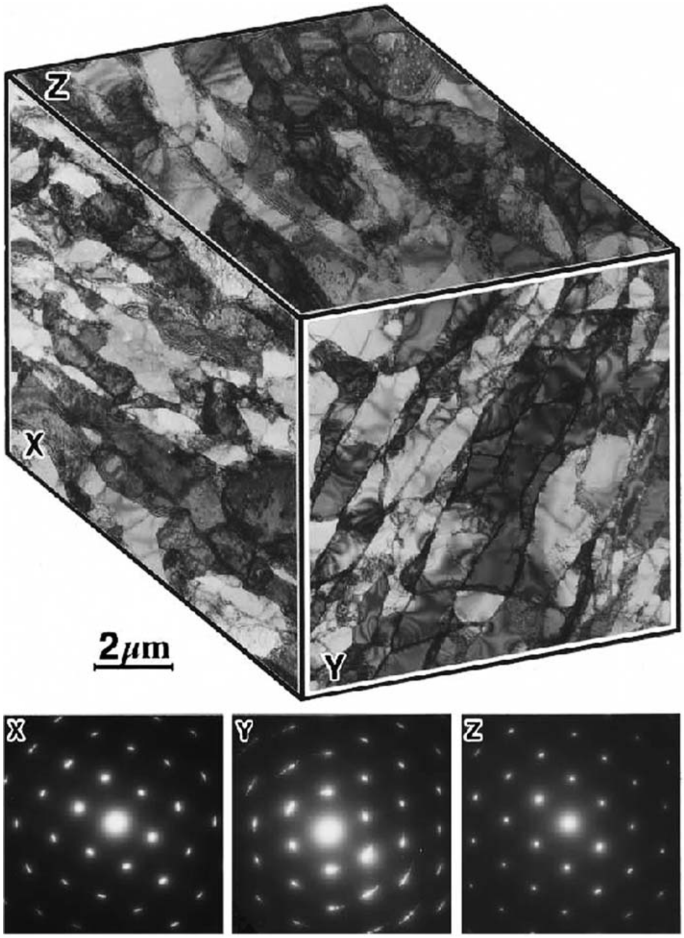

Fig. 39. Microstructures on the X, Y and Z planes for polycrystalline aluminum after ECAP through one pass and the associated SAED patterns [170].

are equivalent after only two passes [170]. For this condition, it is apparent that the experimental observations are again in excellent agreement with the predictions based on the shearing patterns in Fig. 20 and this agreement becomes especially obvious when the shearing is restricted to a set of parallel planes. For example, Fig. 20 shows that for route C the shearing is confined exclusively to the horizontal plane parallel to the Y direction when viewed on the X plane, to the plane at 45° to the horizontal and therefore to the X direction when viewed on the Y plane and perpendicular to the flow direction and therefore to the Y direction when viewed on the Z plane. All of these predicted characteristics are in excellent agreement with the microstructures visible on the various planes for route C in Fig. 40.

When the pressing is continued to a total of four passes, equivalent to an imposed strain of ~4 [105], the visible microstructure becomes less closely aligned with the individual shearing patterns shown in Fig. 20 because many of the sub-grain boundaries evolve into

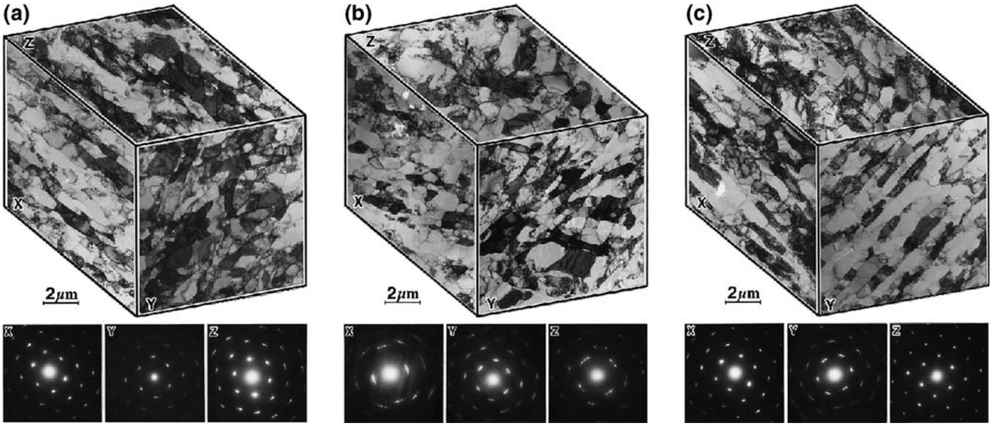

Fig. 40. Microstructures on the X, Y and Z planes for polycrystalline aluminum after ECAP through two passes using (a) route A, (b) route B and (c) route C together with the associated SAED patterns [170].

high-angle boundaries and there is a concomitant evolution of the arrays of well-defined cell or subgrain bands into arrays of reasonably equiaxed ultrafine grains. This evolution is apparent in Fig. 41 which shows the microstructures visible in pure aluminum on the X

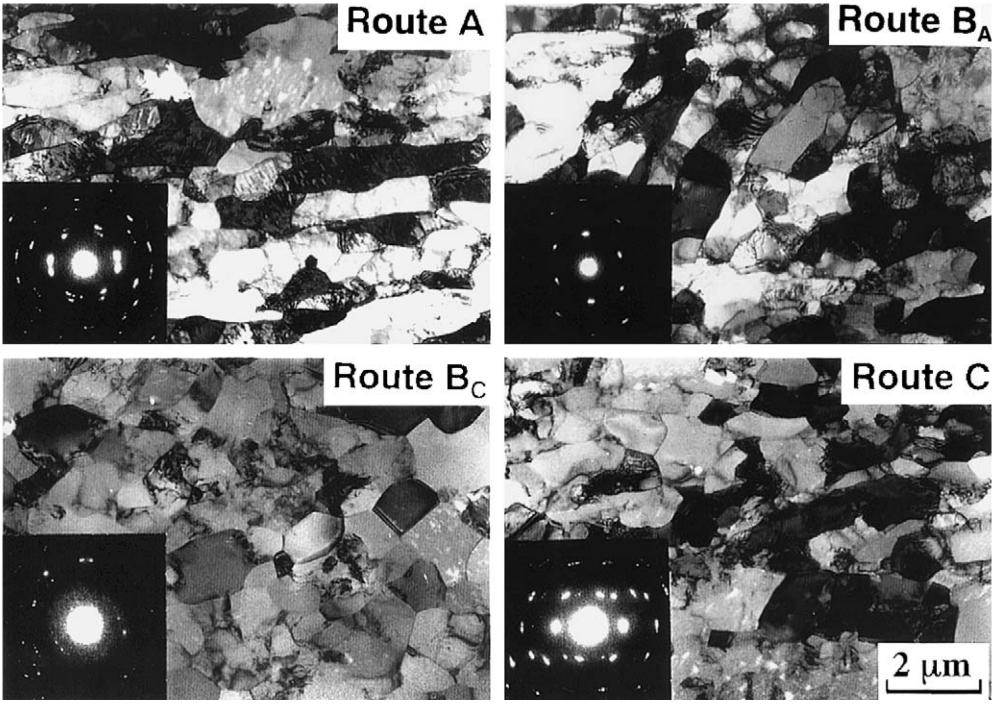

Fig. 41. Appearance of the microstructures on the X plane for polycrystalline aluminum after ECAP through 4 passes using routes A [170], B_A [171], B_C [170] and C [170] together with the associated SAED patterns.

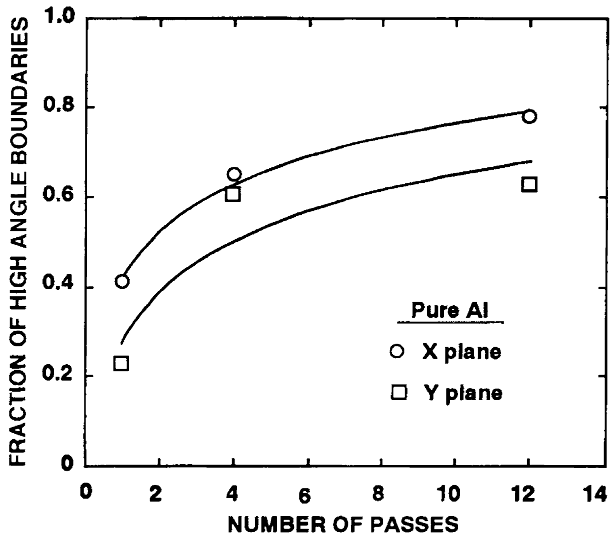

Fig. 42. Variation of the fraction of high-angle boundaries with the number of passes through the die for pure aluminum using route B_C: datum points are shown for the X and Y planes [172].

plane after four passes using (a) route A [170], (b) route B_A [171], (c) route B_C [170] and (d) route C [170]. It is apparent from these photomicrographs that route B_C leads most expeditiously to an array of reasonably equiaxed ultrafine grains [171] whereas elongated grains are visible after four passes when processing through routes A, B_A and C. It is important to note also that, when processing pure aluminum using route B_C, essentially identical equiaxed arrays of ultrafine grains were visible on each of the three orthogonal planes of sectioning [170]. Detailed examinations of this type show that route B_C leads to the most rapid evolution into an array of high-angle grain boundaries [170,171]. This evolution is illustrated in Fig. 42 where the fraction of high-angle boundaries in pure aluminum processed by route B_C is plotted against the number of passes in ECAP for the X and Y planes [172]: following conventional practice, high-angle boundaries are defined as boundaries having misorientation angles >15° [173,174] and the more rapid evolution on the X plane is attributed to the larger angular range of shearing on this plane as shown in Table 1 in Section 3. Thus, it is concluded from these results that route B_C is the optimum ECAP processing route at least for the pressing of pure aluminum.

Similar investigations on Cu and Ti [15], as well as Ni [175], have demonstrated that after one or two passes of ECAP the dislocation structures in various initial grains, having different orientations with respect to the shear stresses, vary essentially from a banded to an equiaxed cellular structure. However, as the number of passes in ECAP is increased, the dislocation structure becomes more homogeneous and there occurs a gradual transition from arrays of predominantly low-angle grain boundaries to a predominantly high-angle configuration.

The results obtained on pure aluminum for the influence of the processing routes are similar to those reported in other materials. Thus, route B_C was identified as the optimum route for producing an ultrafine-grained structure in commercial purity aluminum [176] and titanium [177] with a channel angle of 90° although route A was identified as the optimum procedure in two aluminum alloys when using a die with $\Phi = 120°$ [178]. A possible explanation for this difference has been proposed based upon the dominance of the accumulated strain when using a 90° die and the dominance of the interaction of the shearing plane with the crystal structure and the deformation texture when using a 120° die [179].

5.3. Factors governing the ultrafine grain size in polycrystalline materials

5.3.1. Significance of the grain size in ECAP

It is important to note that the microstructures recorded in Figs. 39–41 were taken near the centers of the as-pressed billets but nevertheless there is good evidence that the microstructure produced in pure aluminum by ECAP becomes essentially homogeneous over the cross-section of the billet after pressing through four passes when using route B_C except only for a very narrow peripheral region, having a width of <0.2 mm, along the edge of the lower surface [180]. The occurrence of a homogeneous microstructure through processing by ECAP has been demonstrated directly in experimental results showing that the tensile properties of an Al–3%Mg–0.2%Sc alloy are essentially identical when miniature specimens are cut from the as-pressed billets with their tensile axes oriented parallel to the three major orthogonal directions, *X*, *Y* and *Z* [181]. It is reasonable to conclude, therefore, that no significant anisotropy is produced in this alloy when processing by ECAP. Further testing of this type is now required to evaluate the degree of any anisotropy that may be introduced in mechanical testing for materials having significant textures in the as-pressed condition.

An important characteristic of the equiaxed microstructure attained in pure aluminum when using route B_C, as shown in Fig. 41, is that the average grain size is measured as ~1.2–1.3 μm and this is identical both to the width of the cell or subgrain bands visible on the *Y* plane in the single crystal after a single pass as shown in Fig. 38 and to other detailed measurements of the equilibrium grain size in polycrystalline pure aluminum after ECAP [172]. Thus, the ultimate equilibrium grain size is determined by the width of the elongated cell or subgrain array which is formed on the first pass through the die [170] and this array develops so that the longer sides of the subgrain bands are oriented parallel to the primary slip plane [165].

In order to obtain a more complete understanding of these results, it is important to examine both the factor determining the size of the ultrafine grains formed in ECAP and any procedures that may be undertaken to produce even smaller grain sizes.

It has been shown that the equiaxed grain size visible in Fig. 41 for route B_C is almost identical to the subgrain sizes reported using conventional cold-working operations such as compression or extrusion [182]. Thus, it was reported that a commercial-purity aluminum was compressed at ambient temperature using high strain rates from 10^{-1} to $2.23 \times 10^{2}\ s^{-1}$ and this produced arrays of subgrains having sizes within the range of ~1.00–1.13 μm [183]. These sizes are very close to the equiaxed grain size of ~1.2–1.3 μm obtained in pure aluminum processed by ECAP at room temperature under a strain rate within the ECAP die which may be estimated as ~3.8 s^{-1} [182]. The similarity suggests that the deformation occurring in ECAP is analogous to, and is a natural extension to even higher strains, the deformation occurring in more conventional metal-working processes. The significant feature of ECAP is that, because the billet retains the same cross-sectional area so that repetitive pressings are feasible, materials processed by ECAP may be deformed to very high strains wherein the subgrain boundaries evolve into high-angle boundaries through the absorption of dislocations, thereby producing arrays of ultrafine grains separated by high-angle grain boundaries. By contrast, this evolution cannot be achieved in more conventional metal-working processes because of the natural limit imposed on the total strain introduced during deformation.

The equilibrium grain size achieved in the pure aluminum sample shown in Fig. 41 is ~1.2–1.3 μm which is large by comparison with most materials processed by ECAP. It is possible to attain much smaller grain sizes by alloying but the production of an array of equiaxed grains may then require continuing the pressing to a larger number of passes. For example, experiments on Al–Mg solid-solution alloys show that the equilibrium grain size is reduced to ~0.45 μm after 6 passes in an Al–1%Mg alloy and to ~0.27 μm after 8 passes in an Al–3%Mg alloy: these two microstructures are shown in Fig. 43 together with the relevant SAED patterns which confirm the presence of high-angle boundaries [184]. The occurrence of smaller grain sizes on alloying with magnesium is attributed to the decreasing rates of recovery in these solid solution alloys [184]. Similarly, a grain size of ~0.70 μm was achieved in an Al–0.2%Sc alloy by pressing at room temperature and this was reduced even further to ~0.20 μm through the addition of 3% Mg [185]. However, a slightly larger grain size of ~0.30 μm was achieved in an Al–5%Mg–0.2%Sc alloy because additional intermediate anneals were then required to prevent cracking during the pressing operation [185].

An alternative procedure for decreasing the grain size is to combine processing by ECAP with some other post-ECAP procedure. For example, experiments on pure Ti showed a potential for achieving additional grain refinement by combining ECAP at 723 K with either cold extrusion [186] or cold-rolling [187]. An alternative possibility is to cut small disks from the as-pressed billets for processing by high-pressure torsion (HPT). This combination of ECAP and HPT was successfully used both with pure Ti where the grain size was reduced from ~300 nm after ECAP to ~200 nm after ECAP + HPT [188] and high-purity nickel where the grain size was reduced from ~350 nm to ~140 nm using these two processes, respectively [189]. Fig. 44 shows the distributions of grain boundary misorientations for these two processing routes [189] and it is apparent that the combination of ECAP + HPT both decreases the fraction of low-angle boundaries and leads to a distribution which is closer to the solid line representing the theoretical curve predicted for a random distribution of misorientation angles [190].

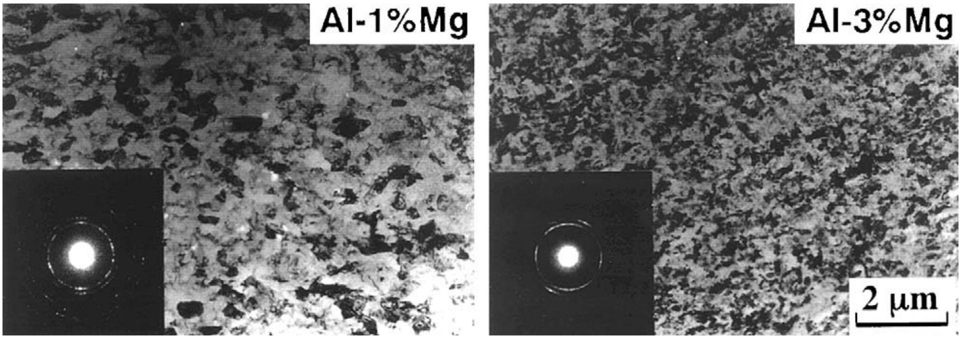

Fig. 43. Microstructures in Al–1%Mg after ECAP through 6 passes and Al–3%Mg after ECAP through 8 passes together with the associated SAED patterns [184].

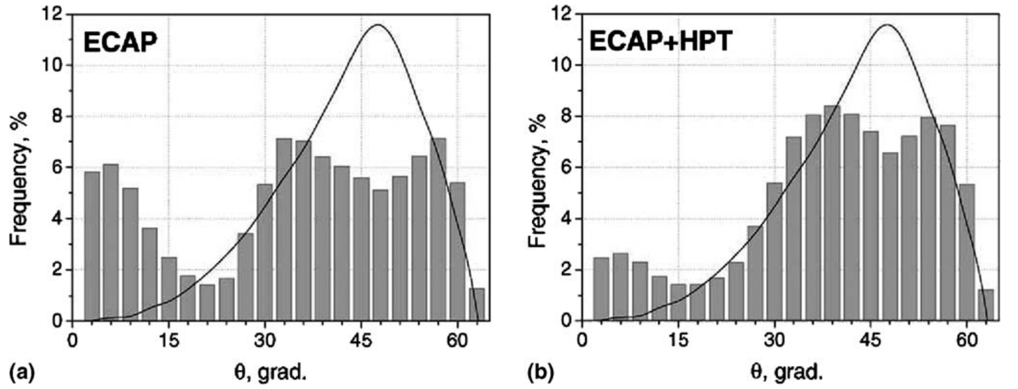

Fig. 44. The grain boundary misorientation distributions in pure Ni after processing by (a) ECAP and (b) ECAP + HPT: the solid lines show the predicted relationship for a random distribution of misorientation angles [189].

A recent analysis considered the problem of the ultimate grain refinement that may be produced by ECAP [191]. On the basis of the fragmentation theory [192], which states that the structure of a severely-strained metal represents a system of junction disclinations [193], it was demonstrated that the ultimate grain refinement should depend both on the nature of the metal and on the straining regimes including the temperature, the rate of pressing and the applied pressure [191]. This conclusion is in general agreement with a number of sets of experimental data, as discussed in Section 4, but the analytical treatment now requires confirmation through the use of more systematic experimental investigations.

5.3.2. Using ECAP in grain boundary engineering

It is apparent from Fig. 44(a) that the distribution of grain boundary misorientations after ECAP reveals a reasonable fraction of high-angle boundaries but also an excess of low-angle boundaries. Similar trends have been reported following ECAP processing for many other materials [145,162,172,178,194–204]. It is reasonable to anticipate that the presence of a high fraction of low-angle boundaries, which is a recurrent feature of the misorientation distributions after ECAP, is a natural consequence of the large numbers of excess dislocations which are introduced into the billet on each separate passage through the ECAP die. Nevertheless, the tendency for the average boundary misorientation to increase with increasing numbers of passes, as shown in Fig. 42, provides a unique opportunity to make use of ECAP processing for the production of materials having different, but controlled, boundary misorientation distributions.

This approach is important in the concept of grain boundary engineering or grain boundary design [205] where it has been proposed that the properties of materials may be effectively changed by deliberate and careful tailoring of the distributions of boundary angles. This approach has been used successfully for several studies including, for example, improving the susceptibility to intergranular stress corrosion cracking [206]. However, there are generally difficulties in achieving different boundary distributions and the optimum current procedure appears to be through the use of magnetic annealing [207]. The evidence available to date shows that ECAP processing provides an alternative procedure for achieving different misorientation distributions because there is a high fraction of low-angle boundaries after a small number of passes but a lower fraction of low-angle boundaries when the number of passes is increased [208]. This approach was used successfully with an Al–3%Mg–0.2%Sc alloy by processing samples through either 2 passes using route C or 8 passes using route B_C, measuring the misorientation distributions, and then using these samples to measure the interdiffusion characteristics and especially the role of any enhanced grain boundary diffusion [209].

5.4. Microstructural features after ECAP

The principles of ECAP are now understood reasonably well and the processing procedure has been applied to a very wide range of metals and metallic alloys. Examples of these materials are fcc metals such as Al [113,170,180,210–215], Cu [210,216–221], Ni [175,189,222] and Au [223], hcp metals such as Mg [224–226], Ti [102,177,227,228] and Zr [199], iron [229,230] and steel [231–238], hard-to-deform materials such as tungsten [122], eutectic [239,240] and eutectoid [241,242] alloys, metal–matrix composites [243–246] and others, where the cited references provide representative reports for these various materials. Although there are some common trends among these metals, there are also some significant microstructural differences. These variations are therefore considered in this section with reference to single-phase materials. The more complex processing of precipitation-hardened alloys, multi-phase alloys and composites is considered in Section 6.

It is important to note that the selection of the testing material influences both the equilibrium grain size attained after ECAP and the homogeneity of the microstructure. For example, it was noted in Section 5.3 that the equilibrium grain size in pure Al is ~1.2–1.3 μm and the microstructure is extremely homogeneous after pressing at room temperature. By contrast, when pure Cu is pressed at room temperature the equilibrium grain size is much smaller (typically ~ 0.27 μm) and the microstructure is not fully homogeneous [216]. This difference arises because of the low stacking-fault energy and the associated low rate of recovery in Cu. In this respect, pure Ni appears to represent an ideal material for ECAP because, with a stacking-fault energy which is intermediate between pure Al and pure Cu, the equilibrium grain size is very small after pressing at room temperature (~0.30 μm) and the microstructure is essentially homogeneous [222]. Furthermore, additional considerations may be needed for more complex materials. For example, the application of ECAP processing to a metal–matrix composite may lead to the breaking of the reinforcement due to the high applied pressures. An example of this effect is the development of some limited cracking of the large alumina particulates during pressing of an Al-6061 alloy reinforced with 10 vol% of Al_2O_3 particulates [244]. These problems are considered in more detail in Section 6.

Processing by ECAP involves the imposition of a very high strain in each passage through the die so that very large numbers of dislocations are introduced into the material. It was recognized in very early investigations that the microstructures produced by ECAP are often highly heterogeneous with poorly-delineated transition zones between the individual grains and irregular extinction contours along the grain boundaries [13,47,247]. These observations show that the boundaries introduced by ECAP are in a high-energy non-equilibrium configuration. Fig. 45 shows examples of the microstructures in an Al–3%Mg solid-solution alloy after pressing at room temperature and annealing for 1 h at 423 K [248]. In Fig. 45(a) at the lower magnification, the grain size is ~0.3 μm, which is

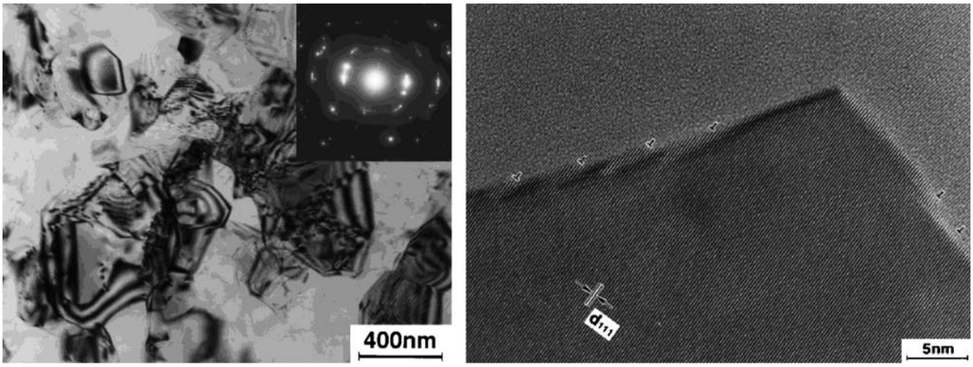

Fig. 45. (a) Typical microstructure for Al–3%Mg after ECAP at room temperature and annealing for 1 h at 423 K together with an SAED pattern; (b) image for the Al–3%Mg alloy shown in (a) using high-resolution electron microscopy with the locations of dislocations along the grain boundary marked by "T" [248].

similar to the grain size immediately after ECAP, and the grain boundaries contain bright and dark irregular fringes denoting the varying inclinations of the boundaries to the foil surface. These irregularities confirm that, even after annealing for 1 h at 423 K, the boundaries are irregular and in high-energy configurations. The SAED pattern in Fig. 45(a) was taken with a beam diameter of 1.3 μm and it shows the grains are oriented preferentially in $\langle 110 \rangle$ directions but the boundaries have high angles of misorientation. The image in Fig. 45(b) was taken from the same sample using high-resolution electron microscopy and it shows the presence of moire fringes at the two lower boundaries and the presence of dislocations, marked with the designation "T", at the points where the extra atomic planes terminate within the lattice on one side of the boundary. The presence of an excess of dislocations in a zone adjacent to the boundary is similar to observations reported on samples produced using high-pressure torsion [249,250] and it confirms again the presence of non-equilibrium grain boundaries.

The sample shown in Fig. 45 was annealed at the relatively low temperature of 423 K but it is important to evaluate the thermal stability of these ultrafine grains over a wide range of temperatures. There are several reports describing the thermal stability of the ultrafine grains produced by ECAP [251–258]. In general terms, the grains grow when heated but the extent of grain growth depends upon the nature of the microstructure. In pure metals and solid-solution alloys, the grains grow rapidly at elevated temperatures because there are no precipitates within the crystalline lattice to restrict the movement of the grain boundaries. By contrast, submicrometer grains may be retained to relatively high temperatures in materials containing a distribution of fine precipitates: examples include an Al–3%Mg–0.2%Sc alloy containing Al_3Sc precipitates [259] and an Al-7034 Al–Zn–Mg alloy containing $MgZn_2$ and Al_3Zr precipitates [260].

Figs. 46 and 47 show the effect of annealing for 1 h on pure Al and an Al–1%Mg alloy, respectively, using annealing temperatures from 423 to 573 K [255]. These materials were processed by ECAP at room temperature for totals of 4 and 6 passes using route B_C to give as-pressed grain sizes of ~1.3 μm in aluminum and ~0.45 μm in the Al–1%Mg alloy, and they were then cut into small pieces and annealed for 1 h at the temperatures shown in Figs. 46 and 47 up to a maximum of 573 K. It is apparent that both of these materials

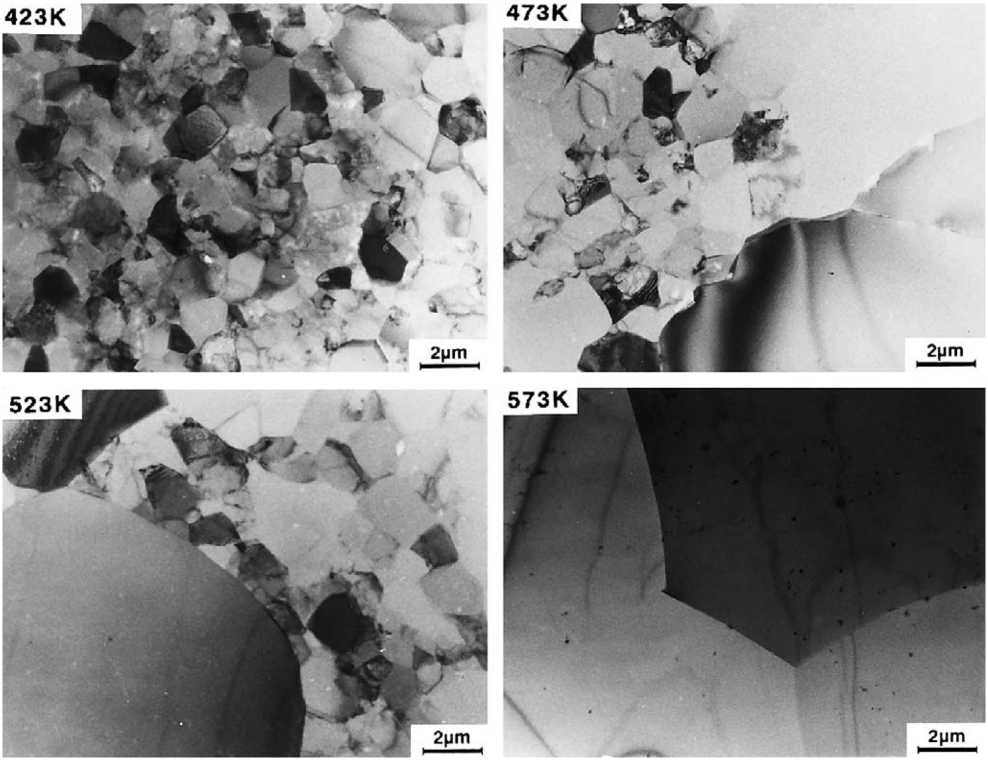

Fig. 46. Microstructures of pure Al after ECAP and annealing for 1 h at 423, 473, 523 and 573 K [255].

exhibit good thermal stability at temperatures up to 423 K but a duplex microstructure of small and large grains is visible in both materials at 473 K. This duplex structure persists at 523 K but with an increase in the fraction of the larger grains. Finally, the duplex structure is no longer present at 573 K and the microstructure consists of large grains with no evidence for the original small grains. It is also apparent that both materials behave in a qualitatively similar manner except only that the grain sizes are smaller in the solid-solution alloy shown in Fig. 47. Similar results were obtained also for an Al–3%Mg alloy where the as-pressed grain size was ∼0.3 μm after 8 passes [255].

5.5. Textures produced by ECAP

A study of the nature of the evolution of the predominant crystallographic orientations resulting from SPD is of primary importance in ECAP processing, especially since the crystallographic texture has a significant effect on many structure-sensitive properties so that a careful texture analysis makes it possible to estimate the mechanisms responsible for the progress of plastic straining and phase transformations. It is well known that the principle of plastic straining, which is a direct consequence of simple shear, is the basic process underlying the ECAP processing technique.

In this connection, a comparison was made between the textures developed during the ECAP processing of copper using route A and the established textures resulting from large

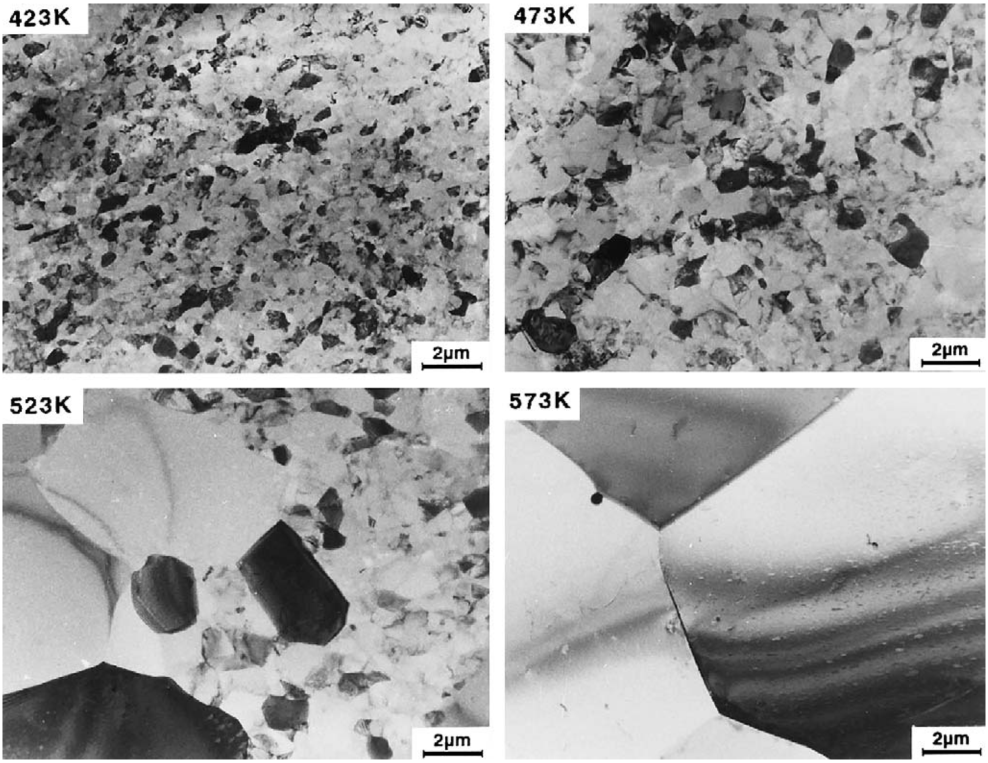

Fig. 47. Microstructures of Al–1%Mg after ECAP and annealing for 1 h at 423, 473, 523 and 573 K [255].

strain simple shear [261]. It was demonstrated that there is a good similarity between these two cases both in terms of the main ideal components and their intensity variations. A peculiarity of the ECAP textures was also noted: the ideal orientations appear in significantly rotated positions, where these rotations are 10° after the first pass but decrease to 5° in the subsequent passes. An important difference between simple shear and ECAP textures is that the tilts of the components are in the opposite sense.

Fig. 48 shows experimental pole figures for UFG (a) Cu, (b) W and (c) Ti processed by ECAP using route B_C [262]. An analysis of the experimental data showed that the basic texture peaks for Cu subjected to SPD, shown in Fig. 48(a), belong to the ideal orientations $\{111\}\langle 110\rangle$ and $\{111\}\langle 112\rangle$ that are either close to each other or coinciding and also to $\{112\}\langle 110\rangle$ and $\{100\}\langle 110\rangle$. These orientations were described as ideal orientations of torsion or shear with two texture components, $\{111\}\langle uvw\rangle$ and $\{hkl\}\langle 110\rangle$, that also coincided with the results from modeling of torsional shear textures [263]. The texture in W after ECAP, shown in Fig. 48(b), is characterized by the ideal orientations $\{001\}\langle 110\rangle$ and $\{111\}\langle 211\rangle$ which are also typical of the shear textures [263]. Hence, it can be asserted that the process of ECAP in both cases, for an fcc lattice and a bcc lattice, proceeds by pure shear. Studies of the crystallographic texture of CP Ti show that ECAP leads to a domination of the basal ideal orientations of the type $\{0001\}\langle 11\bar{2}0\rangle$ and $\{0001\}\langle 10\bar{1}0\rangle$, as shown in Fig. 48(c). The selection of different ECAP pressing routes predetermines the prevailing slip direction as $\langle 11\bar{2}0\rangle$ or $\langle 10\bar{1}0\rangle$ in the basal plane

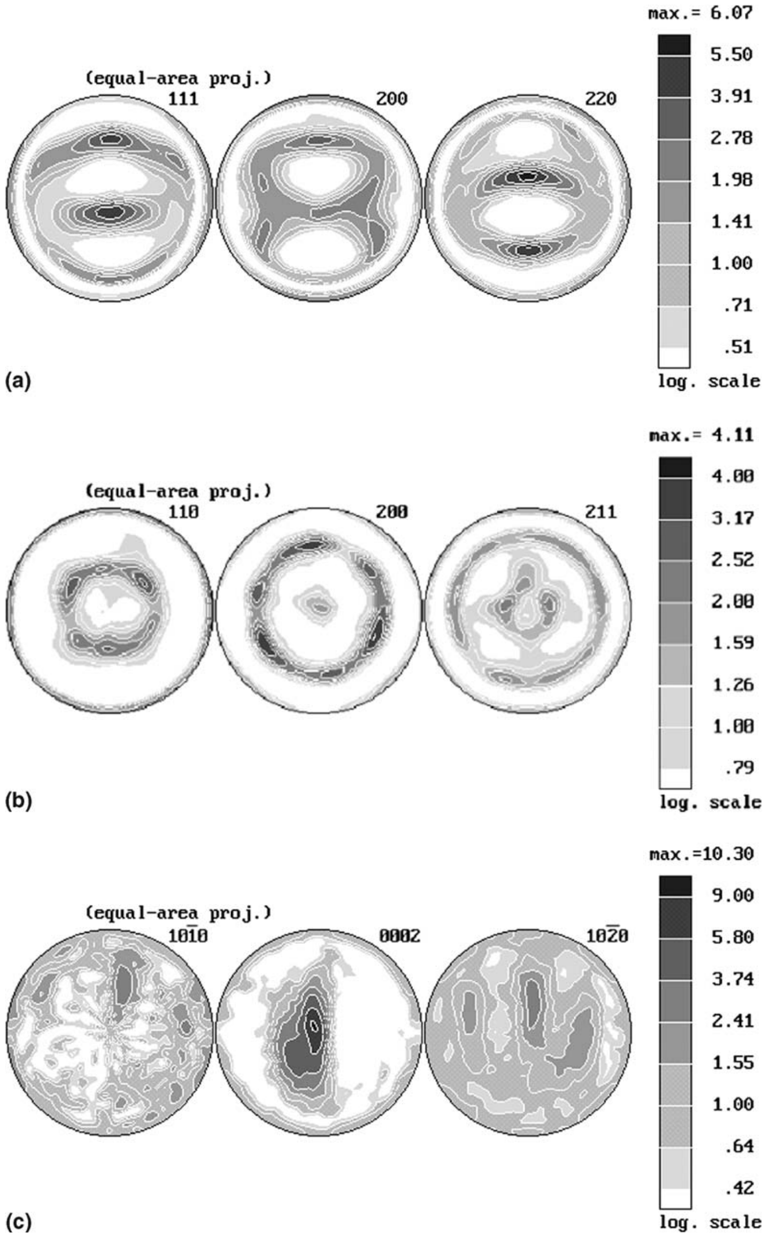

Fig. 48. Experimental pole figures from the cross-sections of samples of (a) Cu, (b) W and (c) Ti after ECAP through 8 passes using route B_C [262].

placed at an angle of 45° with respect to the plane of intersection of the angles of pressing. It was found that, for all of the investigated states of α-titanium processed by ECAP, the most sharp crystallographic texture was produced by ECAP using route B_C. In spite of some scattering of the main texture peaks along the direction of pressing, the basal planes

{0001} were positioned parallel to the longitudinal section of the billets. This leads, therefore, to the emergence of an anisotropy in the physical and mechanical properties in UFG Ti.

The data presented in Fig. 48 were obtained from the central parts of the billets after ECAP. However, investigations of the texture at several locations across the billet in Cu after the first ECAP pass [264] revealed significant spatial variations in texture, in good agreement with the results from OIM observations. The experimental study was extended for routes A and C up to a total of 16 passes. For route A, the textures in the upper and middle regions of the billet were similar, they remained much stronger than in the lower region and they strengthened with the number of passes. In route C, the textures in the upper and lower positions became similar after the second pass but they were quite different from the textures in the center of the billet. Furthermore, the heterogeneity in the texture was smaller for odd-numbered passes than for even-numbered passes.

In recent years, within the framework of modeling of the ECAP deformation, active work has been initiated on the simulation of texture evolution during processing [264,265]. These simulations lead to the conclusion that the use of a combined finite element–polycrystalline modeling approach is most effective in the prediction of texture, and this is true not only for the first pass in ECAP but also for multi-pass deformation [265].

6. Pressing of more complex alloys and metal–matrix composites

Since ECAP processing involves the rapid imposition of an exceptionally high strain, the primary microstructural change associated with ECAP is the introduction of a very high density of dislocations into the crystalline lattice. However, it is important to recognize that ECAP may also influence the microstructure in other significant ways. For example, the high pressure involved in the pressing operation may lead to the breaking and fragmentation of internal precipitates. Furthermore, depending upon the processing regimes, ECAP may lead also to precipitate dissolution and/or precipitate formation and coarsening. The interactions between these various processes will depend in practice upon both the composition of the alloy and the pressures and temperatures used in the pressing operation. As in processing by high-pressure torsion, where nevertheless the strain intensity is much higher, it is reasonable to expect evidence for the formation of metastable states during ECAP associated with the generation of supersaturated solid solutions, disordering or even amorphization [15].

6.1. Influence of ECAP on precipitation

The potential for precipitate fragmentation during ECAP was first recognized for θ'-precipitates in an Al–Cu alloy [266] and subsequently there were similar reports of the fragmentation of β'-precipitates [267] and metastable β''-precipitates [268] in Al–Mg–Si alloys and η-phase $MgZn_2$ precipitates in Al-7050 [81] and Al-7034 alloys [214,260].

For the Al-7034 alloy, the material was received in a spray-cast condition with reasonably equiaxed grains and an initial grain size of ~2.1 μm: the chemical composition (in wt%) was Al–11.5% Zn, 2.5% Mg, 0.9% Cu and 0.2% Zr. Fig. 49 shows the microstructure of this alloy in the as-received condition and close inspection revealed the presence of three different types of precipitates [214]. There are large rod-shaped precipitates in Fig. 49 which were identified as the η-phase ($MgZn_2$), with two examples marked by arrows,

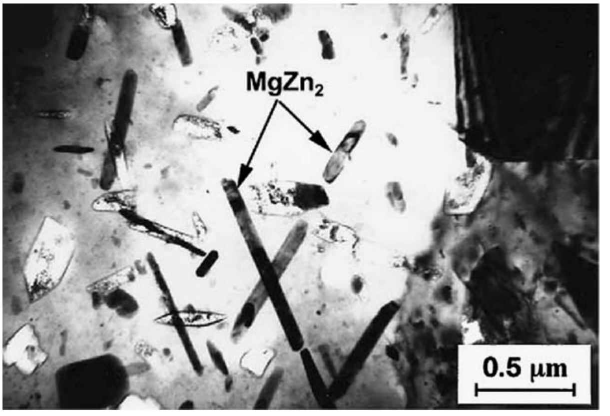

Fig. 49. Microstructure in the as-received unpressed Al-7034 alloy showing the presence of rod-shaped $MgZn_2$ precipitates [214].

and there is also an array of very fine particles which was identified as primarily representing the metastable hardening η′-phase but with additional Al_3Zr particles that were identified through the presence of Ll_2 superlattice reflection spots in the SAED patterns. For the as-received condition, measurements showed that the large rod-shaped $MgZn_2$ precipitates had lengths and widths of ~0.48 and ~0.07 μm, respectively, but the very fine particles had dimensions of the order of ~10 nm. All of these results are typical of the microstructures that are generally present in 7xxx-series aluminum alloys containing additions of Zn, Mg and Zr [269–272].

The effect of ECAP is documented in Fig. 50(a) and (b) which show the microstructures after one and two passes, respectively [214]. The η-phase $MgZn_2$ was again identified after ECAP and examples are marked by arrows in Fig. 50. It is clear from these photomicrographs that the large rod-shaped precipitates have become fragmented by the high pressure imposed in ECAP. By contrast, inspection showed the very fine spherical particles of Al_3Zr appeared to be unaffected by the ECAP processing but there were also arrays of fine and reasonably spherical precipitates having sizes in the range of ~30–100 nm. These spherical precipitates were also identified as the η-phase and it was concluded that, although many of the more irregular particles were formed by fragmentation of the larger precipitates, it was reasonable nevertheless to anticipate that many of the smaller $MgZn_2$ precipitates formed through a direct transformation of the η′-phase into the η-phase with subsequent coarsening. Thus, it is anticipated that this transformation occurs easily at the ECAP temperature of 423 K.

To check this possibility, Fig. 51 shows thermograms obtained by differential scanning calorimetry (DSC) where the material was subjected to a heating rate of 10 K min^{-1} in the as-received condition and after 1, 4 and 8 passes in ECAP; Fig. 51(a) shows the heat flow over the entire range of temperature but Fig. 51(b) places emphasis on temperatures above 640 K [273,274]. These curves are also similar to those anticipated for 7xxx-series aluminum alloys in peak-aged and over-aged tempers [275,276] but they reveal some additional trends associated specifically with the ECAP processing. For simplicity in interpretation of these data, the separate regions identified in the DSC curves are labeled from I to VI in Fig. 51 where I corresponds to the dissolution of the Guinier–Preston (GP) zones and/or

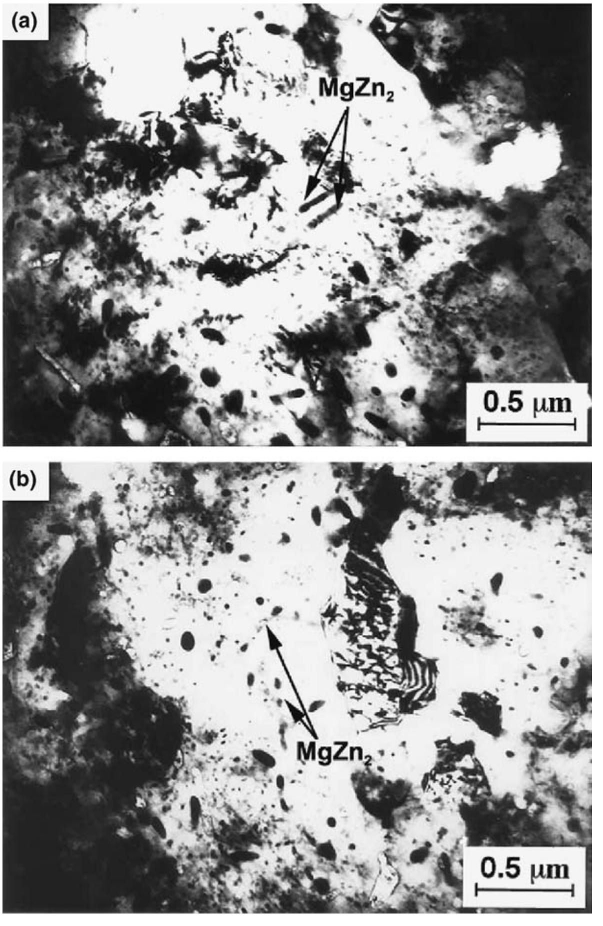

Fig. 50. Microstructures in the Al-7034 alloy after ECAP at 473 K through (a) 1 pass and (b) 2 passes showing the fragmentation of the $MgZn_2$ precipitates [214].

the η′-phase, II corresponds to the formation of the η-phase, III corresponds to the coarsening of the rounded disks of η-phase precipitates, IV corresponds to dissolution of the η-phase, V corresponds to incipient melting of the T-phase which represents a quarternary phase based on $Mg_3Zn_3Al_2$ and finally VI is the onset of full melting of the Al-7034 alloy.

Inspection of the curves in Fig. 51 reveals several significant trends. First, there is a dissolution of the GP zones and/or the η′-phase in the as-received alloy on heating to the ECAP temperature of 473 K but precipitation of the η-phase commences as the alloy approaches the pressing temperature. It is reasonable to assume this reaction continues both during the period of temperature equilibration prior to pressing and during the pressing operation. As a result, it is apparent in Fig. 51(a) that regions I and II are no longer present for the alloy pressed through a single pass or for the alloys pressed through 4 and 8 passes. Furthermore, coarsening of the η-phase will occur on subsequent passes and in this respect it is anticipated that the very high density of dislocations introduced by ECAP will provide many potential nucleation sites for the precipitation event [277].

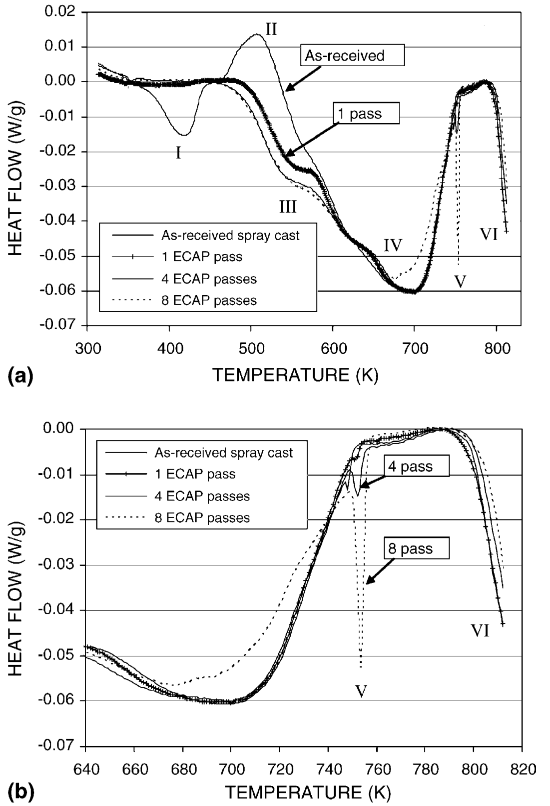

Fig. 51. The DSC thermograms for the Al-7034 alloy in the as-received condition and after ECAP through 1, 4 and 8 passes: (a) over the entire range of temperature and (b) for temperatures above 640 K [274].

Additional information is available in Fig. 51(b) where it is apparent that the trough in the curve associated with a dissolution of the η-phase generally occurs at a temperature in the vicinity of ~700 K for the as-received condition and after 1 and 4 passes whereas it is displaced to a lower temperature of ~670 K after a total of 8 passes of ECAP. Thus, dissolution is more favored and occurs at a lower temperature after 8 passes because the η-phase particles are now fully fragmented so that they dissolve more readily. Fig. 51(b) reveals also the presence of a clearly-defined melting of the T-phase after 8 passes and to a minor extent after 4 passes. Thus, the presence of melting after larger numbers of passes in ECAP processing at 473 K confirms the occurrence of T-phase precipitation at the pressing temperature, with more precipitation occurring after larger numbers of passes because the billets are then held at temperature for longer periods of time. The occurrence of this precipitation is consistent with data reported for similar alloys at this temperature [278].

6.2. The pressing of multi-phase alloys and composites

Several recent investigations have addressed the application of ECAP to multi-phase alloys and metal–matrix composites. In contrast to the pressing of pure metals and simple metallic alloys, the ECAP processing of multi-phase alloys and composite materials is a significantly more complex procedure since these materials are normally less ductile and harder to deform. In addition, the various strain capacities of the different phases within multi-phase alloys often lead to precipitous cracking which may occur even during the initial passes of ECAP.

6.2.1. Multi-phase alloys

A good example of the successful multipass pressing of a multi-phase alloy with low workability is the recent processing of a two-phase Ti–6Al–4V alloy [279]. An enhancement of the alloy deformability during ECAP was achieved using an initial globular structure of the alloy and optimizing the pressing temperature and geometry of the die-set. In this way it was possible to produce an ultrafine-grained structure in the alloy using ECAP.

After thermal treatment, the microstructure of the initial Ti–6Al–4V alloy was in the form of a globular ($\alpha + \beta$) type with equiaxed grains of α-phase, ~3–5 μm in size, and with a small amount of intercrystalline β-phase. Special ECAP die-sets were fabricated in order to process the alloy with enlarged channel angles, Φ, of 135° and 120° and the pressing operation was conducted using route B_C and a temperature of ~700 °C. This combination of a large channel angle and a high pressing temperature was successful in permitting the multi-pass pressing of the alloy. For example, with $\Phi = 135°$ at 700 °C the billets were pressed for 12 passes without any cracking and using the die-set with $\Phi = 120°$ the pressing was successfully completed to a total of 8 passes. For both of these situations, the total accumulated true strain was of the order of ~6.

Optical metallography was conducted on billets of the alloy subjected to ECAP using either the die-set with $\Phi = 135°$ after 12 passes or the die-set with $\Phi = 120°$ after 8 passes. These results are shown in Fig. 52(a) and (b) and they reveal a significant refinement of the grain structure of the α-phase in both the longitudinal direction and in the cross-section [279]. Furthermore, the initial boundaries of the α-phase are no longer visible and uniform etching of the section area demonstrates the homogeneous nature of the processed structure. At the same time, Fig. 52(a) shows that elongated grains are visible in the longitudinal section of billets processed at an angle of $\Phi = 135°$ whereas most grains are equiaxed in

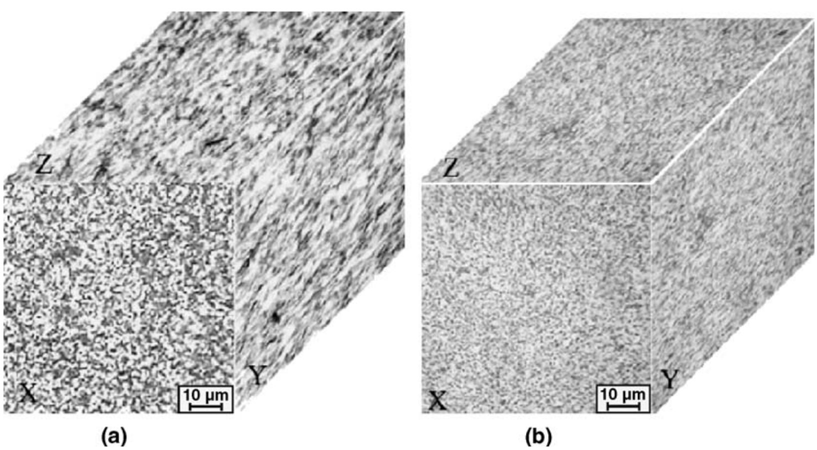

Fig. 52. Optical micrographs showing the structure of the Ti–6%Al–4%V alloy after ECAP using route B_C at ~700 °C (a) with $\Phi = 135°$ for 12 passes and (b) with $\Phi = 120°$ for 8 passes [279].

the cross-section. Processing by ECAP through 8 passes in a die-set with a channel angle of 120° led to the formation of a more equiaxed structure both in the longitudinal direction and in the cross-section, as shown in Fig. 52(b).

Fig. 53(a) and (b) present typical TEM images of the microstructures produced by ECAP on the die-sets with $\Phi = 120°$ and 135°, respectively [279]. It is apparent that a considerable structural refinement has taken place in both situations but the types of structure formation are different. After ECAP with $\Phi = 135°$ in Fig. 53(a), there is both grain refinement and the formation of thin twins with a thickness of ~50 nm inside many grains having sizes of ~400–600 nm. The SAED pattern in Fig. 53(a) shows highly blurred spots indicative of the presence of high internal stresses in the structure. By contrast, Fig. 53(b) shows that no twins are observed in the UFG microstructure after ECAP with $\Phi = 120°$ and the SAED pattern suggests instead the presence of many boundaries having low angles of misorientation so that the processed microstructure consists of an array of grains and subgrains. The SAED pattern in Fig. 53(b) shows more equiaxed spots which are indicative of a decrease in the internal stresses. Close inspection showed that twins were present in only about 10–15% of the grains in this condition and X-ray analysis suggested that ECAP led to a slight decrease in the amount of β-phase by up to ~8%.

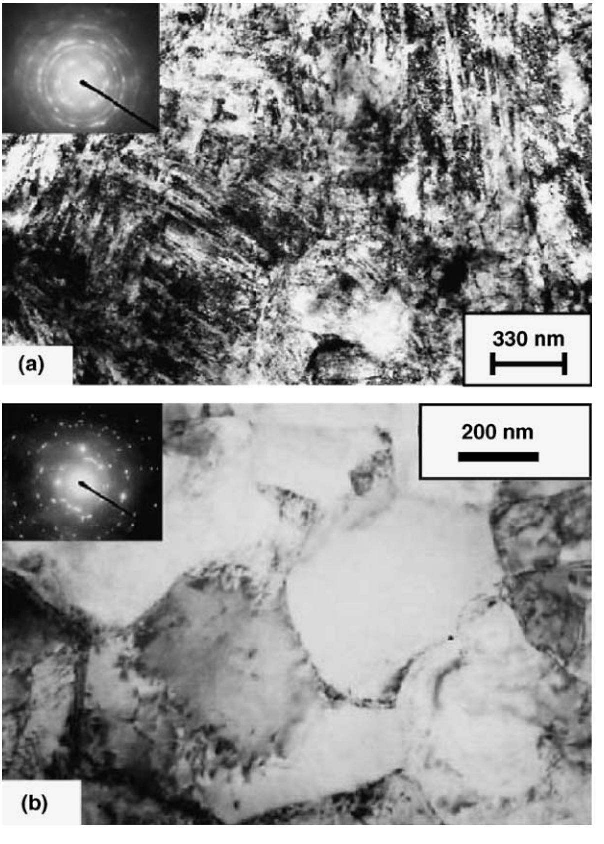

Fig. 53. The structure by TEM in the cross-section of the Ti–6%Al–4%V alloy after ECAP using route B_C at ~700 °C (a) with $\Phi = 135°$ for 12 passes and (b) with $\Phi = 120°$ for 8 passes [279].

Tensile tests were conducted on this material at room temperature and they revealed significant strengthening of the alloy after ECAP. Thus, ECAP gave a 20% increase in the alloy strength at room temperature by comparison with the initial state. A combined treatment by ECAP and subsequent extrusion led to an additional enhancement in strength with a final value for the ultimate tensile strength of ~1510 MPa and sufficient ductility of $\delta \approx 7\%$.

The overall conclusion from work of this type is that UFG structures can be produced by ECAP even in low ductility and hard-to-deform alloys such as the Ti–6%Al–4%V alloy. It is important also to recognize that, in order to increase the deformability of alloys of this type, it is necessary to consider not only increasing the ECAP processing temperature and changing the tool geometry but also examining the different possible initial microstructures. Thus, the Ti–6Al–4V alloy was pressed successfully by initially forming a globular structure. In this connection it is important to note that ECAP processing is more difficult when using initial lamellar structures [280]. Furthermore, the size of the structural elements and the alloy properties depend upon the geometry of the die-set and especially the value of the channel angle, Φ. For the Ti–6Al–4V alloy, the processed UFG structure is more homogeneous when the alloy is pressed using a die-set with an internal angle of $\Phi = 120°$ rather than 135° despite the fact that the strain accumulation is essentially the same for both angles. Thus, the structures processed at 135° have many thin twins and increased levels of elastic strains.

A recent report described the first studies of ECAP using the multi-phase Pr_{20}-$Fe_{73.5}B_5Cu_{1.5}$ alloy which is known to be a hard magnetic material [281]. An homogenized cast alloy produced by crystallization in a metal crucible (Cu mould) was subjected to ECAP for one pass. The diameter of the ingot was 13 mm and the length was 110 mm. The ingot was enclosed within a metal shell during ECAP to prevent oxidation and cracking during the deformation. A die-set with a channel diameter of 20 mm and a channel angle of $\Phi = 110°$, together with a hydraulic press with 160 ton-force, was used for ECAP at 750 °C.

The microstructure of the cast alloy in the homogenized state was coarse-grained with an average grain size of about 20 μm. However, processing by ECAP even for a single pass produced considerable grain refinement. Fig. 54 shows an optical micrograph of the $Pr_{20}Fe_{73.5}B_5Cu_{1.5}$ alloy after ECAP for a single pass. The microstructure shows the presence of small grains of ~1–3 μm in diameter together with comparatively coarse grains having a size up to ~10 μm. It was noted in the processed samples that the grain shape became more rounded and the Pr-rich phase was distributed more uniformly along the grain boundaries of the matrix phase. Magnetic measurements demonstrated also a considerable enhancement of the magnetic properties in terms of the coercivity and the specific magnetization of the alloy after ECAP. For example, the value for the coercivity increased by almost four times by comparison with the unpressed cast alloy.

Finally, it should be noted that the pressures exerted in ECAP are not necessarily sufficiently high in order to achieve a good mixing of the two separate phases when pressing two-phase alloys. For example, experiments on the Zn–22%Al eutectoid alloy showed that processing by ECAP produced a submicrometer grain size but with separate agglomerates of ultrafine Al-rich and Zn-rich phases whereas some mixing of the two phases was more easily achieved after processing by high-pressure torsion [241]. In addition, the pressing of steels through multiple passes requires the use of a back-pressure in the ECAP facility or alternatively the use of an elevated temperature for the pressing operation [282].

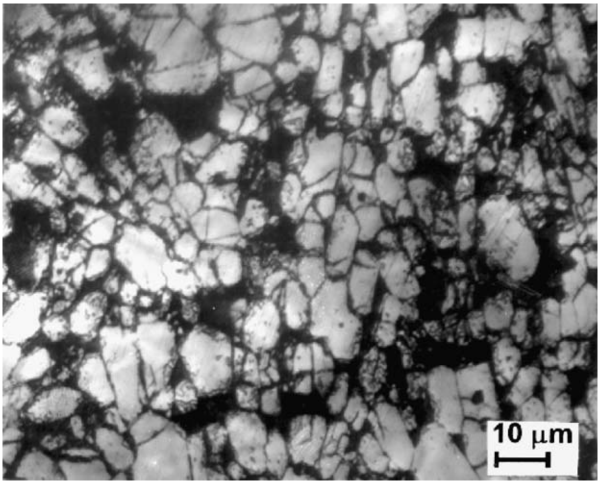

Fig. 54. Optical micrograph showing the microstructure of the $Pr_{20}Fe_{73}B_{5.5}Cu_{1.5}$ alloy after ECAP for one pass at 750 °C [281].

6.2.2. Metal–matrix composites

Although ECAP processing has been used for achieving grain refinement in numerous experiments reported over the last decade, there appears to have been only a limited number of investigations in which this procedure was used with metal–matrix composites. The first paper on composites described a series of experiments in which ECAP was applied to an Al-6061 metal–matrix composite reinforced with 10 vol% of Al_2O_3 particulates [243] and it was demonstrated that intense plastic straining has a potential for both reducing the grain size of the matrix material to the submicrometer level and increasing the strength of the composite at room temperature by a factor in the range of ~2.

These experiments were conducted using a metal–matrix composite designated Al-6061 10 vol% Al_2O_3(p) where p denotes particulates [243]. This composite was fabricated commercially using a proprietary casting technique in which an Al-6061 matrix alloy was reinforced with 10 vol% of irregularly-shaped Al_2O_3 particulates. These Al_2O_3 particulates were in the size range from ~6 to ~13 μm with an average size close to ~10 μm. The as-received grain size of the composite was measured as ~35 μm.

Severe plastic straining was introduced into the material using an ECAP die with a channel angle of $\Phi = 90°$. In the investigation, the samples were pressed for 8 passes at a temperature of 673 K plus an additional 2 passes at 473 K, thereby giving a total strain of ~10. All of the ECA pressing was conducted using processing route B_C. Fig. 55 shows a typical microstructure in a sample subjected to ECAP together with the appropriate SAED pattern [243]. Detailed inspection showed there was substantial grain refinement after ECAP with a mean grain size estimated as ~0.6 μm. Measurements of the Vickers microhardness showed the measured microhardness in the as-received condition was ~650 MPa but this value increased to ~1200 MPa after ECAP. Thus, severe plastic straining increased the strength of the composite by a factor of the order of ~2.

Detailed measurements indicated also there was little or no breaking of the Al_2O_3 particulates after ECA pressing to a strain of ~10 and the average particulate sizes were measured as 7.5 ± 3.1 and 7.5 ± 3.3 μm in the as-received and in the ECA pressed condition,

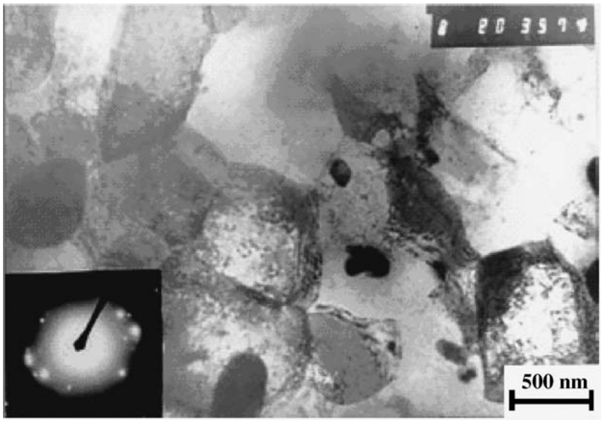

Fig. 55. Microstructure and associated SAED pattern for the Al-6061 10 vol% Al_2O_3(p) composite after ECAP through 8 passes at 673 K and an additional 2 passes at 473 K using route B_C [243].

respectively. In addition, the distributions of particulate sizes were similar in these two conditions, as indicated in Fig. 56(a) and (b) where the sizes are plotted in increments of 2 μm [243]. In practice, it is reasonable to anticipate that particulate cracking may be minimized when processing by ECAP because, unlike conventional extrusion, there is no confining aperture and thus no reduction in the sample cross-section as it passes through the die.

The propensity for particulate breaking in ECAP is a function of several parameters including the temperature employed for the pressing and the initial size of the reinforcing particulates. Cracking becomes more prevalent when the pressing temperature is reduced and some limited cracking of the particulates was reported when the same Al-6061 10vol%Al_2O_3(p) composite was pressed exclusively at room temperature instead of 473 K [244]. However, cracking becomes less likely when the particulate size is reduced and in this respect detailed measurements using TEM revealed no reduction in the average particulate size when an Al-6061 10vol%Al_2O_3(p) composite with a very small particulate size of only ~270 nm was pressed for one pass at room temperature and then through a total of 11 additional passes at 473 K [283].

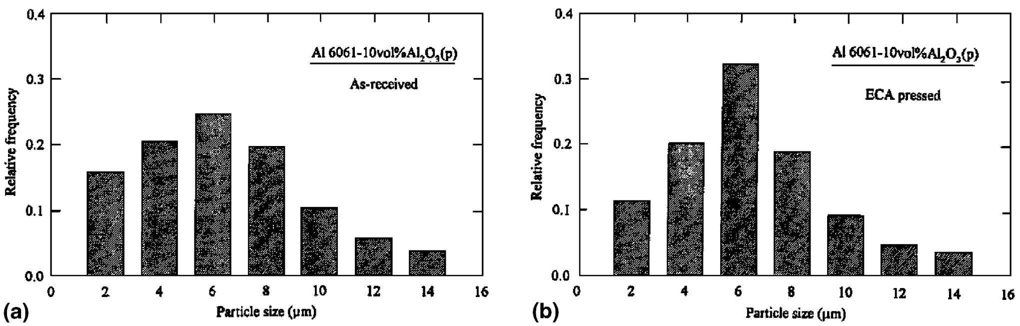

Fig. 56. Distribution of sizes of the Al_2O_3 particulates in (a) the as-received condition and (b) after ECAP through 8 passes at 673 K and an additional 2 passes at 473 K using route B_C [243].

In another investigation, ECAP was applied as an additional procedure in order to improve the homogeneity of the particle distribution and the mechanical properties of a metal–matrix composite with particle clusters [284]. An Al-6061 20% Al_2O_3 powder metallurgy composite with a strongly-clustered particle distribution was subjected to ECAP at a temperature 643 K and the evolution of homogeneity of the particle distribution during ECAP was monitored using the quadrat method. Fig. 57 illustrates the improvement of the particle distribution with an increasing number of ECAP passes, where Fig. 57(a)–(c) correspond to the as-fabricated condition and Fig. 57(d) and (e) show the microstructures after 4 and 7 passes of ECAP, respectively. In the as-fabricated condition, there are clearly-defined particle-free zones with sizes up to ~200 μm in the extrusion direction and

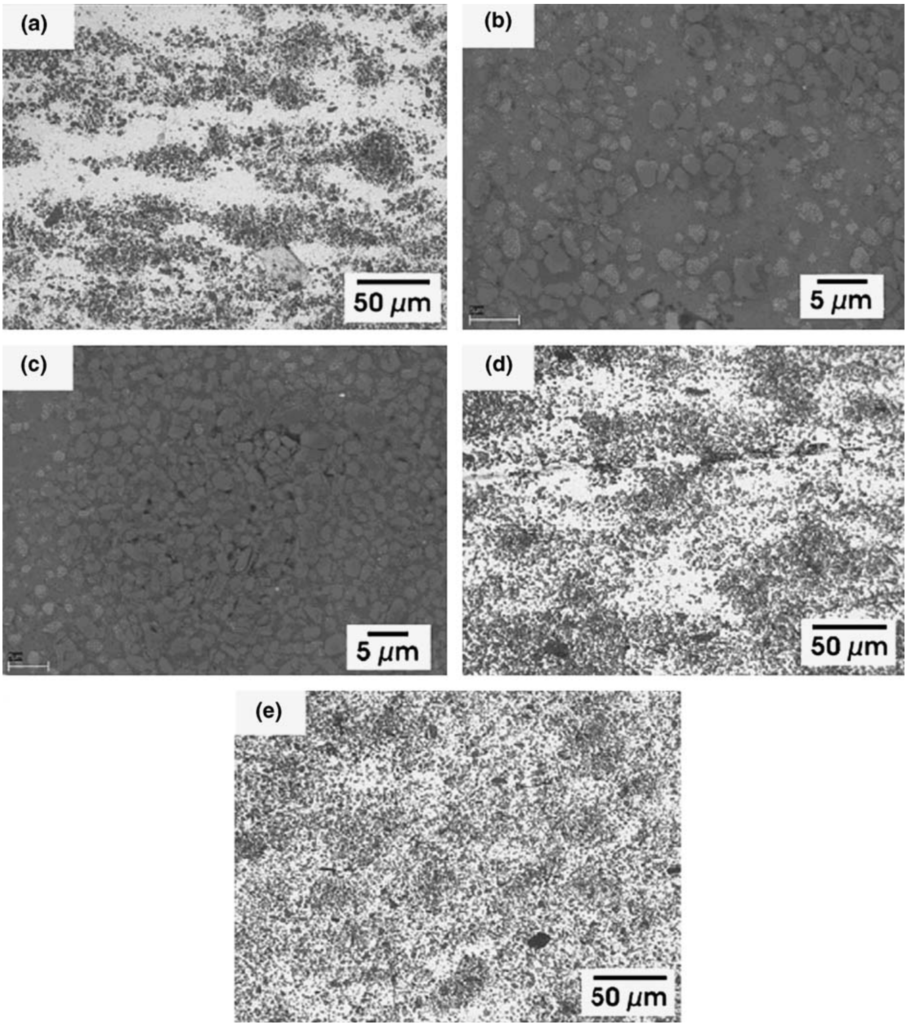

Fig. 57. Microstructure of an Al-6061 20% Al_2O_3 powder metallurgy composite: (a) in the as-fabricated condition, (b) in the as-fabricated condition showing a dense particle cluster, (c) in the as-fabricated condition showing diffuse particle clusters, (d) after ECAP through 4 passes and (e) after ECAP through 7 passes [284].

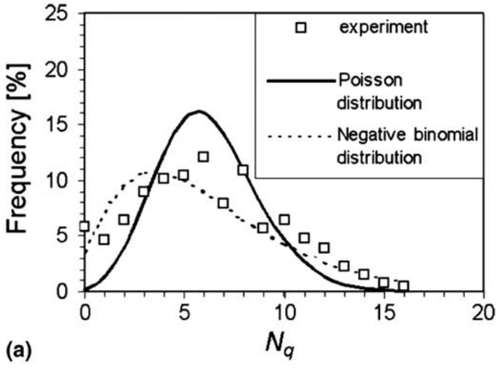

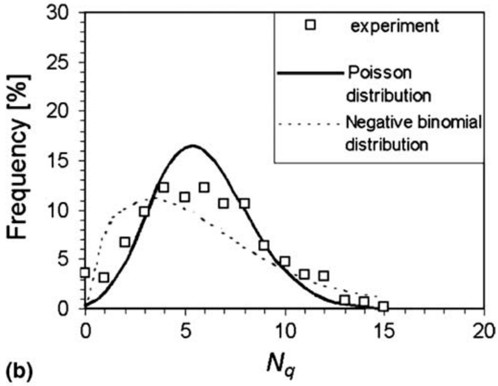

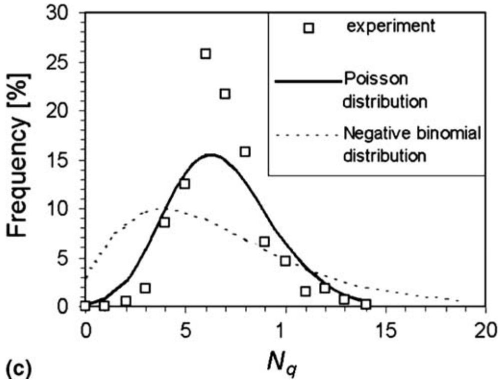

Fig. 58. Theoretical distribution curves and experimental results from the quadrat analysis of the Al-6061 20% Al_2O_3 powder metallurgy composite (a) in the as-fabricated condition, (b) after ECAP through 4 passes and (c) after ECAP through 7 passes [284].

up to ~40 μm in the direction perpendicular to the extrusion direction as is evident in Fig. 57(a). There are also both dense particle clusters as in Fig. 57(b) and relatively diffuse particle clusters as in Fig. 57(c). After 4 ECAP passes, shown in Fig. 57(d), a declustering process is initiated and the particle-free zones become smaller; whereas after 7 ECAP passes, shown in Fig. 57(e), there are no particle-free zones and the particle distribution appears to be reasonably homogeneous except only for the occurrence of a few dense particle clusters.

The frequency histograms of the number of alumina particles per quadrat, N_q, are plotted in Fig. 58 for each separate condition corresponding to the as-fabricated material in (a) and after 4 and 7 ECAP passes in (b) and (c), respectively [284]. These histograms show that the frequencies of empty quadrats and quadrats containing 10 or more particles decrease with increasing numbers of ECAP passes. Furthermore, the histogram for the as-fabricated condition in Fig. 58(a) follows a negative binomial distribution indicative of a clustered particle distribution. The histogram of the particle distribution for the material after 7 ECAP passes, shown in Fig. 58(c), resembles a Poisson distribution which is consistent with the presence of a homogeneous particle distribution. Detailed microstructural investigations showed that the alumina particles did not break during ECAP. Indeed, there was no significant change in the mean values of the number of particles per quadrat during ECAP, with values of 6.2, 5.9, and 6.7 for the as-fabricated condition and after 4 and 7 ECAP passes, respectively. Finally, testing revealed an important consequence of the improvement in the microstructure due to processing by ECAP. There was an increase in both the global fracture initiation toughness and the total crack growth resistance with increasing homogeneity of the particle distribution.

It can be seen from the results of this investigation that processing by ECAP may represent a useful procedure for improving the homogeneity of the particle distributions in metal–matrix composites containing small particles. It is important to note also that processing by ECAP does not degrade the microstructure of the material. Thus, no voids were formed and there was no evidence for any breaking of the particles in the interiors of the samples used in this investigation.

Although there have been no investigations to date of the influence of ECAP on the uniformity of particle distributions in cast metal–matrix composites, these results suggest that ECAP may be useful in this regard also. Indeed, the difficulty of achieving homogeneous distributions of reinforcements within the matrix is one of the problems generally associated with the production of cast composites [285,286]. Thus, in cast metal–matrix composites the distribution of the reinforcement particles in the matrix alloy is influenced by several factors such as the rheological behavior of the matrix melt, the method of particle incorporation, the interactions between the particles and the matrix before, during and after mixing and the changing particle distribution during solidification [285,286]. It has been shown that the post-solidification processing of cast composites by extrusion or rolling can effectively modify the particle distribution but nevertheless a complete declustering cannot be achieved even at very high extrusion ratios [287]. Therefore, based on the present evidence, it is reasonable to suggest that the application of ECAP processing may be a useful tool in improving the microstructure and the mechanical properties of these cast composites.

7. Mechanical and functional properties achieved using ECAP

The small grain sizes and high defect densities inherent in UFG materials processed by severe plastic deformation lead to much higher strengths than in their coarse-grained counterparts. Moreover, according to the constitutive relationship for superplasticity, it is reasonable to expect the appearance in UFG metals of low-temperature and/or high-rate superplasticity [15,288–290]. The realization of these capabilities will become important for the future development of high strength and wear-resistant materials, advanced superplastic alloys and metals having high fatigue life. The potential for achieving all of these possibilities has raised a keen interest among scientists and engineers in studying the mechanical and functional properties of these UFG materials.

In this connection, the fabrication of bulk samples and billets using ECAP was a crucial first step in initiating investigations into the properties of UFG materials and nanomaterials because the use of ECAP processing permitted, and subsequently fully supported, a series of systematic studies using various nanostructured metallic materials including commercial alloys [45,291–294]. The results of these recent studies are discussed in this section.

7.1. Properties at ambient temperature

7.1.1. Strength and ductility

During the last decade it has been widely demonstrated that a major grain refinement, down to the nanometer range, may lead to a very high hardness in various metals and alloys but nevertheless these materials invariably exhibit low ductility under tensile testing [295,296]. A similar tendency is well known for metals subjected to heavy straining by other processes such as rolling, extrusion or drawing. Strength and ductility are the key mechanical properties of any material but these properties typically have opposing characteristics. Thus, materials may be strong or ductile but they are rarely both.

The reason for this dichotomy is of a fundamental nature. As discussed in more detail in Section 7.1.3, the plastic deformation mechanisms associated with the generation and movement of dislocations may not be effective in ultrafine grains or in strongly-refined microstructures. This is generally equally true for SPD-processed materials. Thus, most of these materials have a relatively low ductility but they usually demonstrate significantly higher strength than their coarse-grained counterparts. Despite this limitation, it is important to note that SPD processing leads to a reduction in the ductility which is generally less than in more conventional deformation processing techniques such as rolling, drawing and extrusion. For example, experiments were conducted to compare the strength and ductility of the 3004 aluminum alloy processed by ECAP and cold-rolling [297]. As illustrated by the data plotted in Fig. 59, the yield strength increased monotonically with the increasing equivalent strain imparted into the alloy by either cold rolling or ECAP [298]. However, it is apparent also that the overall ductility exhibits different trends for these two processing methods. After one ECAP pass, equivalent to a strain of ~1, the elongation to failure or the ductility of the alloy decreases from ~32% to ~14%. However, there is no additional reduction in the ductility with additional ECAP passes and therefore with the imposition of even larger strains. By contrast, cold-rolling decreases the ductility by a similar magnitude initially but thereafter the ductility continues to decrease with increasing rolling strain although at a slower rate. Consequently, processing by ECAP leads ultimately to a greater retention of ductility than conventional cold-rolling.

In this connection, recent findings of extraordinary high strength and good ductility in several bulk ultrafine-grained metals produced by severe plastic deformation are also of special interest [3,158,215,299,300]. It is important to consider in detail the three different approaches that were used in these investigations.

In the first study, high purity (99.996%) Cu was processed at room temperature using ECAP with a 90° clockwise rotation around the billet axis between consecutive passes in route B_C [158]. The strength and ductility were measured by uniaxial tensile tests and the

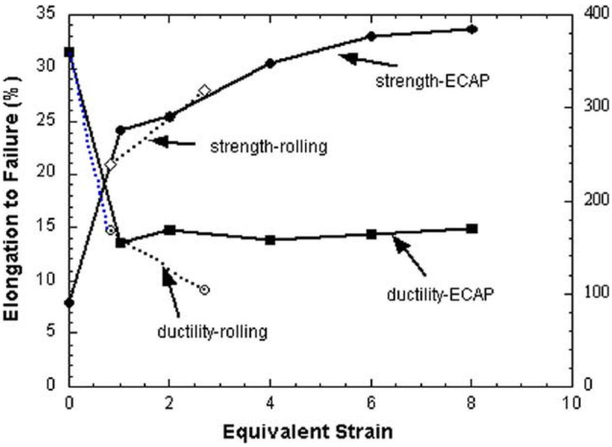

Fig. 59. A comparison of yield strength and ductility for an Al-3004 alloy processed by cold-rolling or ECAP [298].

resulting engineering stress–strain curves are shown in Fig. 60 for the Cu samples tested at room temperature in the initial coarse-grained condition and in three processed states [158]. It is apparent that the initial coarse-grained Cu, with a grain size of about 30 μm, has a typical low yield stress with significant strain hardening and a large elongation to failure. At the same time, cold-rolling of the copper to a thickness reduction of 60% significantly increases the strength, as shown by curve 2 in Fig. 60, but dramatically decreases the elongation to failure. This result is consistent with the classical mechanical behavior of metals that are deformed plastically. The same tendency is true also for Cu subjected to two passes of ECAP. However, further straining of Cu to 16 passes of ECAP, as shown by curve 4 in Fig. 60, simultaneously increases both the strength and the ductility. Furthermore, the increase in ductility is much more significant than the relatively minor increase in strength.

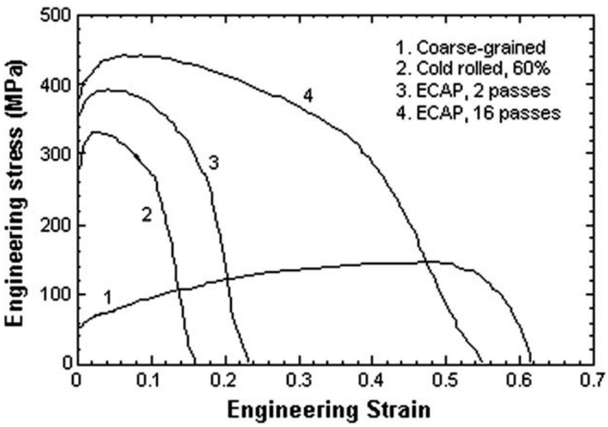

Fig. 60. Tensile engineering stress–strain curves for Cu tested at 22 °C with a strain rate of $10^{-3}\ s^{-1}$: the processing conditions for each curve are indicated [158].

Thus, the data shown in Fig. 60 for Cu processed by ECAP clearly demonstrate an enhancement of strength as well as ductility with accumulated deformation due to an increase in the number of passes from 2 to 16 [158]. This is a very remarkable result that, at the time of the investigation in 2002, had never been observed in metals processed by plastic deformation. Accordingly, the effect was termed the "paradox of strength and ductility in SPD-processed metals" and the principles of this paradox are illustrated in Fig. 61 where it is apparent that conventional metals lie within the lower shaded quadrant [158]. As seen in Fig. 61 for Cu and Al, cold-rolling (the reduction in thickness is marked by each datum point) increases the yield strength but decreases the elongation to failure or ductility [301,302]. The extraordinary combination of high strength and high ductility shown in Fig. 61 for the nanostructured Cu and Ti after processing by SPD clearly sets them apart from the other coarse-grained metals.

In recent years, similar tendencies have been reported in a number of metals, including Al [303,304], Cu [219], Ni [175] and Ti [158,300], after processing through various types of severe plastic deformation such as ECAP, high-pressure torsion or accumulative roll bonding. Concerning the origin of this phenomenon, it has been suggested that it is associated with an increase in the fraction of high-angle grain boundaries with increasing straining and with a consequent change in the dominant deformation mechanisms due to the increasing tendency for the occurrence of grain boundary sliding and grain rotation [3,158]; recent experimental evidence for this change in deformation mechanism is described in Section 7.1.3.

Another new approach to the problem of ductility enhancement was suggested through the introduction of a bimodal distribution of grain sizes [299]. In this study, nanostructured copper was produced through a combination of ECAP and subsequent rolling at the low temperature of liquid nitrogen prior to heating to a temperature close to ~450 K. This procedure gave a bimodal structure of micrometer-sized grains, with a volume fraction of around 25%, embedded in a matrix of nanocrystalline grains. The material

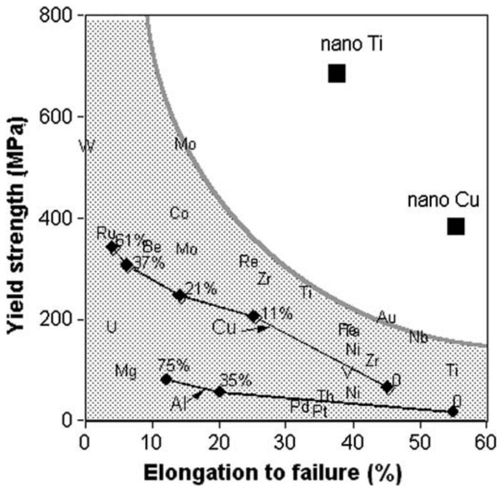

Fig. 61. The paradox of strength and ductility in metals subjected to SPD: the extraordinary combination of high strength and high ductility in nanostructured Cu and Ti processed by SPD (two upper points) clearly sets them apart from conventional coarse-grained metals (lower points relating to metals of 99.5–99.9% purity) [158].

produced in this way exhibited an extraordinarily high ductility but also retained a very high strength. The reason for this behavior is that, while the nanocrystalline grains provide strength, the embedded larger grains stabilize the tensile deformation of the material. Other evidence for the importance of grain size distribution comes from investigations on zinc [305], copper [306] and an aluminum alloy [307]. Furthermore, the investigation of copper [306] showed that bimodal structures may increase the ductility not only during tensile testing but also during cyclic deformation. This observation is important in improving the fatigue properties of materials, as discussed in Section 7.1.2.

A third approach has been suggested for enhancing strength and ductility based on the formation of second-phase particles in the nanostructured metallic matrix [296] where it is anticipated these particles will modify the shear-band propagation during straining and thereby it will lead to an increase in the ductility.

The principle of achieving high strength and high ductility through the introduction of intermediate metastable phases was successfully realized recently in a commercial Al–Zn–Mg–Cu–Zr alloy [308] and an Al–10.8%Ag alloy subjected to ECAP and subsequent ageing [215]. The principle of this approach is illustrated in Fig. 62 for the Al–Ag alloy where the Vickers microhardness is plotted against the ageing time at 373 K for samples in a solution treated condition (ST) and after cold-rolling (CR) and ECAP [215]. For the ST condition, the hardness is initially low but increases with ageing time to a peak value after 100 h (3.6×10^5 s). For the CR condition, the hardness is higher but there is only a minor increase with ageing. The hardness is even higher after ECAP and further increases with ageing to a peak value after 100 h. The relatively lower values of hardness recorded after CR by comparison with ECAP are due to the lower equivalent strain imposed on the sample: these strains were ~1.4 in CR and ~8 in ECAP so that the microstructure after CR consisted of subgrains or cell boundaries having low angles of misorientation. It was shown, using scanning TEM, that the peak hardness achieved after ECAP and ageing for 100 h is due to precipitation within the grains of spherical particles with diameters

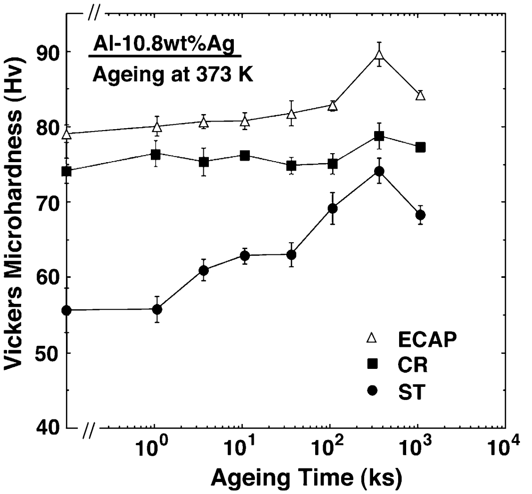

Fig. 62. Variation of the Vickers microhardness with ageing time for the Al–10.8%Ag alloy after solution treatment (ST), cold-rolling (CR) and ECAP [215].

of ~10 nm and elongated precipitates with lengths of ~20 nm. The spherical particles were identified as η-zones consisting of arrays of solute atoms lying parallel to the (001) planes and the elongated precipitates were identified as the plate-like γ' particles. It was shown also that additional ageing up to 300 h led to a growth in the γ' particles and a very significant reduction in the density of the fine η-zones, thereby giving a consequent loss in hardening at the longest ageing time recorded in Fig. 62.

The introduction of ageing after ECAP has an important influence on the stress–strain behavior at room temperature, as demonstrated in Fig. 63 where the tensile stress–strain curves are shown after ECAP and after ST, CR and ECAP with additional ageing for 100 h at 373 K: each sample in Fig. 5 was tested at room temperature at an initial strain rate of $1.0 \times 10^{-3}\ s^{-1}$ [215]. Thus, ST and ageing gives a reasonable tensile strength, an extensive region of uniform strain and good ductility, whereas CR and ageing gives an increased strength but very limited uniform strain and a marked reduction in the total ductility. For the ECAP condition, the strength is high in the absence of ageing but there is a negligible region of uniform strain and no significant strain hardening. By contrast, the sample processed by ECAP and aged for 100 h shows a similar high strength, a region of strain hardening and good ductility. In practice, the uniform strain of ~0.14 achieved in this specimen is similar to the uniform strain of ~0.17 in the sample after ST and ageing and the elongation to failure of ~0.40 is comparable to, and even slightly exceeds, the elongation of ~0.37 recorded in the ST and aged condition. These results demonstrate, therefore, the potential for producing high strength and good ductility in precipitation-hardened alloys. Furthermore, although the results documented in Figs. 62 and 63 relate to a model Al–Ag alloy, it is reasonable to anticipate that it should be possible to achieve similar results in commercial engineering alloys where the ageing treatments are generally well documented.

It is worth noting also that in UFG metals processed by ECAP both strength and ductility can be improved by performing mechanical tests at lower temperature. As an

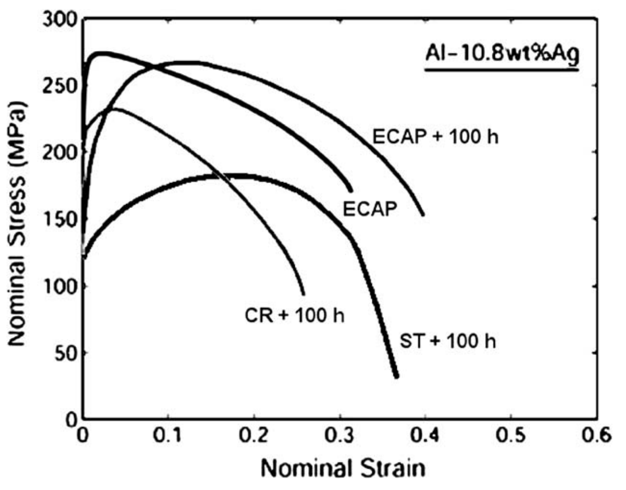

Fig. 63. Tensile plots of stress versus strain at room temperature for the Al–10.8%Ag alloy after solution treatment (ST) or cold-rolling (CR) with ageing at 373 K for 100 h or ECAP without subsequent ageing and ECAP with ageing at 373 K for 100 h [215].

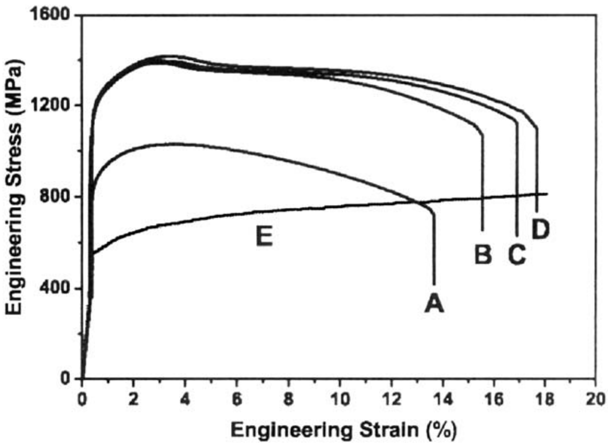

Fig. 64. Engineering stress–strain curves for nanostructured Ti where curve A is for testing at room temperature at a strain rate of $1 \times 10^{-3}\ s^{-1}$ and curves B–D for the same Ti tested at 77 K for strain rates of $1 \times 10^{-3}\ s^{-1}$, $1 \times 10^{-2}\ s^{-1}$ and $1 \times 10^{-1}\ s^{-1}$, respectively; for comparison, curve E shows the behavior of coarse-grained Ti over the initial 18% of strain when testing at 77 K [309].

example, Fig. 64 displays the tensile engineering stress–strain curves of UFG Ti with a grain size of 260 nm tested at room temperature and 77 K [309]. At room temperature, the Ti has some ductility and a small uniform elongation, as shown by Curve A obtained at a strain rate of $1 \times 10^{-3}\ s^{-1}$. However, at 77 K the strength of the material is drastically elevated to ~1.4 GPa. There is also a simultaneous increase in the elongation to failure and this increases with strain rate up to a maximum close to ~20%, as shown in Fig. 64 where curves B–D are for strain rates of $1 \times 10^{-3}\ s^{-1}$, $1 \times 10^{-2}\ s^{-1}$ and $1 \times 10^{-1}\ s^{-1}$, respectively. These results for strength and ductility are better than, or at least comparable to, those of Ti alloys with a large percentage of alloying elements. Here, pronounced necking is delayed even for this very strong metal, resulting in a large area under the stress–strain curve and a generally tough behavior of the material. For comparison, curve E shows the initial 18% of strain for a conventional coarse-grained Ti sample tested at 77 K.

It is well known that UFG Cu with high ductility was found to have a higher strain rate sensitivity, m, where m is defined as $\{d \ln \sigma / d \ln \dot{\varepsilon}\}$ where σ is the applied stress and $\dot{\varepsilon}$ is the strain rate [158]. The value of m was equal to ~0.14 for ECAP-processed Cu taken through 16 passes compared with a value of m of ~0.06 for ECAP-processed Cu taken through only 2 passes. A high value for the strain rate sensitivity indicates viscous flow and renders the material more resistant to necking and therefore more ductile. Increased values for the strain rate sensitivities were also revealed in a number of other studies [304,310]. At the same time, there are also some reports illustrating low values of m after ECAP. It is possible these apparent differences are due to microstructural features in the samples since, as already shown, the microstructures produced by SPD processing may differ significantly depending upon the processing conditions.

In conclusion, recent results show that grain refinement by ECAP can lead to a unique combination of strength and ductility in metallic materials. Such superior mechanical properties are highly desirable in the development of advanced structural materials for the next generation [3]. However, the achievement of these properties is associated with the tailoring of specific microstructures which, in turn, are determined by the precise processing regimes and the nature of any further treatments. In general, any microstructural refinement by severe plastic deformation will lead to a hardening of the material and the formation of specific UFG structures appears to be a necessary condition for the development of new and viable structural materials.

7.1.2. Fatigue behavior

Fatigue is associated with the processes of damage accumulation and the resulting fracture of materials under cyclic loading at stress levels below the tensile strength. The total fatigue life has been conventionally divided into two regions corresponding to the times required for crack nucleation and crack propagation [311,312]. The resistance to crack initiation naturally requires strength while the tolerance to crack advance requires ductility. The most promising feature of SPD materials, which suggests the possibility of obtaining significantly enhanced fatigue properties, is associated with a combination of high strength and good ductility in the nanostructured state [3,15,215]. The low-cycle fatigue (LCF) and high-cycle fatigue (HCF) regimes are conventionally distinguished in accordance with the applied stain amplitude. Testing in the HCF regime corresponds to probing the resistance of a material to crack initiation whereas testing in the LCF regime corresponds to assessing the defect tolerance of a material.

Experimental results concerning the cyclic behavior are currently available for several UFG SPD materials in the form of both pure metals and metal alloys and the data show that the ultimate tensile strength and the fatigue limit follow the standard Hall–Petch relationship [313]. Hence, it was reasonably anticipated that UFG materials produced by SPD should generally demonstrate a great potential for an enhancement of the high-cycle fatigue life.

It has been established experimentally for a number of materials that ultrafine structures usually exhibit higher fatigue resistance than materials with a conventional grain size under stress-controlled loading. For example, the fatigue life and endurance limit for constant stress amplitude cycling of Ni and an Al–Mg alloy increases when the microstructure changes from microcrystalline to ultrafine-grained and nanocrystalline [314]. In the case of Cu, which is probably the most closely-studied material, an improvement in the fatigue lifetime was observed in UFG copper when compared to Cu with a conventional grain size [315–319].

A very pronounced improvement of the fatigue limit was observed in a planar slip material, ECAP-processed Ti produced at an elevated temperature of 400 °C, subjected to further strengthening by cold-rolling to an area reduction of 75%, and further annealing for structural stabilization at 300 °C for 1–2 hours [320]. The fatigue limit of 500 MPa in pure SPD-processed titanium is close to that of conventional Ti alloys, as shown in Fig. 65 [320].

However, the results of strain-controlled tests expressed on the basis of the Coffin–Manson plot show nearly the same or even a somewhat shorter lifetime for UFG Cu than for their counterpart with a conventional grain size [315,318,319,321]. The effect of lifetime shortening is more pronounced at the higher plastic strain amplitudes. The explanation of this behavior lies in the often-reported low thermal and mechanical stability and a strong tendency to recover the highly-deformed UFG structure.

Cyclic softening, grain growth and strain localization appear to be the main mechanisms responsible for the lower fatigue resistance of UFG structures under the same plastic

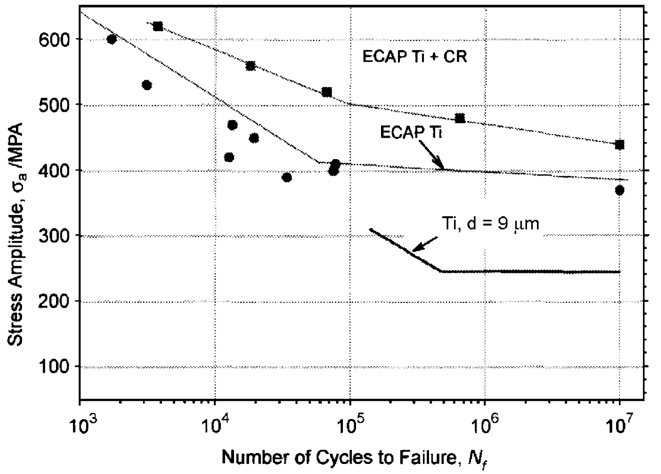

Fig. 65. Characteristic *S–N* plots and fatigue limits for Ti processed by ECAP and Ti processed by ECAP and cold-rolling: data are also shown for conventional Ti with a grain size of 9 μm [320].

strain amplitude [313]. Cyclic softening caused by total strain-controlled cyclic loading was observed in early studies of UFG Cu [321]. It was concluded that the softening is due to a general decrease in the defect density and perhaps changes in the boundary misorientations. At low strain amplitudes, the softening is less pronounced. The cyclic hardening/softening curve was found to be nearly flat during most of the fatigue life and no softening was observed under a plastic strain amplitude, ε_{ap}, below 10^{-3} [322]. The softening behavior depends in practice upon both the loading and microstructural parameters. A microstructure characterized by nearly equiaxed subgrains (termed Type A) exhibits a nearly stable cyclic behavior when cycled at $\varepsilon_{ap} = 10^{-3}$ whereas a microstructure consisting of mainly elongated subgrains or lamellar subgrains (termed Type B) undergoes marked softening under the same loading conditions [315,318].

Grain growth and changes of microstructure due to fatigue are frequently observed in UFG Cu and there is evidence also for a significant increase of cell size [321]. Areas with recrystallized grains develop in UFG structures of Type B whereas recrystallization and grain growth are not evident in structures of Type A [323]. There is evidence for a pronounced recrystallization in UFG copper of high purity after constant plastic strain-controlled loading with a plastic strain amplitude of the order of 10^{-4} [324]. In recent work it was assumed that no characteristic dislocation structure can develop in ultrafine grains [319] whereas a specific dislocation structure develops in coarse grains. At higher strain amplitudes, a well-defined cell and subgrain structure is observed in UFG copper.

Cyclic strain localization, resulting in fatigue crack initiation, is an important feature of the fatigue process in UFG materials. The development of macroscopic shear bands (SBs) is considered the major form of fatigue damage in wavy slip UFG materials processed by ECAP. Thus, SBs oriented at 45° to the loading axis were observed on the surface of cyclically-loaded Cu specimens [321,322,325–327] where these bands are macroscopically parallel to the shear plane of the last extrusion pass. These SBs have been shown to be "persistent" in the sense that they appear on the surface after re-polishing [318]. This persistent nature suggests that they are sites of easier and more intensive cyclic deformation.

Observations after low-cycle fatigue also reveal extrusions and intrusions which are similar to the features known from fatigue studies on Cu single crystals [321]. For UFG materials, the average dimensions of the extrusions, both in terms of their lengths along the slip lines and their elevations above the surrounding surface, are larger than the very small grain size. Accordingly, the details for the formation of these SBs are not entirely clear. It has been proposed that the mechanism responsible for the formation of SBs is an interaction between cyclically-induced grain coarsening and grain rotation [328]. In this mechanism, local grain coarsening takes place first and shear localization appears later. It was also suggested that recrystallization occurs preferentially in some regions of microstructural inhomogeneity in the form of banded structures [320]. The occurrence of grain growth triggered by cyclic deformation is believed to be a very common feature of cyclically-deformed UFG metals. On the other hand, no detectable grain coarsening was observed in the vicinity of SBs which suggests there is no relationship between SBs and grain coarsening [327].

There has been some discussion of the effect of ECAP processing on fatigue and the procedure for the optimization of the fatigue performance [313]. It was noted that pressing through an increasing number of passes in ECAP leads to an increasing monotonic strength and fatigue limit [329–332]. Furthermore, the fatigue properties of UFG metals can be improved by gaining some ductility and by reducing the constraints for dislocation motion as, for example, by decreasing the tendency for shear banding and strain localization which is common in many hardened metals. Thus, it may be advantageous in improving the fatigue properties to employ materials with partially-recovered structures. The positive effect of the heat treatment on LCF was revealed in early fatigue studies of ECAP-processed materials [333]. It was shown, using the acoustic emission technique and microscopic surface observations, that susceptibility to shear banding in ECAP-processed Cu decreases dramatically after a short-term annealing of only 10 min at the relatively low temperature of 250 °C [334] and the LCF life can be improved by a factor of ~5–10 after a heat treatment that gives no significant grain growth [316,335,336]. While processing by ECAP leads to a considerable reduction in the tensile and cyclic ductility, the same materials subjected to a post-ECAP annealing can potentially obtain a higher ductility than their conventional coarse-grained counterparts with shifts in the Coffin–Manson line towards higher fatigue lives [336]. Since metals processed by SPD retain some ductility after fabrication, their tensile and high cyclic strengths can be further improved after processing through the use of conventional cold-rolling with or without intermediate annealing at a moderate temperature. This has been shown for several Al–Mg alloys [337] and commercial purity Ti [336,338].

The effect of precipitation in SPD-processed nanostructured metals is complex. On the one hand, it was noted earlier that precipitates can dramatically increase the thermal stability of SPD-processed metals and, on the other hand, the grain boundaries may recover during ageing thereby reducing their susceptibility to strain localization and premature cracking. As an example, it was shown that optimal ageing of an ECAP-processed UFG Cu–Cr–Zr alloy gives a structure having high strength with a grain size of ~200 nm which remains fine after subsequent annealing at temperatures as high as 500 °C [330]. It was shown that ECAP of the solid-solution treated Al-2024 alloy through one pass, followed by low temperature ageing, can impressively enhance both the strength and the ductility. Thus, samples aged at 100 °C for 20 h exhibited an ultimate tensile strength of $\sigma_{\mathrm{UTS}} \approx 715$ MPa and a total elongation to failure of $\delta = 16\%$ [339]. It was shown also that the yield stress and tensile strength of the Al-6061 alloy benefits from multiple ECAP up to four passes by comparison with a solution-treated sample pressed by ECAP through only a single pass at 125 °C with no subsequent heat treatment [340]. Although the effect of the single pass of ECAP on the 6061 aluminum alloy is impressive, it is not clear whether it would be possible to achieve the same strength and ductility in Al alloys after conventional treatments.

Hence it appears there are several principal competing approaches for the enhancement of fatigue properties via ECAP processing [313,341]. The first is the achievement of a compromise between strength and ductility in a minimum number of passes of ECAP, where only a single pass is used whenever possible since this is a cost-effective procedure employing relatively small imposed strains. The second is the achievement of the maximum possible strength leading to high cycle fatigue life. The third is the achievement of both high strength and ductility through multipass ECAP leading to enhanced low and high cycle fatigue lives.

It is reasonable to conclude that there is a good body of results available to date on the effects of ECAP on the subsequent fatigue properties but nevertheless there remain significant opportunities for developing optimum processing schemes for attaining the desired fatigue properties of SPD-produced materials.

7.1.3. Alternative deformation mechanisms at very small grain sizes

When the grain sizes of UFG materials processed by SPD become very small, typically less than ~100 nm, new deformation mechanisms may be initiated that play a significant role in the mechanical behavior [298]. Thus, it has been revealed using both dynamic molecular simulations [342–344] and experimental observations [345–348] that materials with nanocrystalline grain sizes deform via mechanisms not accessible to their coarse-grained counterparts. For example, the emission of partial dislocations from grain boundaries becomes a major deformation mechanism when the grain size is less than ~50–100 nm [342–349]. This emission leads also to the formation of deformation twins, as observed experimentally in UFG copper and aluminum [345–349]. It is important to note in this respect that conventional coarse-grained aluminum never deforms by twinning even at low temperatures and high strain rates. High-resolution transmission electron microscopy of copper processed by HPT [345] has shown the occurrence of regions forming a twinning relationship. There are also many stacking faults extending from grain boundaries into the grains but failing to reach the opposite grain boundaries, thereby providing direct evidence that partial dislocations are emitted from sources within the boundaries.

Moreover, nanostructured materials produced by SPD techniques often have non-equilibrium grain boundaries characterized by an excess of non-geometrically necessary dislocations [3,15]. Some of these dislocations may dissociate into pairs of Shockley partials that are capable of moving away from the grain boundary under the action of an applied stress. The grain boundaries of this type can act both as sources and sinks for partial dislocations. In addition, partial dislocations may also be emitted from the grain boundaries through atomic reshuffling [342].

Since the number of grain boundaries per volume increases as the grain size is reduced, it is reasonable to expect that another deformation mechanism, in the form of grain boundary sliding, may become increasingly important at these small grain sizes. In addition, grain rotation is intricately linked to the role of grain boundary sliding. Thus, dislocation glide on preferred slip systems gives rise to grain rotation and to crystallographic texture. By contrast, it is reasonable to anticipate also that rotation via grain boundary sliding alone will randomize the grain orientation distribution. It is therefore significant to note that experiments on nanocrystalline Pd, deformed to a large true strain of 0.6 by rolling at room temperature, showed that the random grain orientation distribution of the initial material was maintained whereas in coarse-grained Pd deformed under identical conditions a pronounced rolling texture was developed [350]. These results provide strong evidence for a significant role of grain rotation in the deformation of the nanocrystalline metal, where this rotation is mechanistically similar to the grain rotation occurring during superplastic deformation of materials with micrometer grain sizes at elevated temperatures.

In UFG metals produced by ECAP, grain boundary sliding was revealed experimentally in early work on UFG copper with a mean grain size of 210 nm by observing the formation of step relief on the polished surface of the sample after testing in compression [351]. The contribution of grain boundary sliding to the total strain was estimated in this investigation as ~20%. More recently, there are reports of long mesoscopic shear traces appearing on the surfaces of samples of UFG Cu [352], Ni [352] and Al [353] after tensile testing at room temperature, where these observations are consistent with the mesoscopic sliding model developed for nanocrystalline materials [354]. In very recent experiments, the active development of grain boundary sliding was revealed directly in UFG aluminum during deformation at room temperature through the use of atomic force microscopy and depth-sensing indentation testing [355]. The sliding contribution in these experiments was estimated as ~70% from measurements of the surface profiles around hardness indentations, thereby confirming the significance of sliding in the deformation of UFG structures. It is important to note also that these data correlate closely with results demonstrating an increased strain rate sensitivity of the flow stress in UFG metals (see Section 7.1.1), where a high strain rate sensitivity is indicative of a more viscous type of flow and therefore with a process such as grain boundary sliding where, as documented in Section 7.2, the strain-rate sensitivity is 0.5.

The question remains why grain boundary sliding takes place in nanostructured materials produced by SPD at temperatures that are relatively low by comparison with the absolute melting temperatures of the materials. Thus, ambient temperature for pure aluminum corresponds to an homologous temperature of only $\sim 0.32T_m$ where T_m is the absolute melting temperature of the material. Since grain boundary sliding is a diffusion-controlled process, it should occur preferentially at high temperatures where diffusion rates are reasonably rapid. Nevertheless, it is interesting to note that the possibility of low temperature sliding was discussed in very early work on the creep of metals [356]. A possible explanation for the occurrence of sliding in UFG metals is that diffusion is more rapid in SPD-produced metals with highly non-equilibrium grain boundaries. Experiments have shown that in metals produced by SPD the diffusion coefficient increases considerably, often by two or three orders of magnitude, and this is associated directly with the presence of non-equilibrium grain boundaries [357,358]. Accordingly, it appears that grain boundary sliding is easier in these ultrafine-grained metals and develops during straining at lower temperatures leading to the possibility of observing increased ductility. It is well known in this connection that enhanced sliding in nanostructured metals may lead to superplasticity even at relatively low temperatures [289].

The recent results obtained from modeling and experiments provide strong support for the proposal that new deformation mechanisms, that are not typical under the experimental conditions in conventional coarse-grained materials, may proceed actively in metals with UFG microstructures. An important task in future studies is therefore to identify and quantify the interrelationships between these alternative deformation mechanisms and thus to determine their influence on the mechanical behavior of UFG metals.

7.2. Properties at high temperatures

High temperature deformation refers to the plastic flow or creep of materials at elevated temperatures where the rates of flow are governed by diffusion-controlled processes. In broad terms, the creep mechanisms occurring in crystalline solids divide into two groups depending upon whether the mechanisms occur intragranularly or whether the mechanisms are associated specifically with the presence of grain boundaries [359,360]. Examples of intragranular processes include creep controlled by dislocation climb [361] or dislocation glide [362] and examples of grain boundary processes include the occurrence of grain boundary sliding in creep or superplasticity [363] and the stress-directed flow of vacancies in diffusion creep [364–366]. The occurrence of intragranular and grain boundary processes lead to distinct differences in the deformation behavior because intragranular dislocation mechanisms give conventional power-law creep where the strain rate, $\dot{\varepsilon}$, varies with the applied stress, σ, raised to an exponent of ~3–5 whereas grain boundary processes such as superplasticity and diffusion creep have stress exponents of 2 and 1, respectively. In practice, it is especially attractive to make use of ECAP processing to achieve superplastic ductilities because this provides a potential for producing materials that may be used in industrial superplastic forming operations. To consider this possibility, it is first necessary to examine the requirements inherent in attaining superplastic deformation.

In evaluating the characteristics of ultrafine-grained materials processed by ECAP in high temperature deformation, it is very important to recognize that generally these ultrafine grains are unstable at elevated temperatures. Thus, if the ultrafine-grained structures are lost through grain growth when the samples are heated, no advantageous properties are achieved in high temperature deformation. Nevertheless, it is often feasible to retain an array of ultrafine grains even at very high temperatures by using materials containing second phases or arrays of precipitates. Fig. 66 gives an example of the potential for retaining ultrafine grain sizes in a range of aluminum-based alloys [367] where samples were processed by ECAP, separate pieces were cut from the as-pressed materials and annealed for 1 h at selected elevated temperatures, and the plot shows the measured grain sizes as a function of the annealing temperature. Data are shown in Fig. 66 for samples of pure aluminum [255], an Al–3%Mg solid solution alloy [255], an Al–3%Mg–0.2%Sc alloy [368], and commercial Al-2024 [369] and Al-7034 [260] alloys. It is apparent that the as-pressed grain size is slightly larger than ~1 μm in pure aluminum but the grains grow rapidly when the material is heated to temperatures above ~500 K. The behavior is similar for the Al–3%Mg solid solution alloy where the grains are much smaller after ECAP but rapid grain growth occurs again at temperatures above ~500 K. By contrast, the addition of 0.2% Sc to the Al–3%Mg alloy introduces a distribution of fine Al_3Sc precipitates and these are sufficient to retain an ultrafine grain size in the submicrometer range up to temperatures >700 K. Ultrafine grains are also retained in the Al-2024 alloy because of the presence of $CuMgAl_2$ precipitates and in the Al-7034 alloy due to the presence of Al_3Zr and $MgZn_2$ precipitates. It is reasonable to conclude from inspection of Fig. 66 that the

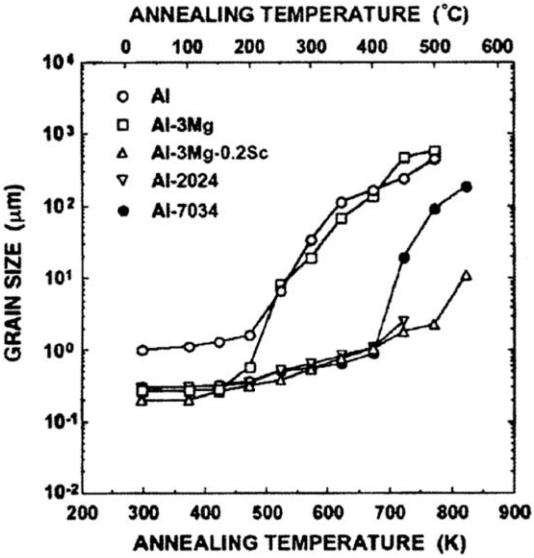

Fig. 66. Grain size versus annealing temperature for samples annealed for 1 h after ECAP: pure Al [255], Al–3%Mg [255], Al–3%Mg–0.2%Sc [368], Al-2024 alloy [369] and Al-7034 alloy [260].

Al–3%Mg–0.2%Sc alloy and the Al-2024 and Al-7034 alloys are potential candidates for achieving superplastic ductilities in high temperature testing.

7.2.1. Achieving superplasticity in tensile testing

There are two requirements for attaining superplastic ductilities in tensile testing [370]. First, superplasticity requires a very small and stable grain size, typically less than ~10 μm. Second, since superplastic flow is a diffusion-controlled process, it occurs at high temperatures when the rate of diffusion is reasonably rapid: typically, superplasticity is achieved at temperatures at and above $\sim 0.5T_m$ where T_m is the absolute melting temperature of the material. When materials deform superplastically, it can be shown both experimentally [371] and theoretically [363] that the steady-state strain rate in the superplastic regime, $\dot{\varepsilon}_{sp}$, is given by a relationship of the form

$$\dot{\varepsilon}_{sp} = \frac{AD_{gb}G\mathbf{b}}{kT}\left(\frac{\mathbf{b}}{d}\right)^2\left(\frac{\sigma}{G}\right)^2 \tag{7}$$

where A is a dimensionless constant, D_{gb} is the coefficient for grain boundary diffusion, G is the shear modulus, $\mathbf{b}$ is the Burgers vector, k is Boltzmann's constant, T is the absolute temperature and d is the grain size. Thus, the strain rate varies with the stress raised to a power of 2 which is equivalent to a strain rate sensitivity of $m = 0.5$, with the reciprocal of the grain size raised to a power of 2 and with the rate of grain boundary diffusion.

When materials are produced for use in the superplastic forming industry, it is a standard procedure to produce sheet metals with small grain sizes through the use of appropriate thermomechanical processing [372]. However, these procedures have very significant disadvantages. First, different processing routes must be developed for each separate alloy. Second, the grain sizes achieved in this way typically lie within the range of

~2–5 μm. By contrast, processing by ECAP is capable of producing materials having grain sizes in the submicrometer range and it follows from Eq. (7) that a reduction in grain size by one order of magnitude will increase the strain rate associated with optimum superplasticity by two orders of magnitude. Furthermore, a reduction in grain size leads to the potential for achieving superplastic deformation at lower testing temperatures.

Since industrial superplastic forming is generally performed at strain rates within the range of $\sim 10^{-3}$–10^{-2} s^{-1} where the forming times for each individual component are of the order of ~20–30 min [373], there is the potential for using ECAP to produce ultra-fine-grained materials and thereby achieving superplasticity at strain rates of $\sim 10^{-2}$–1 s^{-1} with a consequent reduction in the forming time to <60 s [288]. It should be noted that high strain rate superplasticity is defined formally as the occurrence of superplastic elongations when pulling in tension at strain rates at and above 10^{-2} s^{-1} [374]. Thus, if this is achieved, it is reasonable to anticipate that it may be feasible to expand the use of superplastic forming from the current emphasis on aerospace and other high-cost low-volume components to the fabrication of low-cost high-volume components for the automotive and consumer product industries [375].

The first direct demonstration of the occurrence of high strain rate superplasticity in commercial aluminum-based alloys processed by ECAP occurred in 1997 when elongations of 1180% without failure and 970% at failure were reported in commercial Al–Mg–Li–Zr and Al–Cu–Zr (Al-2004) alloys, where these high elongations were achieved at strain rates of 1×10^{-2} s^{-1} within the regime of high strain rate superplasticity [376]. An example of this first report is shown in Fig. 67 for the Al–Mg–Li–Zr alloy where the central specimen pulled out to 1180% without failure and the lower specimen pulled to failure at 910% at 623 K at a strain rate of 1.0×10^{-1} s^{-1}: the upper specimen is untested [376].

Subsequently, there have been numerous reports describing the use of ECAP to produce very high tensile elongations of >2000% in various Al–Mg–Sc [377–383], Al–Mg–Sc–Zr [384] and Al–Mg–Li–Sc–Zr [385] alloys and in the magnesium ZK60 alloy [386,387]. In practice, however, these exceptionally high tensile elongations are not a strict

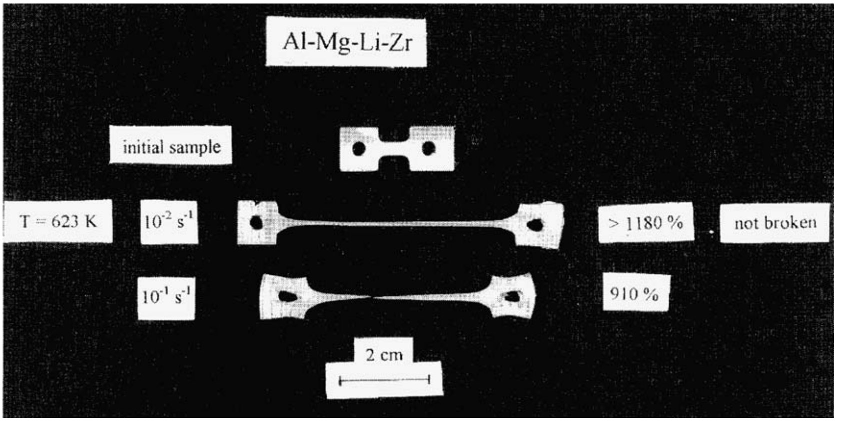

Fig. 67. A first demonstration of the occurrence of high strain rate superplasticity in a commercial Al–Mg–Li–Zr alloy after processing by ECAP: the upper specimen is untested [376].

requirement for the utilization of sheet metals in superplastic forming operations because complex parts can be readily formed using alloys exhibiting maximum elongations of ~400% [388]. Thus, it is encouraging to note that tensile elongations of >500% have been achieved after ECAP processing in alloys of Al–Mg–Li–Zr [389–393], Al–Mg–Li–Sc–Zr [212,394,395], Al–Cu–Li–Zr [394], Al–Mg–Sc [181,259,368,396–400], Al–Zn–Mg–Cu–Zr (Al-7034) [214,260,401,402], Al–Mg–Mn–Cr–Sc (modified Al-5083) [403,404], Al–Cu–Mg–Mn (Al-2024) [369], Al–Zn–Mg–Cu–Zr (Al-7055) [405], Cu–Zn [217], Cu–Zn–Sn [406], Mg–Al [407], Mg–Al–Zr [225], Mg–Al–Zn (AZ61) [408,409] and (AZ91) [410–413], Mg–Zn–Zr (ZK60) [412–414] and Zn–Al [241].

Another advantage of the UFG structure is the occurrence of superplasticity at lower temperatures by comparison with the effects observed in conventional micrometer-grained materials. This effect was demonstrated for the first time using Al and Mg alloys subjected to high pressure torsion [13,415] but in later work the same effect was also demonstrated using processing by ECAP [47]. At the present time, there are many examples confirming the possibility of reducing the temperature of superplasticity by 100–200 °C through the use of the ECAP process and this trend is clearly of great practical importance for any future use of these materials in commercial superplastic forming operations.

7.2.2. Effects of different types of ECAP processing on superplasticity

The potential for achieving excellent superplastic properties after ECAP is clearly demonstrated in Fig. 68 where experimental data are presented for a commercial spray-cast Al-7034 alloy [260]. This alloy was produced by spray-casting and the grain size was only ~2.1 μm in the as-received condition. Nevertheless, processing by ECAP reduced the grain size to ~0.3 μm after 6 passes at a pressing temperature of 473 K. Fig. 68 shows a plot of the elongation to failure versus strain rate for tensile tests conducted at temperatures from 573 to 698 K for (a) the as-received condition and (b) the as-pressed condition after ECAP: in addition, points are shown in Fig. 68(b) after pressing through both 6 and 8 passes of ECAP. The relatively high elongations attained in the as-received alloy reflect both the very small grain size in the spray-cast condition and the typical occurrence of enhanced

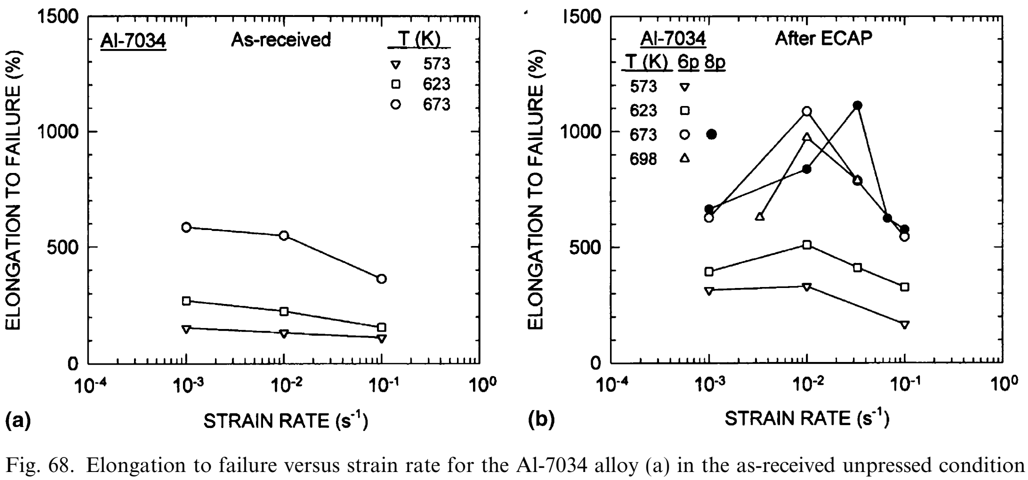

Fig. 68. Elongation to failure versus strain rate for the Al-7034 alloy (a) in the as-received unpressed condition and (b) after processing by ECAP for 6 or 8 passes [260].

ductilities in dilute Al–Mg alloys where dislocation glide and the dragging of solute atom atmospheres is generally the dominant rate-controlling process within the intragranular creep regime [416,417] but the datum points in Fig. 68(b) show the very enhanced ductilities that may be attained after ECAP. Furthermore, high elongations are achieved at a strain rate of 10^{-2} s^{-1} and there is evidence from the points for specimens pressed through 8 passes that the curve of elongation versus strain rate may be displaced to faster strain rates when samples are pressed to larger numbers of passes.

The latter trend is more clearly visible in Fig. 69 which shows experimental data for an Al–Mg–Li–Zr alloy [392]. Both plots delineate the elongation to failure versus the strain rate for testing temperatures from 573 to 723 K with the open points depicting samples processed by ECAP and the solid points depicting unpressed samples tested at a temperature of 603 K. Two different processing conditions are represented in Fig. 69: in Fig. 69(a) the samples were pressed using route B_C for a total of 4 passes at 673 K and in Fig. 69(b) the samples were pressed using route B_C for 8 passes at 673 K and, in order to minimize the extent of grain growth during ECAP, an additional 4 passes at the lower temperature of 473 K. Thus, the open points in Fig. 69(a) correspond to a total imposed strain of ~4 whereas the open points in Fig. 69(b) correspond to a total imposed strain of ~12. Two important conclusions may be reached by inspection of Fig. 69. First, the elongations to failure are significantly enhanced by ECAP processing by comparison with the unpressed material. Second, the peak elongations are displaced to faster strain rates when the samples are subjected to larger numbers of passes in ECAP. Thus, exceptionally high elongations are achieved at strain rates of 10^{-1} to 1 s^{-1} after pressing through 12 passes with elongations to failure up to >1000% in this strain rate range. The displacement to faster strain rates with increasing numbers of passes through the die is consistent with experimental results for pure aluminum showing that the fraction of high-angle grain boundaries increases with increasing numbers of passes through the ECAP die as illustrated earlier in Fig. 42 [172].

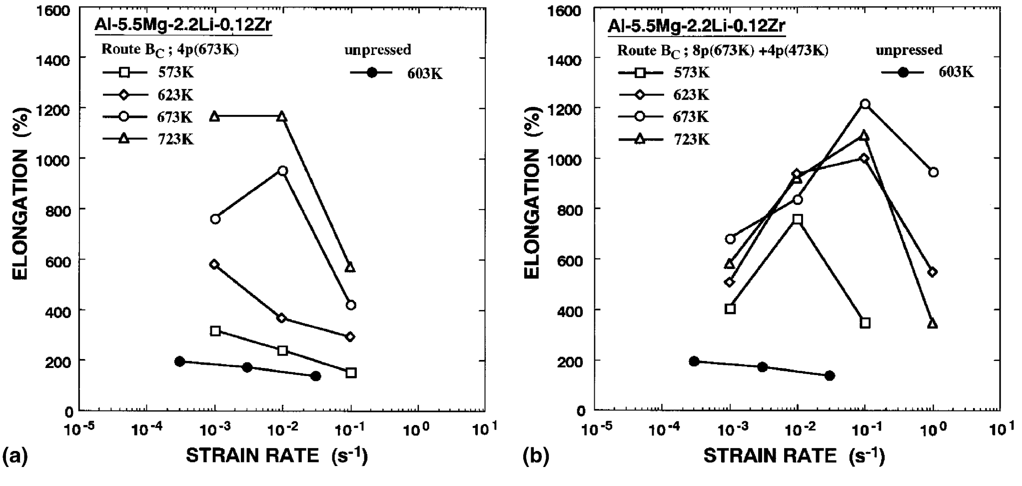

Fig. 69. Elongation to failure versus strain rate for an Al–Mg–Li–Zr alloy after ECAP (a) through 4 passes at 673 K and (b) through 8 passes at 673 K and an additional 4 passes at 473 K: the solid points denote the as-received unpressed condition [392].

Another ECAP parameter which may have a strong effect on the development of superplasticity is the temperature of pressing. This issue was investigated in detail recently focusing on the Al-1420 alloy (Al–5.5%Mg–2.2%Li–0.12%Zr) subjected to ECAP with 8 passes at the three different temperatures of 340, 370 and 400 °C [393]. It was established in this work that the elongation to failure achieved at a temperature of 400 °C with a strain rate of 10^{-2} s^{-1} depended strongly on the temperature used in the ECAP processing and in practice the maximum superplastic elongation of over 1500% was observed after pressing at 370 °C. This effect is associated with the presence of precipitations of the second phase of $Al(Mg,Li,Zr)_x$, the morphology of which is determined by the precise processing regime of ECAP.

The ECAP processing of magnesium alloys is often difficult because of the limited number of slip systems in the hexagonal crystal structure: for example, the application of ECAP to samples of cast pure magnesium was effective only in reducing the grain size from ~400 μm to ~120 μm after 3 passes of ECAP at 673 K [418]. However, Mg-based alloys are becoming increasingly important because of their low density, good machinability and excellent recycling capabilities [419]. Accordingly, efforts were made to develop a processing procedure that may be used to produce a superplastic forming capability in dilute magnesium alloys.

Experiments suggest that ECAP is most effective in Mg-based alloys when using a two-step procedure in which the material is prepared initially by extrusion and then subsequently processed by ECAP [420]. This two-step process, designated EX-ECAP, was used effectively with a Mg–Zr alloy [224,420] and subsequently with Mg–Al [407], Mg–Al–Zr [225] and Mg–Al–Zn [409] alloys. An example of the success of this approach is shown in Fig. 70 for a Mg–9%Al alloy where data are shown for the cast condition, for the cast condition after extrusion and for the cast condition followed by the two-step EX-ECAP procedure [407]. For the latter condition, the elongations to failure extend to >800% at the slowest experimental strain rate. The success of the intermediate extrusion step is attributed to the production of a texture in extrusion where a majority of the basal

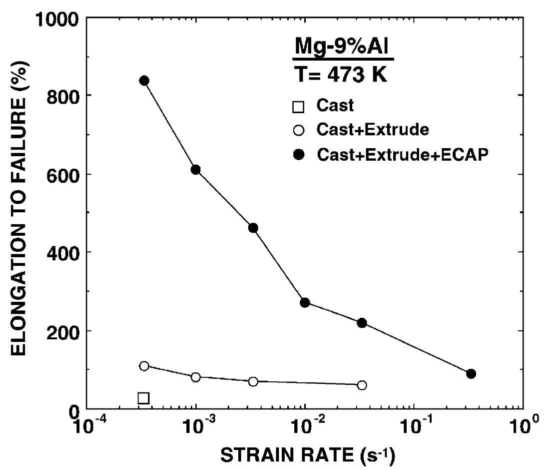

Fig. 70. Elongation to failure versus strain rate at 473 K for a cast Mg–9%Al alloy, for the cast alloy after extrusion and for the cast alloy after extrusion and ECAP for 2 passes at 473 K [407].

(0001) planes lie parallel to the extrusion direction [421,422] so that the basal planes are no longer oriented for easy slip in the subsequent processing by ECAP.

7.2.3. Developing a superplastic forming capability

The production of polycrystalline metals with ultrafine grain sizes suggests that, if the grain sizes are reasonably stable at elevated temperatures, these materials will readily exhibit superplastic characteristics. The preceding section demonstrates the potential for achieving superplastic elongations in tensile testing in the laboratory but it is necessary also to evaluate the potential for making use of these materials in industrial superplastic forming operations.

The Al–3%Mg–0.2%Sc alloy exhibits remarkable superplastic properties after pressing for 8 passes at room temperature using route B_C, including elongations to failure exceeding 2000% when testing in tension at temperatures of 673 and 723 K [379]. This suggests, therefore, that this alloy will be formed relatively easily under an external pressure. To check this hypothesis, thin disks were cut from a pressed billet after pressing through 8 passes at room temperature and these disks were inserted individually into a biaxial gas-pressure forming facility. Each disk was heated to 673 K and then subjected to a constant pressure of argon gas for a very short period of time.

Examples of representative disks achieved in this die-less facility are shown in Fig. 71 where the disk on the left at (a) is untested and the other disks were held under a gas pressure of 10 atmospheres, equivalent to 1 MPa, for periods of 30 s for disk (b) and 60 s for disk (c) [377]. The formation of the domes demonstrates the excellent superplastic forming capability of this alloy in the as-pressed condition especially when it is noted that the domes were formed using a pressure that is representative of conventional superplastic forming operations. Furthermore, by sectioning the domes and measuring the local thicknesses at incremental points around each dome, it was possible to estimate a thinning factor denoting the ratio of the measured thickness at any point on the dome to the average thickness assuming constant volume and uniform deformation [423]. The significance of the value of the thinning factory is that an ideal solid has a value of 1.0 but all real materials have values <1.0 with the lower values associated with materials where the forming operation is less uniform. The value of the thinning factor was estimated as ~0.85–0.89 for the dome shown on the right at Fig. 71(c) where the forming time was only 60 s. In practice, it is important to note that this value is exceptionally high and provides a very clear demonstration that processing by ECAP produces materials that can be superplastically-formed by blowing out in a very uniform manner. The high degree of uniformity experienced in this alloy after processing by ECAP is attributed to the extremely fine grain size produced in the pressing operation.

Despite the success of the forming operation shown in Fig. 71, industrial superplastic forming is conducted using sheet metals whereas the billets processed by ECAP are generally in the form of rods or bars. To evaluate the potential for maintaining a superplastic capability when these bars or rods are rolled into sheets, it is necessary to evaluate the mechanical behavior of materials subjected to ECAP followed by rolling. Experiments were conducted using the same Al–3% Mg–0.2%Sc alloy shown for the dome formation in Fig. 71. Billets, in the form of rods with diameters of 10 mm, were processed by ECAP to various numbers of passes at room temperature using route B_C and then they were subjected to cold-rolling (CR) by machining two flat parallel faces to give a bar with a thickness of 7 mm and rolling at room temperature to a final thickness of 2.2 mm equivalent to

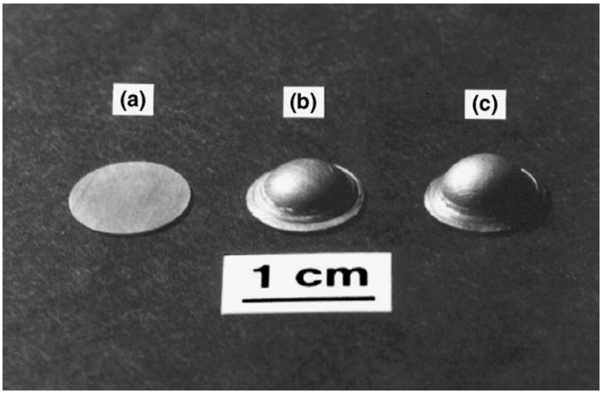

Fig. 71. Examples of superplastic forming at high strain rates in a gas-pressure forming facility: the Al–Mg–Sc disk at (a) is untested after ECAP and the other disks were processed by ECAP and then held at 673 K and subjected to a gas pressure of 10 atmospheres for (b) 30 s and (c) 60 s [377].

a reduction of ~70%. This reduction was achieved through incremental reductions of ~0.2 mm on each separate pass. Fig. 72 shows the measured elongations to failure as a function of the number of ECAP passes when testing at 673 K with an initial strain rate of $3.3 \times 10^{-2}\ s^{-1}$ for specimens after ECAP (open points) and after ECAP plus cold-rolling (closed points) [397]. These results confirm that the superplastic characteristics are retained in the subsequent rolling operation thereby suggesting that the grain boundaries retain their high angles of misorientation and thus their capacity for exhibiting grain boundary sliding during superplastic flow. It is apparent also from Fig. 72 that slightly larger elongations are achieved after ECAP and cold-rolling after 4 passes through the die, where this extra straining is due to the additional microstructural evolution that occurs in the rolling operation.

Alternative results were also reported recently using a modified Al-5154 alloy containing 0.13% Sc where the samples were taken to only 4 passes of ECAP, which is below the

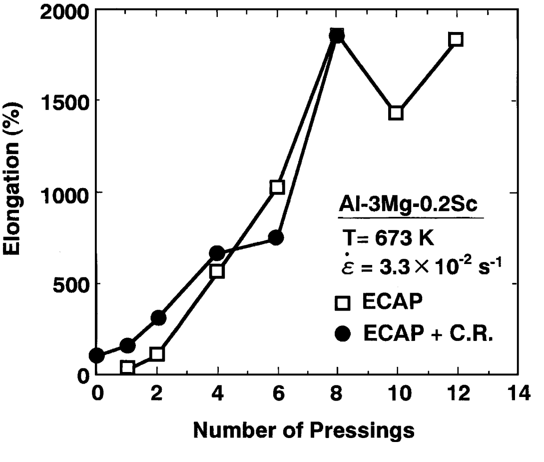

Fig. 72. Elongation to failure versus number of passes for an Al–Mg–Sc alloy after ECAP (open points) and after ECAP and cold-rolling (closed points) [397].

optimum superplastic condition, and then cold rolled to different reduction ratios before testing in tension at 723 K [399,400]. The results from this investigation suggested that it may be feasible to increase the superplastic forming capability of the alloy by rolling after ECAP since the measured elongations to failure gradually increased for rolling reductions at and above ∼70%. These results suggest that conventional rolling may be combined usefully with ECAP in the production of sheet metals for superplastic forming operations.

Finally, it is important to note that superplastic materials generally fail through the nucleation, growth and coalescence of internal cavities and it is important therefore to evaluate the cavitation characteristics of materials processed by ECAP and subsequently tested under superplastic conditions. There is only one report to date providing quantitative data to document the significance of cavitation in an alloy processed by ECAP and subsequently tested in tension within the regime of superplasticity [402]. In this work, which was conducted on an Al-7034 alloy tested in tension at 673 K, it was shown that the superplastic diffusion growth of cavities plays an important role in the early stages of cavity development but with a transition to plasticity-controlled growth at the larger cavity radii.

7.3. Functional properties: inelasticity and shape-memory effects

Processing by ECAP can have a strong effect not only on the mechanical properties but also on the functional properties of materials. However, detailed investigations into this topic have started only recently and so far there are very few individual interesting examples. Among them, however, and worthy of special emphasis, are the considerable enhancement of the coercive force in hard magnetic alloys after ECAP [281,424] and the modification of the corrosion behavior of UFG-structured Cu [425]. In recent years, an exhibition of the capabilities of thermoelastic martensitic transformations and thermomechanical memory in alloys based on titanium nickelide, which has aroused the greatest scientific and practical interest, has been the object of more systematic studies. These alloys have the highest strength and ductility properties and exhibit thermomechanical memory effects that are unique in both their magnitude and their reproducibility. In addition, they exhibit good weldability, good corrosion resistance, and biocompatibility. The TiNi alloys are generally characterized by good workability in metallurgical processes and in subsequent industrial procedures [426–428].

Using SPD processing by high pressure torsion at room temperature, TiNi alloys can be transformed to an amorphous state and by further annealing to an ultrafine-grained structure with an extremely small grain size of ∼20–30 nm [429,430]. Such a nanocrystalline structure has a strong influence on the kinetics of the martensitic transformation and on the functional properties of the TiNi alloys [431]. However, these alloys cannot be processed by ECAP at room temperature due to their low deformability and accordingly several reports have appeared describing the fabrication of ultrafine-grained alloys using ECAP at elevated temperatures [430,432].

The materials under study, the $Ti_{49.8}Ni_{50.2}$ and $Ti_{49.4}Ni_{50.6}$ alloys, have temperatures for the martensitic transformation, M_s, equaling 75–80 °C. The initial condition was a quenched state with water quenching at 800 °C for 1 h. In this condition, the microstructures of the alloys consisted of polyhedral grains with a mean grain size of ∼80 μm. During ECAP processing of the TiNi alloys, the variable parameters in the processing operation

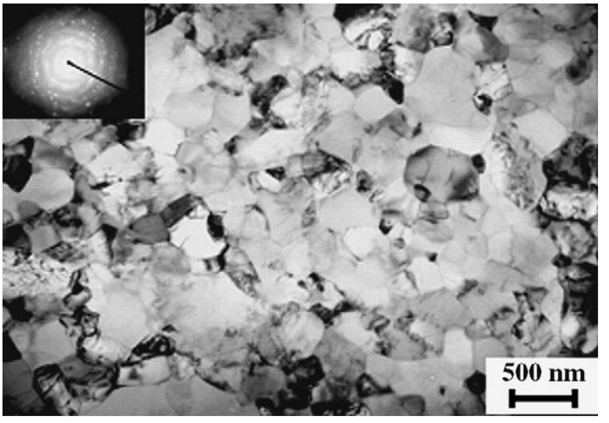

Fig. 73. Microstructure of the $Ti_{49.8}Ni_{50.2}$ alloy on the transverse section after ECAP at 450 °C for 8 passes [433].

are the number of passes (from 1 to 12 passes) and the temperature of the isothermal pressing (from 400 to 500 °C).

Processing by ECAP leads to considerable microstructural refinement and the formation of an ultrafine-grained structure refined down to ~250 nm after ECAP through 8 passes at 450 °C. This microstructure is illustrated in Fig. 73 and the UFG structure is thermally stable during annealing at temperatures up to 500 °C [433].

By comparison with the initial coarse-grained state, processing by ECAP leads to a considerable change in the mechanical properties of TiNi alloys including increases in the coefficient of strain hardening, the yield strength and the ultimate strength. For example, the ultimate strength, σ_B, of the $Ti_{49.8}Ni_{50.2}$ alloy increases with increasing numbers of ECAP passes at a temperature of 450 °C and reaches a maximum value of 1250 MPa after 8 passes while the yield strength increases by more than two times reaching a maximum of 1150 MPa. These results are shown in Fig. 74 and it is important to emphasize that the maximum ultimate strength is 30% higher and the yield strength is two times higher than in the initial coarse-grained state [433]. Additional annealing after ECAP at a temperature of 500 °C for 1 h leads to an increase in the elongation to failure, with values of δ up to ~50% and only a minor change in the strength properties.

The characteristic temperatures of the martensitic transformations, M_s, M_f, A_s, A_f, were determined in the TiNi alloys using the dilatometric method [433]. To characterize the functional properties, the maximum fully-recoverable strain, ε_r, and the maximum reactive stress, σ_r, were estimated. It was found that processing by ECAP leads to a fall in all of the characteristic temperatures of the martensitic transformations of the TiNi alloys by comparison with the quenched state. In the $Ti_{49.8}Ni_{50.2}$ alloy, this effect increases in magnitude when the number of passes is increased to 4 and thereafter it becomes stabilized or may even become slightly weaker. At 4–8 passes of ECAP, the fall in temperatures is of the order of 20 ± 5 °C by comparison with the quenched state.

The maximum fully recoverable strain, ε_r^{max}, increases with an increasing number of passes reaching a maximum at 4 passes (9%) and then slightly decreases with additional passes (down to 8–7.5%). At the same time, the maximum reactive stress, σ_r^{max}, increases with an increasing number of passes to reach the largest value of 1100 MPa at 12 passes. The growth in σ_r^{max} with increasing accumulated strain correlates well with the behavior of

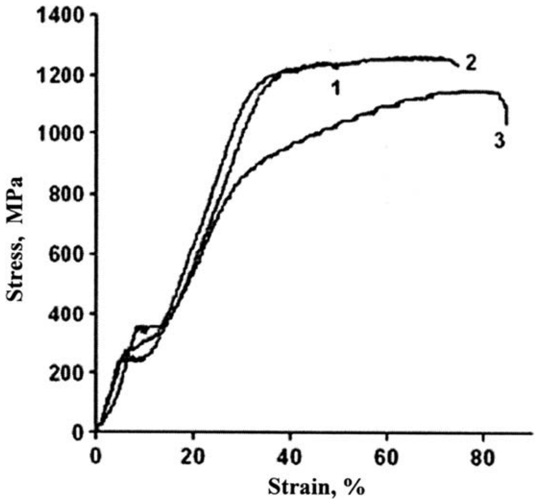

Fig. 74. Engineering stress–strain curves in tension for the $Ti_{49.8}Ni_{50.2}$ alloy (1) after ECAP at 450 °C for 8 passes and after ECAP and subsequent annealing for 1 h at temperatures of (2) 500 °C and (3) 600 °C [433].

the yield strength which in turn is dictated by a decrease in the grain/subgrain size and an increase in the dislocation density.

It is apparent, therefore, that ECAP processing leads to an enhancement of the two most important functional characteristics of the shape-memory alloys, namely the maximum reactive stress and the maximum fully-recoverable strain [433]. It is important to note also that this trend is not observed when other types of mechanical processing or thermomechanical treatments are employed. The maximum reactive stress of 1100 MPa is much higher than the corresponding values both in the coarse-grained state and after conventional treatments. At the same time, such a high value of the fully-recoverable strain in the TiNi alloy (9%), which was achieved as a result of ECAP conducted at 450 °C, represents a record value that has never been previously observed in alloys such as TiNi subjected to conventional thermomechanical treatments.

Processing by ECAP of the $Ti_{49.4}Ni_{50.6}$ alloy conducted over a broad range of temperatures from 23 to 60 °C led to the observation of a superelasticity effect and this result is quite significant [432]. It is known that there is no noticeable superelasticity effect in the coarse-grained alloy. Nevertheless, in the alloy processed by ECAP there was a perfect superelasticity effect even at 20 °C with a value reaching $\sim$7% while the residual strain was $\leqslant$0.2%.

It can be concluded from these experiments that ECAP processing of TiNi alloys has introduced a high-strength state and simultaneously introduced a unique combination of functional characteristics [432–435]. These results are therefore very promising for the future expansion of the application areas for these alloys.

8. Future prospects for applying ECAP in manufacturing

At the present time, SPD techniques are beginning to emerge from the domain of laboratory-scale research and to receive serious consideration for their potential in the commercial production of various ultrafine-grained materials [4,436–439]. This change is revealed in several features. First, it is characterized by the fact that not only pure metals are under investigation but also extensive research is currently underway on commercial alloys for special applications. Second, it is demonstrated by the attention which is now focused on the requirement for developing an economically-feasible production procedure for the processing of ultrafine-grained metals and alloys.

Processing by ECAP is at present one of the most promising techniques for manufacturing UFG structures in different metals and alloys and the various parameters associated with the processing operation have been described in detail in this review. Concerning the economically-feasible production of UFG metals, there are several tasks which must be addressed during processing development. Among these tasks are a reduction of the material waste, the fabrication of bulk billets and semi-products in the form of rods, sheets and wires with a homogeneous UFG structure and superior properties and, most important, raising the efficiency of the ECAP processing technique.

As an example of an approach to the solution of these tasks, consider the results obtained from developing two processing routes, including ECAP, for the fabrication of long rods of nanostructured Ti materials for medical applications [438]. In developing nanostructured Ti materials for medical use, a very clear advantage was demonstrated in combining ECAP with other techniques of metal forming such as rolling, forging or extrusion [186,440]. These advantages are connected with the effective shaping of long-size semi-products in the form of sheets or rods together with the further enhancement of properties introduced by ECAP in UFG materials. For example, in Grade 2 commercial purity (CP) Ti, high strength with a yield stress of 980 MPa and UTS of 1100 MPa and a reasonable elongation to failure of $\delta = 12\%$ was attained using a combination of ECAP and extrusion. These investigations used ECAP and thermomechanical treatments (TMT), including forging and rolling, and this permitted the fabrication of Ti rods with a diameter of 6.5 mm and lengths of more than 800 mm [441].

Fig. 75 presents TEM micrographs of CP Ti subjected to a combination of ECAP and subsequent TMT to a strain, ε, of 80%, where (a) is the cross-section and (b) is a longitudinal section [441]. It can be seen that this combined processing leads to very significant additional grain refinement from $\sim$300–400 nm after ECAP to $\sim$100 nm after the combined operation although the additional refinement is associated with considerable elongation of the grains. It was shown through mechanical testing, as documented in Table 2, that TMT after ECAP leads to an increase in the strength of CP Ti as recorded by the values for $\sigma_{0.2}$ and the UTS and at the same time there is sufficient ductility as denoted by the values for δ. The final column in Table 2 shows the values for the reductions in area in the failed samples, Λ, for the three different testing conditions. It is important to note that these values of strength for nanostructured CP Ti are significantly higher than those associated with the Ti–6%Al–4%V alloy which is widely used in current medical applications and other aspects of engineering.

It is also interesting that the microstructure and properties of the rods processed in this way were reasonably uniform with a dispersion in the mechanical properties along the length of the rods not exceeding ±5% [441]. In addition, the rate of material utilization was more than 65%. These results demonstrate, therefore, the great potential for using a combination of SPD processing and TMT for the commercial production of semi-products from Ti for medical applications. It is reasonable to anticipate that similar approaches may be used also to fabricate UFG materials for a range of other applications as, for

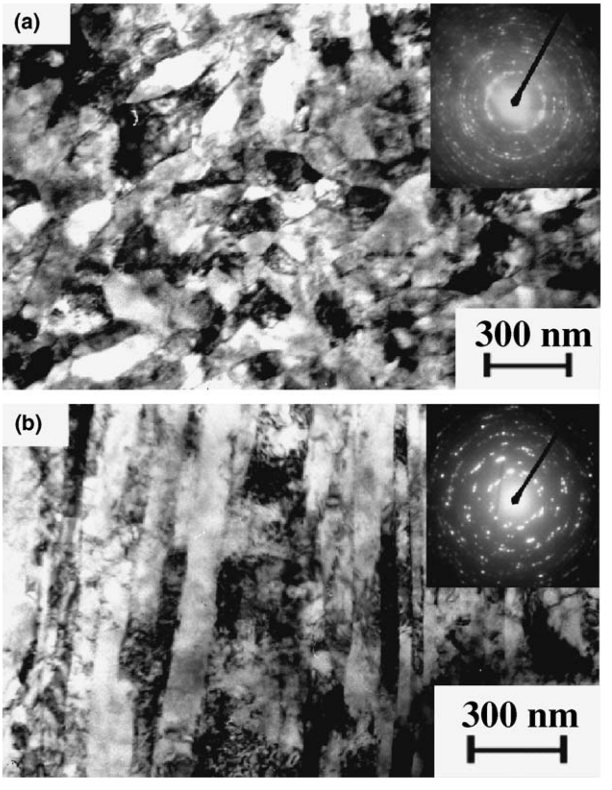

Fig. 75. Micrographs in TEM showing the microstructure of Grade 2 Ti after ECAP + TMT to a strain of 80%: (a) cross-section and (b) longitudinal section [438].

Table 2
Mechanical properties of Ti billets at different stages of processing [438]

State	$\sigma_{0.2}$ {MPa)	UTS (MPa)	δ {%}	Λ{%}
Initial	370	440	38	60
ECAP after 4 passes	545	630	22	51
ECAP after 4 passes + TMT to a strain of $\varepsilon = 80\%$	1100	1150	11	56

example, in weight-sensitive products such as high-performance mountain bicycles and automotive components [4].

Scaling to larger billet sizes is equally feasible in ECAP. For example, Fig. 76 shows three types of billets of ultrafine-grained Ti with different diameters of 20, 40 and 60 mm [442,443]. A second example is shown in Fig. 77 where specimens of a commercial Al-1100 alloy were pressed at room temperature with diameters of 6, 10 and 40 mm [444]. An examination of the microstructures of the latter samples confirmed that the refinement of the initial microstructure was essentially independent of the specimen size [444]. However, care must be exercised because there is evidence that frictional effects between the samples and the die walls may influence the internal microstructures when the cross-sectional diameter is reduced to a size below $\sim$5 mm [54]. This latter effect may be important

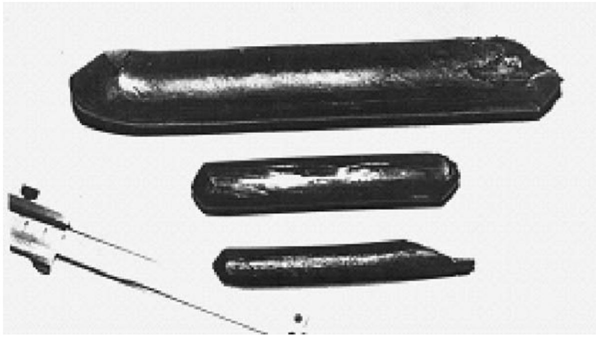

Fig. 76. Bulk titanium billets with diameters of 20, 40 and 60 mm after processing by ECAP [442,443].

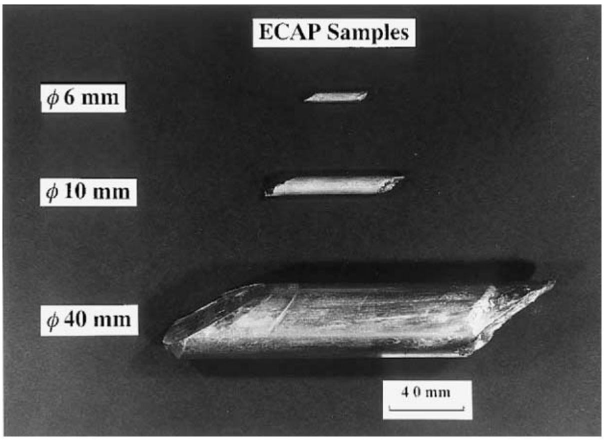

Fig. 77. Typical appearance of the samples of an Al-1100 alloy after ECAP with diameters of 6, 10 and 40 mm [444].

if, for example, processing by ECAP is used for the fabrication of materials for MEMS applications. A very recent investigation evaluated the effect of scaling-up on the mechanical properties, microstructure and the hot-workability of the Al-6061 alloy from a laboratory scale with a diameter of 12.5 mm to an industrial scale with a diameter of 100 mm [445]. This latter investigation and all earlier studies have consistently confirmed the feasibility of successfully scaling ECAP processing in the fabrication of large-scale components.

With regard to the reduction of material waste, a continuous process, such as a combination of ECAP and Conform-processing [93] as described in Section 2.5.2, is especially effective in minimizing the wastage. For example, the material utilization rate is very high in the ECAP–Conform process and typically exceeds ~90%.

Thus, although work on the application of ECAP in the manufacturing of UFG metals was initiated only recently, the examples reported to date provide very clear demonstrations of the broad prospects that are now becoming apparent for the future utilization of ECAP in the successful commercialization of ultrafine-grained materials.

9. Summary

During the last two decades, equal-channel angular pressing has progressed from being a relatively minor metal processing technique to becoming a well-established and recognized procedure for achieving very significant grain refinement in a wide range of metallic alloys. Starting from the mid-1990s, processing by ECAP has attracted the close attention of researchers from many different laboratories and the procedure has experienced active development in several areas. These developments include not only the application of ECAP to many different metals and alloys but also the establishment of the basic principles of ECAP for microstructural refinement.

At the present time, ECAP is the most well developed of all potential SPD processing techniques. Furthermore, the fundamental principles of ECAP, dealing with the mechanics of metal flow and the microstructural evolution, provide useful tools that can be utilized both in the development of new SPD methods and in the future exploitations of some of the existing but underdeveloped SPD techniques. In this context it is important to recognize that processing by ECAP represents an effective tool for achieving grain refinement but the basic principles of this refinement are not unique to the ECAP process. Thus, it is reasonable to assume that the same fundamental principles may be applied in interpreting, and ultimately in successfully developing, other SPD procedures. Using the definitions introduced in Section 1, there is now a good understanding of the basic principles of SPD processing and the role of these principles in the production of bulk ultrafine-grained materials. Nevertheless, there is an important requirement in future investigations both to more rigorously establish the physical mechanisms of UFG structure formation under intense plastic straining and to define and quantify the parameters of SPD processing that dictate the minimum achievable grain size.

From the practical point of view, it is important to acknowledge that recent studies have demonstrated very clearly a great potential for the use of SPD processing and the incorporation of ECAP in industrial applications. There are very good reasons for believing that, in the relatively near future, SPD processing will become established as the basis for the commercial production of semi-products and products with UFG structures using a wide range of metals and alloys.

Acknowledgements

Our understanding of ECAP has developed over a period of several years through our many close interactions with colleagues and associates around the world. We are pleased to have this opportunity to express our sincere appreciation to all who have contributed to the development and understanding of the principles of the ECAP process. It is a special pleasure to acknowledge our co-authors for their stimulating collaborations and for actively working with us to publish many joint publications: a number of these papers are cited in the reference section.

Many people contributed to the preparation of this article but we must especially thank Julia Bazhenova of Ufa State Aviation Technical University for assisting in the preparation of several parts of this overview and Cheng Xu and Megumi Kawasaki of the University of Southern California for assistance in preparing the Figures. The preparation of this paper was made possible through the support of the International Science and Technology Center (Moscow) under NIS-IPP projects LANL-T2-0193 and LANL-T2-0197 and the

Russian Federation for Basic Research (RZV) and the support of the National Science Foundation of the United States under Grant No. DMR-0243331 and the U.S. Army Research Office under Grant No. W911NF-05-1-0046 (TGL).

References

[1] Hall EO. Proc Roy Soc B 1951;64:747.
[2] Petch NJ. J Iron Steel Inst 1953;174:25.
[3] Valiev RZ. Nature Mater 2004;3:511.
[4] Zhu YT, Lowe TC, Langdon TG. Scripta Mater 2004;51:825.
[5] Gleiter H. In: Hansen N, Horsewell A, Leffers T, Lilholt H, editors. Deformation of polycrystals: Mechanisms and microstructures. Roskilde, Denmark: Risø National Laboratory; 1981. p. 15.
[6] Gleiter H. Prog Mater Sci 1989;33:223.
[7] Erb U, El-Sherik AM, Palumbo G, Aust KT. Nanostruct Mater 1993;2:383.
[8] Koch CC, Cho YS. Nanostruct Mater 1992;1:207.
[9] Luton MJ, Jayanth CS, Disko MM, Matras S, Vallone J. Mater Res Soc Symp Proc 1989;132:79.
[10] Witkin DB, Lavernia EJ. Prog Mater Sci 2006;51:1.
[11] Han BQ, Matejczyk D, Zhou F, Zhang Z, Bampton C, Lavernia EJ, et al. Metall Mater Trans 2004;35A:947.
[12] Valiev RZ, Mulyukov RR, Ovchinnikov VV. Philos Mag Lett 1990;62:253.
[13] Valiev RZ, Krasilnikov NA, Tsenev NK. Mater Sci Eng 1991;A137:35.
[14] Musalimov RSh, Valiev RZ. Scripta Metall Mater 1992;27:1685.
[15] Valiev RZ, Islamgaliev RK, Alexandrov IV. Prog Mater Sci 2000;45:103.
[16] Wang JT. Mater Sci Forum 2006;503–504:363.
[17] Sherby OD, Wadsworth J. J Mater Proc Tech 2001;117:347.
[18] Srinivasan S, Ranganathan S. India's legendary wootz steel: An advanced material of the ancient world. Bangalore, India: National Institute of Advanced Studies and Indian Institute of Science; 2004.
[19] Bridgman PW. Studies in large plastic flow and fracture. New York (NY): McGraw-Hill; 1952.
[20] Segal VM, Reznikov VI, Drobyshevskiy AE, Kopylov VI. Russian Metall 1981;1:99.
[21] Segal VM. Mater Sci Eng 1995;A197:157.
[22] Segal VM, Dobatkin SV, Valiev RZ, editors. Equal-channel angular pressing of metallic materials: Achievements and trends. Thematic issue, Part 1, Russian Metall, vol. 2004, no. 1, pp. 1–102 [translated from Metally 2004, no. 1, p. 3–119].
[23] Smirnova NA, Levit VI, Pilyugin VI, Kuznetsov RI, Davydova LS, Sazonova VA. Fiz Met Metalloved 1986;61:1170.
[24] Valiev RZ, Kaibyshev OA, Kuznetsov RI, Musalimov RSh, Tsenev NK. Proc USSR Acad Sci 1988;301:864.
[25] Zhilyaev AP, Nurislamova GV, Kim BK, Baró MD, Szpunar JA, Langdon TG. Acta Mater 2003;51:753.
[26] Salishchev GA, Valiahmetov OR, Galeev RM. J Mater Sci 1993;28:2898.
[27] Valitov VA, Salishchev GA, Muhtarov ShH. Russian Metall 1994;3:127.
[28] Sitdikov O, Sakai T, Goloborodko A, Miura H, Kaibyshev R. Mater Trans 2004;45:2232.
[29] Beygelzimer Y, Varyukhin V, Orlov D, Synkov S, Spuskanyuk A, Pashinska Y. In: Zehetbauer MJ, Valiev RZ, editors. Nanomaterials by severe plastic deformation. Weinheim, Germany: Wiley–VCH Verlag; 2004. p. 511.
[30] Varyutkhin VN, Beygelzimer YY, Synkov S, Orlov D. Mater Sci Forum 2006;503–504:335.
[31] Richert J, Richert M. Aluminium 1986;62:604.
[32] Richert M, Liu Q, Hansen N. Mater Sci Eng 1999;A260:275.
[33] Chu HS, Liu KS, Yeh JW. Metall Mater Trans 2000;31A:2587.
[34] Chu HS, Liu KS, Yeh JW. Scripta Mater 2001;45:541.
[35] Huang JY, Zhu YT, Jiang H, Lowe TC. Acta Mater 2001;49:1497.
[36] Zhu YT, Jiang H, Huang J, Lowe TC. Metall Mater Trans 2001;32A:1559.
[37] Shin DH, Park JJ, Kim YS, Park KT. Mater Sci Eng 2002;A328:98.
[38] Zhao X, Jing TF, Gao YW, Zhou JF, Wang W. Mater Lett 2004;58:2335.
[39] Saito Y, Tsuji N, Utsunomiya H, Sakai T, Hong RG. Scripta Mater 1998;39:1221.
[40] Saito Y, Utsunomiya H, Tsuji N, Sakai T. Acta Mater 1999;47:579.

[41] Rhodes CG, Mahoney MW, Bingel WH, Spurling RA, Bampton CC. Scripta Mater 1997;36:69.
[42] Mishra RS, Ma ZY. Mater Sci Eng 2005;R50:1.
[43] Hofmann DC, Vecchio KS. Mater Sci Eng 2005;A402:234.
[44] Segal VM. USSR Patent No. 575892, 1977.
[45] Lowe TC, Valiev RZ, editors. Investigations and applications of severe plastic deformation. Dordrecht, The Netherlands: Kluwer Academic Publishers; 2000.
[46] Valiev RZ, Tsenev NK. In: Langdon TG, Merchant HD, Morris JG, Zaidi MA, editors. Hot deformation of aluminum alloys. Warrendale (PA): The Minerals, Metals and Materials Society; 1991. p. 319.
[47] Valiev RZ, Korznikov AV, Mulyukov RR. Mater Sci Eng 1993;A168:141.
[48] Valiev RZ, editor. Ultrafine-grained materials prepared by severe plastic deformation: Special issue. Annales de Chimie, Sci Mater 1996;21:369.
[49] Segal VM. Mater Sci Eng 1999;A271:322.
[50] Furukawa M, Horita Z, Nemoto M, Langdon TG. J Mater Sci 2001;36:2835.
[51] Segal VM. Mater Sci Eng 2002;A338:331.
[52] Segal VM. Mater Sci Eng 2003;A345:36.
[53] Segal VM. Mater Sci Eng 2004;A386:269.
[54] Berbon PB, Furukawa M, Horita Z, Nemoto M, Langdon TG. Metall Mater Trans 1999;30A:1989.
[55] Nakashima K, Horita Z, Nemoto M, Langdon TG. Mater Sci Eng 2000;A281:82.
[56] Furukawa M, Iwahashi Y, Horita Z, Nemoto M, Langdon TG. Mater Sci Eng 1998;A257:328.
[57] Kamachi M, Furukawa M, Horita Z, Langdon TG. Mater Sci Eng 2003;A361:258.
[58] Ferrasse S, Segal VM, Kalidini SR, Alford F. Mater Sci Eng 2004;A368:28.
[59] Ferrasse S, Segal VM, Alford F. Mater Sci Eng 2004;A372:44.
[60] Ferrasse S, Segal VM, Alford F. Mater Sci Eng 2004;A372:235.
[61] Kamachi M, Furukawa M, Horita Z, Langdon TG. Mater Trans 2004;45:2521.
[62] Nishida Y, Arima H, Kim JC, Ando T. J Jpn Inst Metals 2000;64:1224.
[63] Nishida Y, Arima H, Kim JC, Ando T. J Jpn Inst Light Metals 2000;50:655.
[64] Nishida Y, Arima H, Kim JC, Ando T. Scripta Mater 2001;45:261.
[65] Kim JC, Nishida Y, Arima H, Ando T. Mater Lett 2003;57:1689.
[66] Ma A, Suzuki K, Nishida Y, Saito N, Shigematsu I, Takagi M, et al. Acta Mater 2005;53:211.
[67] Ma A, Suzuki K, Saito N, Nishida Y, Takagi M, Shigematsu I, et al. Mater Sci Eng 2005;A399:181.
[68] Sun ZM, Hashimoto H, Keawprak N, Ma AB, Li LF, Barsoum MW. J Mater Res 2005;20:895.
[69] Ma A, Nishida Y, Suzuki K, Shigematsu I, Saito N. Scripta Mater 2005;52:433.
[70] Watazu A, Shigematsu I, Ma A, Suzuki K, Imai T, Saito N. Mater Trans 2005;46:2098.
[71] Ma A, Takagi M, Saito N, Iwata H, Nishida Y, Suzuki K, et al. Mater Sci Eng 2005;A408:147.
[72] Azushima A, Aoki K. Mater Sci Eng 2002;A337:45.
[73] Liu ZY, Liang GX, Wang ED, Wang ZR. Mater Sci Eng 1998;A242:137.
[74] Liu Z, Wang Z. J Mater Proc Tech 1999;94:193.
[75] Raab GI, Valiev RZ, Kulyasov GV, Polozovsky VA. Russian Patent No. 2181314, 2002.
[76] Raab GI. Fizika i Tekhnika Vysokikh Davleniy (Physics and Engineering of High Pressures) 2004;14 (4):83.
[77] Raab GI. Mater Sci Eng 2005;A410-411:230.
[78] Lee JC, Seok HK, Han JH, Chung YH. Mater Res Bull 2001;36:997.
[79] Han JH, Seok HK, Chung YH, Shin MC, Lee JC. Mater Sci Eng 2002;A323:342.
[80] Lee JC, Seok HK, Suh JY, Han JH, Chung YH. Metall Mater Trans 2002;33A:665.
[81] Nam CY, Han JH, Chung YH, Shin MC. Mater Sci Eng 2003;A347:253.
[82] Lee JC, Suh JY, Ahn JP. Metall Mater Trans 2003;34A:625.
[83] Suh JY, Han JH, Oh KH, Lee JC. Scripta Mater 2003;49:185.
[84] Park JW, Kim JW, Chung YH. Scripta Mater 2004;51:181.
[85] Chakkingal U, Suriadi AB, Thomsen PF. Scripta Mater 1998;39:677.
[86] Chakkingal U, Suriadi AB, Thomsen PF. Mater Sci Eng 1999;A266:241.
[87] Alkorta J, Rombouts M, De Messemaeker J, Froyen L, Gil Sevillano J. Scripta Mater 2002;47:13.
[88] Utsunomiya H, Saito Y, Hayashi T, Sakai T. J Mater Eng Perform 1997;6:319.
[89] Saito Y, Utsunomiya H, Suzuki H, Sakai T. Scripta Mater 2000;42:1139.
[90] Utsunomiya H, Hatsuda K, Sakai T, Saito Y. Mater Sci Eng 2004;A372:199.
[91] Green D. J Inst Metals 1972;100:295.
[92] Etherington C. J Eng Indust 1974;96:893.
[93] Raab GJ, Valiev RZ, Lowe TC, Zhu YT. Mater Sci Eng 2004;A382:30.

[94] Xiang S, Matsuki K, Takatsuji N, Tokizawa M, Yokote T, Kusui J, et al. J Mater Sci Lett 1997;16:1725.
[95] Matsuki K, Aida T, Takeuchi T, Kusui J, Yokoe K. Acta Mater 2000;48:2625.
[96] Parasiris A, Hartwig KT. Int J Refract Metals Hard Metals 2000;18:23.
[97] Karaman I, Robertson J, Im JT, Mathaudhu SN, Luo ZP, Hartwig KT. Metall Mater Trans 2003;34A:247.
[98] Haouaoui M, Karaman I, Maier HJ, Hartwig KT. Metall Mater Trans 2004;35A:2935.
[99] Senkov ON, Senkova SV, Scott JM, Miracle DB. Mater Sci Eng 2005;A393:12.
[100] Xia K, Wu X. Scripta Mater 2005;53:1225.
[101] Semiatin SL, DeLo DP, Shell EB. Acta Mater 2000;48:1841.
[102] Semiatin SL, DeLo DP. Mater. Des. 2000;21:311.
[103] Shan A, Moon IG, Park JW. J Mater Proc Tech 2002;122:255.
[104] Xu C, Langdon TG. Scripta Mater 2003;48:1.
[105] Manna R, Agrawal P, Joshi S, Mudda BK, Mukhopadhyay NK, Sastry GVS. Scripta Mater 2005;53:1357.
[106] Iwahashi Y, Wang J, Horita Z, Nemoto M, Langdon TG. Scripta Mater 1996;35:143.
[107] Utyashev FZ, Enikeev FU, Latysh VV. Ann Chim 1996;21:379.
[108] Lee DN. Scripta Mater 2000;43:115.
[109] Xia K, Wang J. Metall Mater Trans 2000;32A:2639.
[110] Aida T, Matsuki K, Horita Z, Langdon TG. Scripta Mater 2001;44:575.
[111] Wu Y, Baker I. Scripta Mater 1997;37:437.
[112] Shan A, Moon IG, Ko HS, Park JW. Scripta Mater 1999;41:353.
[113] Iwahashi Y, Horita Z, Nemoto M, Langdon TG. Acta Mater 1997;45:4733.
[114] Furuno K, Akamatsu H, Oh-ishi K, Furukawa M, Horita Z, Langdon TG. Acta Mater 2004;52:2497.
[115] Nemoto M, Horita Z, Furukawa M, Langdon TG. Metals Mater 1998;4:1181.
[116] Horita Z, Furukawa M, Nemoto M, Langdon TG. Mater Sci Tech 2000;16:1239.
[117] Furukawa M, Horita Z, Langdon TG. Metals Mater 2003;9:141.
[118] Lee S, Langdon TG. Mater Res Soc Symp Proc 2000;601:359.
[119] Furukawa M, Horita Z, Langdon TG. Mater Sci Eng 2002;A332:97.
[120] Nakashima K, Horita Z, Nemoto M, Langdon TG. Acta Mater 1998;46:1589.
[121] Huang WH, Chang L, Kao PW, Chang CP. Mater Sci Eng 2001;A307:113.
[122] Alexandrov IV, Raab GI, Shestakova LO, Valiev RZ, Dowding RJ. In: Greenfield MS, Oakes JJ, editors. Tungsten, hard metals and refractory alloys, vol. 5. Princeton (NJ): Metal Powder Industries Federation; 2000. p. 27.
[123] Prangnell PB, Harris C, Roberts SM. Scripta Mater 1997;37:983.
[124] DeLo DP, Semiatin SL. Metall Mater Trans 1999;30A:1391.
[125] Bowen JR, Gholinia A, Roberts SM, Prangnell PB. Mater Sci Eng 2000;A287:87.
[126] Kim HS, Seo MH, Hong SI. Mater Sci Eng 2000;A291:86.
[127] Kim HS. Mater Sci Eng 2001;A315:122.
[128] Park JW, Suh JY. Metall Mater Trans 2001;32A:3007.
[129] Kim HS, Hong SI, Seo MH. J Mater Res 2001;16:856.
[130] Srinivasan R. Scripta Mater 2001;44:91.
[131] Suh JY, Kim HS, Park JW, Chang JY. Scripta Mater 2001;44:677.
[132] Kim HS. Mater Sci Eng 2002;A328:317.
[133] Kim HS. J Mater Res 2002;17:172.
[134] Pei QX, Hu BH, Lu C, Wang YY. Scripta Mater 2003;49:303.
[135] Baik SC, Hellmig RJ, Estrin Y, Kim HS. Z Metallkd 2003;94:754.
[136] Lee SC, Ha SY, Kim KT, Hwang SM, Huh LM, Chung HS. Mater Sci Eng 2004;A371:306.
[137] Chung SW, Somekawa H, Kinoshita T, Kim WJ, Higashi K. Scripta Mater 2004;50:1079.
[138] Xu C, Langdon TG. In: Jin Z, Beaudoin A, Bieler TA, Radhakrishnan B, editors. Hot deformation of aluminum alloys III. Warrendale (PA): The Minerals, Metals and Materials Society; 2003. p. 373.
[139] Luis Pérez CJ. Scripta Mater 2004;50:387.
[140] Luis Pérez CJ. Modell Simulat Mater Sci Eng 2004;12:205.
[141] Yamaguchi D, Horita Z, Nemoto M, Langdon TG. Scripta Mater 1999;41:791.
[142] Kim IY, Kim JY, Shin DH, Park JT. Metall Mater Trans 2003;34A:1555.
[143] Yamashita A, Yamaguchi D, Horita Z, Langdon TG. Mater Sci Eng 2000;A287:100.
[144] Shin DH, Pak JJ, Kim YK, Park KT, Kim YS. Mater Sci Eng 2002;A325:31.
[145] Chen YC, Huang YY, Chang CP, Kao PW. Acta Mater 2003;51:2005.
[146] Huang WH, Yu CY, Kao PW, Chang CP. Mater Sci Eng 2004;A366:221.

[147] Málek P, Cieslar M, Islamgaliev RK. J Alloys Compounds 2004;378:237.
[148] Goloborodko A, Sitdikov O, Kaibyshev R, Miura H, Sakai T. Mater Sci Eng 2004;A381:121.
[149] Wang YY, Sun PL, Kao PW, Chang CP. Scripta Mater 2004;50:613.
[150] Kim I, Kim J, Shin DH, Lee CS, Hwang SK. Mater Sci Eng 2003;A342:302.
[151] Nishida Y, Ando T, Nagase M, Lim SW, Shigematsu I, Watazu A. Scripta Mater 2002;46:211.
[152] Kim HS. Mater Trans 2001;42:536.
[153] Raab GI, Krasilnikov NA, Valiev RZ. Fizika i Tekhnika Vysokikh Davleniy (Physics and Engineering of High Pressures) 2000;10 (4):73.
[154] Stolyarov VV, Lapovok R, Brodova IG, Thomson PF. Mater Sci Eng 2003;A357:159.
[155] Stolyarov VV, Lapovok R. J Alloys Compounds 2004;378:233.
[156] Krasilnikov NA. Russian Metall 2005;2005 (3):35.
[157] Lapovok RYe. J Mater Sci 2005;40:341.
[158] Valiev RZ, Alexandrov IV, Lowe TC, Zhu YT. J Mater Res 2002;17:5.
[159] Lapovok RYe. Russian Metall 2004;2004 (1):44.
[160] Iwahashi Y, Furukawa M, Horita Z, Nemoto M, Langdon TG. Metall Mater Trans 1998;29A:2245.
[161] Kamachi M, Furukawa M, Horita Z, Langdon TG. Mater Sci Eng 2003;A347:223.
[162] Wang G, Wu SD, Zuo L, Esling C, Wang ZG, Li GY. Mater Sci Eng 2003;A346:83.
[163] Fukuda Y, Oh-ishi K, Furukawa M, Horita Z, Langdon TG. Acta Mater 2004;52:1387.
[164] Furukawa M, Kawasaki Y, Miyahara Y, Horita Z, Langdon TG. Mater Sci Eng 2005;A410–411:194.
[165] Fukuda Y, Oh-ishi K, Furukawa M, Horita Z, Langdon TG. Mater Sci Eng A 2006;A420:79.
[166] Miyamoto H, Erb U, Koyama T, Mimaki T, Vinogradov A, Hashimoto S. Philos Mag Lett 2004;84:235.
[167] Miyamoto H, Fushimi J, Mimaki T, Vinogradov A, Hashimoto S. Mater Sci Eng 2005;A405:221.
[168] Furukawa M, Fukuda Y, Oh-ishi K, Horita Z, Langdon TG. Mater Sci Forum 2006;503–504:113.
[169] Miyamoto H, Fushimi J, Mimaki T, Vinogradov A, Hashimoto S. Mater Sci Forum 2006;503–504:799.
[170] Iwahashi Y, Horita Z, Nemoto M, Langdon TG. Acta Mater 1998;46:3317.
[171] Oh-ishi K, Horita Z, Furukawa M, Nemoto M, Langdon TG. Metall Mater Trans 1998;29A:2011.
[172] Terhune SD, Swisher DL, Oh-ishi K, Horita Z, Langdon TG, McNelley TR. Metall Mater Trans 2002;33A:2173.
[173] Brandon DG. Acta Metall 1966;14:1479.
[174] Winning M, Rollett AD. Acta Mater 2005;53:2901.
[175] Krasilnikov N, Lojkowski W, Pakiela Z, Valiev R. Mater Sci Eng 2005;A397:330.
[176] Sun PL, Kao PW, Chang CP. Metall Mater Trans 2004;35A:1359.
[177] Stolyarov VV, Zhu YT, Alexandrov IV, Lowe TC, Valiev RZ. Mater Sci Eng 2001;A299:59.
[178] Gholinia A, Prangnell PB, Markushev MV. Acta Mater 2001;48:1115.
[179] Zhu YT, Lowe TC. Mater Sci Eng 2000;A291:46.
[180] Xu C, Furukawa M, Horita Z, Langdon TG. Mater Sci Eng 2005;A398:66.
[181] Sakai G, Horita Z, Langdon TG. Mater Trans 2004;45:3079.
[182] Semiatin SL, Berbon PB, Langdon TG. Scripta Mater 2001;44:135.
[183] McQueen HJ, Hockett JE. Metall Trans 1970;1:2997.
[184] Iwahashi Y, Horita Z, Nemoto M, Langdon TG. Metall Mater Trans 1998;29A:2503.
[185] Furukawa M, Utsunomiya A, Matsubara K, Horita Z, Langdon TG. Acta Mater 2001;49:3829.
[186] Stolyarov VV, Zhu YT, Lowe TC, Valiev RZ. Mater Sci Eng 2001;A303:82.
[187] Stolyarov VV, Zhu YT, Alexandrov IG, Lowe TC, Valiev RZ. Mater Sci Eng 2003;A343:43.
[188] Stolyarov VV, Zhu YT, Lowe TC, Islamgaliev RK, Valiev RZ. Nanostruct Mater 1999;11:947.
[189] Zhilyaev AP, Kim BK, Szpunar JA, Baró MD, Langdon TG. Mater Sci Eng 2005;A391:377.
[190] Mackenzie JK. Biometrika 1958;45:229.
[191] Kopylov VI, Chuvil'deev VN. Russian Metall 2004;2004 (1):22.
[192] Rybin VV. Large plastic deformation and fracture of metals. Moscow, USSR: Metallurgia; 1986 [in Russian].
[193] Rybin VV. Izvestiya Vuzov Fizika (Proceedings of Institutes of Higher Education. Physics) 1991;3:7.
[194] Mishin SV, Gertsman VY, Valiev RZ, Gottstein G. Scripta Mater 1996;35:873.
[195] Chang CP, Sun PL, Kao PW. Acta Mater 2000;48:3377.
[196] Huang JC, Hsiao IC, Wang TD, Lou BY. Scripta Mater 2000;43:213.
[197] Chang JY, Yoon JS, Kim GH. Scripta Mater 2001;45:347.
[198] Wang ZC, Prangnell PB. Mater Sci Eng 2002;A328:87.
[199] Choi WS, Ryoo HS, Hwang SK, Kim MH, Kwun SI, Chae SW. Metall Mater Trans 2002;33A:973.

[200] Zhilyaev AP, Kim BK, Nurislamova GV, Baró MD, Szpunar JA, Langdon TG. Scripta Mater 2002;46:575.
[201] Bowen JR, Mishin OV, Prangnell PB, Juul Jensen D. Scripta Mater 2002;47:289.
[202] Sun PL, Yu CY, Kao PW, Chang CP. Scripta Mater 2002;47:377.
[203] Mishin OV, Juul Jensen D, Hansen N. Mater Sci Eng 2003;A342:320.
[204] Goloborodko A, Sitdikov O, Sakai T, Kaibyshev R, Miura H. Mater Trans 2003;44:766.
[205] Watanabe T. Res Mech 1984;11:47.
[206] Watanabe T, Fujii H, Oikawa H, Arai KI. Acta Metall 1989;37:941.
[207] Watanabe T, Suzuki Y, Tanii S, Oikawa H. Philos Mag Lett 1990;62:9.
[208] Furukawa M, Horita Z, Langdon TG. J Mater Sci 2005;40:909.
[209] Fujita T, Horita Z, Langdon TG. Mater Sci Eng 2004;A371:241.
[210] Ferrasse S, Segal VM, Hartwig KT, Goforth RE. Metall Mater Trans 1997;28A:1047.
[211] Apps PJ, Bowen JR, Prangnell PB. Acta Mater 2003;51:2811.
[212] Islamgaliev RK, Yunusova NF, Valiev RZ, Tsenev NK, Perevezentsev VN, Langdon TG. Scripta Mater 2003;49:467.
[213] Apps PJ, Berta M, Prangnell PB. Acta Mater 2005;53:499.
[214] Xu C, Furukawa M, Horita Z, Langdon TG. Acta Mater 2005;53:749.
[215] Horita Z, Ohashi K, Fujita T, Kaneko K, Langdon TG. Adv Mater 2005;17:1599.
[216] Komura S, Horita Z, Nemoto M, Langdon TG. J Mater Res 1999;14:4044.
[217] Neishi K, Horita Z, Langdon TG. Scripta Mater 2001;45:965.
[218] Neishi K, Horita Z, Langdon TG. Mater Sci Eng 2002;A352:129.
[219] Dalla Torre F, Lapovok R, Sandlin J, Thomson PF, Davies CHJ, Pereloma EV. Acta Mater 2004;52:4819.
[220] Rabkin E, Gutman I, Kazakevich M, Buchman E, Gorni D. Mater Sci Eng 2005;A396:11.
[221] Lapovok R, Dalla Torre FH, Sandlin J, Davies CHJ, Pereloma EV, Thomson PF, et al. J Mech Phys Solids 2005;53:729.
[222] Neishi K, Horita Z, Langdon TG. Mater Sci Eng 2002;A325:54.
[223] Suzuki T, Vinogradov A, Hashimoto S. Mater Trans 2004;45:2200.
[224] Matsubara K, Miyahara Y, Horita Z, Langdon TG. Metall Mater Trans 2004;35A:1735.
[225] Miyahara Y, Matsubara K, Horita Z, Langdon TG. Metall Mater Trans 2005;36A:1705.
[226] Lin HK, Huang JC, Langdon TG. Mater Sci Eng 2005;A402:250.
[227] Semiatin SL, Segal VM, Goforth RE, Frey ND, DeLo DP. Metall Mater Trans 1999;30A:1425.
[228] DeLo DP, Semiatin SL. Metall Mater Trans 1999;30A:2473.
[229] Gibbs MA, Hartwig KT, Cornwell LR, Goforth RE, Payzant EA. Scripta Mater 1998;39:1699.
[230] Suś-Ryszkowska M, Wejrzanowski T, Pakiela Z, Kurzydłowski KJ. Mater Sci Eng 2004;A369:151.
[231] Shin DH, Kim BC, Kim YS, Park KT. Acta Mater 2000;48:2247.
[232] Shin DH, Kim BC, Park KT, Choo WY. Acta Mater 2000;48:3245.
[233] Park KT, Kim YS, Lee JG, Shin DH. Mater Sci Eng 2000;A293:165.
[234] Fukuda Y, Oh-ishi K, Horita Z, Langdon TG. Acta Mater 2002;50:1359.
[235] Kim HK, Choi MI, Chung CS, Shin DH. Mater Sci Eng 2003;A340:243.
[236] Son YI, Lee YK, Park KT, Lee CS, Shin DH. Acta Mater 2005;53:3125.
[237] Hwang B, Lee HS, Kim YG, Lee S, Ahn BD, Shin DH, et al. Metall Mater Trans 2005;36A:389.
[238] Kim HS, Ryu WS, Janecek M, Baik SC, Estrin Y. Adv Eng Mater 2005;7:43.
[239] Wang J, Kang SB, Kim HW. Metall Mater Trans 2004;35A:279.
[240] Zhang ZG, Watanabe Y, Kim I. Mater Sci Tech 2005;21:708.
[241] Furukawa M, Ma Y, Horita Z, Nemoto M, Valiev RZ, Langdon TG. Mater Sci Eng 1998;A241:122.
[242] Huang Y, Langdon TG. J Mater Sci 2002;37:4993.
[243] Valiev RZ, Islamgaliev RK, Kuzmina NF, Li Y, Langdon TG. Scripta Mater 1999;40:117.
[244] Li Y, Langdon TG. J Mater Sci 2000;35:1201.
[245] Muñoz-Morris MA, Gutierrez-Urrutia I, Morris DG. Mater Sci Eng 2005;A396:3.
[246] Zheng MY, Qiao XG, Xu SW, Wu K, Kamado S, Kojima Y. J Mater Sci 2005;40:2587.
[247] Wang J, Horita Z, Furukawa M, Nemoto M, Tsenev NK, Valiev RZ, et al. J Mater Res 1993;8:2810.
[248] Oh-ishi K, Horita Z, Smith DJ, Langdon TG. J Mater Res 2001;16:583.
[249] Horita Z, Smith DJ, Furukawa M, Nemoto M, Valiev RZ, Langdon TG. J Mater Res 1996;11:1880.
[250] Horita Z, Smith DJ, Nemoto M, Valiev RZ, Langdon TG. J Mater Res 1998;13:446.
[251] Wang J, Iwahashi Y, Horita Z, Furukawa M, Nemoto M, Valiev RZ, et al. Acta Mater 1996;44:2973.
[252] Furukawa M, Horita Z, Nemoto M, Valiev RZ, Langdon TG. Acta Mater 1996;44:4619.
[253] Wang J, Furukawa M, Horita Z, Nemoto M, Valiev RZ, Langdon TG. Mater Sci Eng 1996;A216:41.

[254] Furukawa M, Iwahashi Y, Horita Z, Nemoto M, Tsenev NK, Valiev RZ, et al. Acta Mater 1997;45:4751.
[255] Hasegawa H, Komura S, Utsunomiya A, Horita Z, Furukawa M, Nemoto M, et al. Mater Sci Eng 1999;A265:188.
[256] Zhao YH, Liao XZ, Jin Z, Valiev RZ, Zhu YT. Acta Mater 2004;52:4589.
[257] Yu CY, Sun PL, Kao PW, Chang CP. Mater Sci Eng 2004;A366:310.
[258] Ferry M, Hamilton NE, Humphreys FJ. Acta Mater 2005;53:1097.
[259] Lee S, Utsunomiya A, Akamatsu H, Neishi K, Furukawa M, Horita Z, et al. Acta Mater 2002;50:553.
[260] Xu C, Furukawa M, Horita Z, Langdon TG. Acta Mater 2003;51:6139.
[261] Tóth LS. Adv Eng Mater 2003;5:308.
[262] Alexandrov IV, Kilmametov AR, Valiev RZ. Russian Metall 2004;2004 (1):63.
[263] Kocks UF, Tomé CN, Wenk HR. Texture and anisotropy. Cambridge, UK: Cambridge University Press; 1998. p. 187.
[264] Li S, Beyerlein IJ, Necker CT, Alexander DJ, Bourke M. Acta Mater 2004;52:4859.
[265] Li S, Beyerlein IJ, Alexander DJ, Vogel SC. Acta Mater 2005;53:2111.
[266] Murayama M, Horita Z, Hono K. Acta Mater 2001;49:21.
[267] Oh-ishi K, Hashi Y, Sadakata A, Kaneko K, Horita Z, Langdon TG. Mater Sci Forum 2002;396–402:333.
[268] Cabibbo M, Evangelista E, Vedani M. Metall Mater Trans 2005;36A:1353.
[269] Stiller K, Warren PJ, Hansen V, Angenete J, Gjønnes J. Mater Sci Eng 1999;A270:55.
[270] Maloney SK, Hono K, Polmear IJ, Ringer SP. Scripta Mater 1999;41:1031.
[271] Berg LK, Gjønnes J, Hansen V, Li XZ, Knutson-Wedel M, Waterloo G, et al. Acta Mater 2001;49:3443.
[272] Hansen V, Karlsen OB, Langsrud Y, Gjønnes J. Mater Sci Tech 2004;20:185.
[273] Starink MJ, Gao N, Furukawa M, Horita Z, Xu C, Langdon TG. Rev Adv Mater Sci 2004;7:1.
[274] Gao N, Starink MJ, Furukawa M, Horita Z, Xu C, Langdon TG. Mater Sci Eng 2005;A410–411:303.
[275] Starink MJ, Li XM. Metall Mater Trans 2003;34A:899.
[276] Starink MJ, Wang SC. Acta Mater 2003;51:5131.
[277] Allen RM, Vande Sande JB. Acta Mater 1980;28:1185.
[278] Deschamps A, Livet F, Bréchet Y. Acta Mater 1999;47:281.
[279] Semenova IP, Raab GI, Saitova LR, Valiev RZ. Mater Sci Eng 2004;A387–389:805.
[280] Ko YG, Jung WS, Shin DH, Lee CS. Scripta Mater 2003;48:197.
[281] Stolyarov VV, Gunderov DV, Popov AG, Puzanova TZ, Raab GI, Yavari AR, et al. J Mag Mag Mater 2002;242–245:1399.
[282] Dobatkin SV, Odesskii PD, Pippan R, Raab GI, Krasil'nikov NA, Arsenkin AM. Russian Metall 2004;2004 (1):110.
[283] Kawasaki M, Huang Y, Xu C, Furukawa M, Horita Z, Langdon TG. Mater Sci Eng 2005;A410–411:402.
[284] Sabirov I, Kolednik O, Valiev RZ, Pippan R. Acta Mater 2005;53:4919.
[285] Hashim J, Looney L, Hashmi MSJ. J Mater Proc Tech 2002;123:251.
[286] Hashim J, Looney L, Hashmi MSJ. J Mater Proc Tech 2002;123:258.
[287] Lloyd DJ, Lagace H, McLeod A, Morris PL. Mater Sci Eng 1989;107:73.
[288] Ma Y, Furukawa M, Horita Z, Nemoto M, Valiev RZ, Langdon TG. Mater Trans JIM 1996;37:336.
[289] McFadden SX, Mishra RS, Valiev RZ, Zhilyaev AP, Mukherjee AK. Nature 1999;398:684.
[290] Langdon TG, Furukawa M, Nemoto M, Horita Z. JOM 2000;52 (4):30.
[291] Zhu YT, Langdon TG, Valiev RZ, Semiatin SL, Shin DH, Lowe TC, editors. Ultrafine-grained materials III. Warrendale (PA): The Minerals, Metals and Materials Society; 2004.
[292] Zehetbauer MJ, Valiev RZ, editors. Nanomaterials by severe plastic deformation. Weinheim, Germany: Wiley–VCH Verlag; 2004.
[293] Zhu YT, Varyukhin V, editors. Nanostructured materials by high-pressure severe plastic deformation. Dordrecht, The Netherlands: Springer; 2006.
[294] Zhu YT, Langdon TG, Horita Z, Zehetbauer MJ, Semiatin SL, Lowe TC, editors. Ultrafine-grained materials IV. Warrendale (PA): The Minerals, Metals and Materials Society; 2006.
[295] Morris DG. Mechanical behaviour of nanostructured materials. Uetikon-Zürich, Switzerland: Trans Tech; 1998.
[296] Koch CC. Scripta Mater 2003;49:657.
[297] Horita Z, Fujinami T, Nemoto M, Langdon TG. Metall Mater Trans 2000;31A:691.
[298] Zhu YT, Langdon TG. JOM 2004;56 (10):58.
[299] Wang Y, Chen M, Zhou F, Ma E. Nature 2002;419:912.
[300] Valiev RZ, Sergueeva AV, Mukherjee AK. Scripta Mater 2003;49:669.

[301] Parker ER. Materials data book for engineers and scientists. New York (NY): McGraw-Hill; 1967.
[302] Brandes EA, Brook GB. Smithells metals reference book. 7th ed. Oxford, UK: Butterworth–Heinemann; 1992 [Chapter 22].
[303] Höppel HW, May J, Eisenlohr P, Göken M. Z Metallkd 2005;96:566.
[304] May J, Höppel HW, Göken M. Scripta Mater 2005;53:189.
[305] Zhang X, Wang H, Scattergood RO, Narayan J, Koch CC, Sergueeva AV, et al. Acta Mater 2002;50:4823.
[306] Mughrabi H, Höppel HW, Kautz M, Valiev RZ. Z Metallkd 2003;94:1079.
[307] Park YS, Chung KH, Kim NJ, Lavernia EJ. Mater Sci Eng 2004;A374:211.
[308] Islamgaliev RK, Yunusova NF, Sabirov IN, Sergueeva AV, Valiev RZ. Mater Sci Eng 2001;A319–321:877.
[309] Wang Y, Ma E, Valiev RZ, Zhu Y. Adv Mater 2004;16:328.
[310] Li YI, Zeng XH, Blum W. Acta Mater 2004;52:5009.
[311] Suresh S. Fatigue of materials. Cambridge, UK: Cambridge University Press; 1991.
[312] Polák J. Cyclic plasticity and low cycle fatigue life of metals. Amsterdam, The Netherlands: Elsevier; 1991.
[313] Vinogradov AYu, Agnew SR. In: Dekker encyclopedia of nanoscience and nanotechnology. New York (NY): Marcel Dekker Inc.; 2004. p. 2269.
[314] Hanlon T, Kwon YN, Suresh S. Scripta Mater 2003;49:675.
[315] Agnew SR, Vinogradov AYu, Hashimoto S, Weertman JR. J Electron Mater 1999;28:1038.
[316] Mughrabi H. In: Lowe TC, Valiev RZ, editors. Investigations and applications of severe plastic deformation. Dordrecht, The Netherlands: Kluwer Academic Publishers; 2000. p. 241.
[317] Höppel HW, Brunnbauer M, Mughrabi H, Valiev, RZ, Zhilyaev AP. Materials Week 2000. Available from: http//www.materialsweek.org/proceedings, Munich, Germany, 2001.
[318] Vinogradov A, Hashimoto S. Mater Trans 2001;42:74.
[319] Mughrabi H, Höppel HW, Kautz M. Scripta Mater 2004;51:807.
[320] Vinogradov AYu, Stolyarov VV, Hashimoto S, Valiev RZ. Mater Sci Eng 2001;A318:163.
[321] Agnew SR, Weertman JR. Mater Sci Eng 1998;A244:145.
[322] Vinogradov A, Hashimoto S. In: Zehetbauer MJ, Valiev RZ, editors. Nanomaterials by severe plastic deformation. Weinheim, Germany: Wiley–VCH Verlag; 2004. p. 663.
[323] Hashimoto S, Kaneko Y, Kitagawa K, Vinogradov A, Valiev RZ. Mater Sci Forum 1999;312–314:593.
[324] Wu SD, Wang ZG, Jiang CB, Li GY. Philos Mag Lett 2002;82:559.
[325] Wu SD, Wang ZG, Jiang CB, Li GY, Alexandrov IV, Valiev RZ. Mater Sci Eng 2004;A387–389:560.
[326] Vinogradov A, Patlan V, Hashimoto S, Kitagawa K. Philos Mag 2002;A82:317.
[327] Wu SD, Wang ZG, Jiang CB, Li GY, Alexandrov IV, Valiev RZ. Scripta Mater 2003;48:1605.
[328] Höppel HW, Xu C, Kautz M, Barta-Schreiber N, Langdon TG, Mughrabi H. In: Zehetbauer MJ, Valiev RZ, editors. Nanomaterials by severe plastic deformation. Weinheim, Germany: Wiley–VCH Verlag; 2004. p. 677.
[329] Stolyarov VV, Alexandrov IV, Kolobov YuR, Zhu M, Zhu Y, Lowe T. In: Wu XR, Wang ZG, editors. Fatigue'99—Proceedings of the 7th international fatigue congress, vol. 3. Beijing, PR China: Higher Education Press; 1999. p. 1345.
[330] Vinogradov A, Suzuki Y, Kopylov VI, Patlan V, Kitagawa K. Acta Metall 2002;50:1636.
[331] Vinogradov A, Kopylov V, Hashimoto S. Mater Sci Eng 2003;A355:277.
[332] Vinogradov A, Hashimoto S. Adv Eng Mater 2003;5:351.
[333] Vinogradov A, Kaneko Y, Kitagawa K, Hashimoto S, Stolyarov V, Valiev R. Scripta Mater 1997;36:1345.
[334] Vinogradov A. Scripta Mater 1998;38:797.
[335] Vinogradov A, Patlan V, Kitagawa K. Mater Sci Forum 1998;312–314:607.
[336] Höppel HW, Zhou ZM, Mughrabi H, Valiev RZ. Philos Mag 2002;A82:1781.
[337] Vinogradov A, Patlan V, Kitagawa K, Kawazoe M. Nanostruct Mater 1999;11:925.
[338] Wang ZG, Wu SD, Jiang CB, Liu SM, Alexandrov IV. In: Blom AF, editor. Fatigue 2002—Proceedings of the 8th international fatigue congress. Warrington, UK: EMAS; 2002. p. 1541.
[339] Kim WJ, Chung CS, Ma DS, Hong SI, Kim HK. Scripta Mater 2003;49:333.
[340] Chung CS, Kim JK, Kim HK, Kim WJ. Mater Sci Eng 2002;A337:39.
[341] Kautz M, Höppel HW, Xu C, Murashkin M, Langdon TG, Valiev RZ, et al. Int J Fatigue, in press.
[342] Van Swygenhoven H. Science 2002;296:66.
[343] Yamakov V, Wolf D, Phillipot SR, Mukherjee AK, Gleiter H. Nature Mater 2002;1:1.
[344] Van Swygenhoven H, Derlet PM, Frøseth G. Nature Mater 2004;3:399.
[345] Liao XZ, Zhao YH, Srinivasan SG, Zhu YT, Valiev RZ, Gunderov DV. Appl Phys Lett 2004;84:592.
[346] Liao XZ, Zhou F, Lavernia EJ, He DW, Zhu YT. Appl Phys Lett 2003;83:5062.

[347] Chen M, Ma E, Hemker KJ, Sheng H, Wang Y, Cheng X. Science 2003;300:1275.
[348] Liao XZ, Srinivasan SG, Zhao YH, Baskes MI, Zhu YT, Zhou F, et al. Appl Phys Lett 2004;84:3564.
[349] Liao XZ, Zhou F, Lavernia EJ, Srinivasan SG, Baskes MI, He DW, et al. Appl Phys Lett 2003;83:632.
[350] Markmann J, Bunzel P, Rösner H, Liu KW, Padmananhan KA, Birringer R, et al. Scripta Mater 2003;49:637.
[351] Valiev RZ, Kozlov EV, Ivanov YuF, Lian J, Nazarov AA, Baudelet B. Acta Metall Mater 1994;42:2467.
[352] Vinogradov A, Hashimoto S, Patlan V, Kitagawa K. Mater Sci Eng 2001;A319–321:862.
[353] Huang Y, Langdon TG. Mater Sci Eng 2003;A358:114.
[354] Hahn H, Padmanabhan K. Philos Mag B 1997;71:1652.
[355] Chinh NQ, Szommer P, Horita Z, Langdon TG. Adv Mater 2006;18:34.
[356] Gifkins RC, Langdon TG. J Inst Metals 1964–65;93:347.
[357] Kolobov YuR, Grabovetskaya GP, Ivanov MB, Zhilyaev AP, Valiev RZ. Scripta Mater 2001;44:873.
[358] Würschum R, Herth S, Brossmann U. Adv Eng Mater 2003;5:356.
[359] Langdon TG. Z Metallkd 2005;96:522.
[360] Langdon TG. Mater Trans 2005;46:1951.
[361] Weertman J. J Appl Phys 1957;28:362.
[362] Weertman J. J Appl Phys 1957;28:1185.
[363] Langdon TG. Acta Metall Mater 1994;42:2437.
[364] Nabarro FRN. In: Report of a conference on strength of solids. London, UK: The Physical Society; 1948. p. 75.
[365] Herring C. J Appl Phys 1950;21:437.
[366] Coble RL. J Appl Phys 1963;34:1679.
[367] Xu C, Furukawa M, Horita Z, Langdon TG. Adv Eng Mater 2003;5:359.
[368] Berbon PB, Komura S, Utsunomiya A, Horita Z, Furukawa M, Nemoto M, et al. Mater Trans JIM 1999;40:772.
[369] Lee S, Furukawa M, Horita Z, Langdon TG. Mater Sci Eng 2002;A342:294.
[370] Langdon TG. Metall Trans 1982;13A:689.
[371] Ball A, Hutchison MM. Metal Sci J 1969;3:1.
[372] Xu C, Horita Z, Furukawa M, Langdon TG. J Mater Eng Perform 2004;13:683.
[373] Barnes AJ. Mater Sci Forum 1999;304–306:785.
[374] Higashi K, Mabuchi M, Langdon TG. ISIJ Int 1996;36:1423.
[375] Xu C, Furukawa M, Horita Z, Langdon TG. J Alloys Compounds 2004;378:27.
[376] Valiev RZ, Salimonenko DA, Tsenev NK, Berbon PB, Langdon TG. Scripta Mater 1997;37:1945.
[377] Horita Z, Furukawa M, Nemoto M, Barnes AJ, Langdon TG. Acta Mater 2000;48:3633.
[378] Komura S, Horita Z, Furukawa M, Nemoto M, Langdon TG. J Mater Res 2000;15:2571.
[379] Komura S, Horita Z, Furukawa M, Nemoto M, Langdon TG. Metall Mater Trans 2001;32A:707.
[380] Komura S, Furukawa M, Horita Z, Nemoto M, Langdon TG. Mater Sci Eng 2001;A297:111.
[381] Musin F, Kaibyshev R, Motohashi Y, Itoh G. Scripta Mater 2004;50:511.
[382] Musin F, Kaibyshev R, Motohashi Y, Itoh G. Metall Mater Trans 2004;35A:2383.
[383] Perevezentsev VN, Chuvil'deev VN, Sysoev AN, Kopylov VI, Langdon TG. Problems Mater Sci 2003;N1 (33):400.
[384] Perevezentsev VN, Chuvil'deev VN, Sysoev AN, Kopylov VI, Langdon TG. Phys Metals Metall 2002;94:S45.
[385] Kaibyshev R, Shipilova K, Musin F, Motohashi Y. Mater Sci Tech 2005;21:408.
[386] Lapovok R, Cottam R, Thomson P, Estrin Y. J Mater Res 2005;20:1375.
[387] Lapovok R, Thomson PF, Cottam R, Estrin Y. Mater Sci Eng 2005;A410–411:390.
[388] Wisbey A, Kearns MW. In: Ridley N, editor. Superplasticity: 50 years after Pearson. London, UK: The Institute of Materials; 1995. p. 305.
[389] Berbon PB, Furukawa M, Horita Z, Nemoto M, Tsenev NK, Valiev RZ, et al. Philos Mag Lett 1998;78:313.
[390] Furukawa M, Berbon PB, Horita Z, Nemoto M, Tsenev NK, Valiev RZ, et al. Metall Mater Trans 1998;29A:169.
[391] Berbon PB, Tsenev NK, Valiev RZ, Furukawa M, Horita Z, Nemoto M, et al. Metall Mater Trans 1998;29A:2237.
[392] Lee S, Berbon PB, Furukawa M, Horita Z, Nemoto M, Tsenev NK, et al. Mater Sci Eng 1999;A272:63.
[393] Islamgaliev RK, Yunusova NF, Valiev RZ. Fiz Met Metalloved 2002;94 (6):88.

[394] Shammazov AM, Tsenev NK, Valiev RZ, Myshlyaev MM, Bikbulatov MM, Lebedich SP. Phys Metals Metall 2000;89:314.
[395] Kolobov YuR, Dudarev EF, Langdon TG, Pochivalova GP, Naidenkin EV. Russian Metall 2004;2004 (2):116.
[396] Komura S, Berbon PB, Furukawa M, Horita Z, Nemoto M, Langdon TG. Scripta Mater 1998;38:1851.
[397] Akamatsu H, Fujinami T, Horita Z, Langdon TG. Scripta Mater 2001;44:759.
[398] Ota S, Akamatsu H, Neishi K, Furukawa M, Horita Z, Langdon TG. Mater Trans 2002;43:2364.
[399] Park KT, Lee HJ, Lee CS, Nam WJ, Shin DH. Scripta Mater 2004;51:479.
[400] Park KT, Lee HJ, Lee CS, Shin DH. Mater Sci Eng 2005;A393:118.
[401] Xu C, Dixon W, Furukawa M, Horita Z, Langdon TG. Mater Lett 2003;57:3588.
[402] Kawasaki M, Xu C, Langdon TG. Acta Mater 2005;53:5353.
[403] Park KT, Hwang DY, Lee YK, Kim YK, Shin DH. Mater Sci Eng 2003;A341:273.
[404] Shin DH, Hwang DY, Oh YJ, Park KT. Metall Mater Trans 2004;35A:825.
[405] Kaibyshev R, Sakai T, Nikulin I, Musin F, Goloborodko A. Mater Sci Tech 2003;19:1491.
[406] Neishi K, Uchida T, Yamauchi A, Nakamura K, Horita Z, Langdon TG. Mater Sci Eng 2001;A307:23.
[407] Matsubara K, Mitahara Y, Horita Z, Langdon TG. Acta Mater 2003;51:3073.
[408] Yoshida Y, Arai K, Itoh S, Kamado S, Kojima Y. Mater Trans 2004;45:2537.
[409] Miyahara Y, Horita Z, Langdon TG. Mater Sci Eng 2006;A420:240.
[410] Mabuchi M, Iwasaki H, Yanase K, Higashi K. Scripta Mater 1997;36:681.
[411] Mabuchi M, Ameyama K, Iwasaki H, Higashi K. Acta Mater 1999;47:2047.
[412] Chuvil'deev VN, Nieh TG, Gryaznov MYu, Kopylov VI, Sysoev AN. J Alloys Compounds 2004;378:253.
[413] Chuvil'deev VN, Nieh TG, Gryaznov MYu, Sysoev AN, Kopylov VI. Scripta Mater 2004;50:861.
[414] Watanabe H, Mukai T, Ishikawa K, Higashi K. Scripta Mater 2002;46:851.
[415] Valiev RZ et al. Doklady AN SSSR (Proceedings of the Academy of Sciences of the USSR) 1988;301 (4):864.
[416] Mohamed FA. Scripta Metall 1978;12:99.
[417] Taleff EM, Lesuer DR, Wadsworth J. Metall Mater Trans 1996;27A:343.
[418] Yamashita A, Horita Z, Langdon TG. Mater Sci Eng 2001;A300:142.
[419] Kubota K, Mabuchi M, Higashi K. J Mater Sci 1999;34:2255.
[420] Horita Z, Matsubara K, Makii K, Langdon TG. Scripta Mater 2002;47:255.
[421] Wilson DV. J Inst Metals 1970;98:133.
[422] Mukai T, Yamanoi M, Watanabe H, Higashi K. Scripta Mater 2001;45:89.
[423] Cornfield GC, Johnson RH. Int J Mech Sci 1970;12:479.
[424] Stolyarov VV, Popov AG, Gundarev DV, Gaviko BS, Korznikova GF, Ermolenko AS, et al. Fiz Met Metalloved 1997;2:100.
[425] Vinogradov A, Mimaki T, Hashimoto S, Valiev R. Scripta Mater 1999;41:319.
[426] Otsuka K, Shimizu K, Sekiguchi Y, Tadaki G, Honma T, Miyazaki S. In: Funakubo H, editor. Shape memory alloys. New York (NY): Gordon and Breach Scientific Publishers; 1987.
[427] Pushin VG, Kondrat'ev VV, Khachin VN. Nikelid titana, struktura i svoistva (Titanium nickelide: Structure and properties). Moscow, Russia: Nauka; 1992.
[428] Pushin VG. Phys Metals Metall 2000;90 (suppl. 1):S68.
[429] Sergueeva AV, Song C, Valiev RZ, Mukherjee AK. Mater Sci Eng A 2003;339:159.
[430] Pushin VG, Valiev RZ. Solid State Phenom 2003;94:12.
[431] Waitz T, Kazykhanov V, Karnthaler HP. Acta Mater 2004;52:137.
[432] Pushin VG, Gunderov DV, Kourov NI, Yurchenko LI, Prokofiev EA, Stolyarov VV, et al. In: Zhu YT, Langdon TG, Valiev RZ, Semiatin SL, Shin DH, Lowe TC, editors. Ultrafine-grained materials III. Warrendale (PA): The Minerals, Metals & Materials Society; 2004. p. 481.
[433] Stolyarov VV, Prokofiev EA, Prokoshkin SD, Dobatkin SV, Trubitsyna IB, Khmelevskaya IY, et al. Phys Metals Metall 2005;100:608.
[434] Pushin VG. In: Zehetbauer MJ, Valiev RZ, editors. Nanomaterials by severe plastic deformation. Weinheim, Germany: Wiley–VCH Verlag; 2004. p. 822.
[435] Prokoshkin SV, Khmelevskaya IYu, Dobatkin SV, Trubitsyna IB, Tatyanin EV, Stolyarov VV, et al. Phys Metals Metall 2004;97 (6):84.
[436] Lowe TC, Zhu YT. Adv Eng Mater 2003;5:373.
[437] Lowe TC, Zhu YT. In: Zehetbauer MJ, Valiev RZ, editors. Nanomaterials by severe plastic deformation. Weinheim, Germany: Wiley–VCH Verlag; 2004. p. 789.

[438] Valiev RZ. Mater Sci Forum 2006;503–504:3.
[439] Lowe TC. Mater Sci Forum 2006;503–504:355.
[440] Zhu YT, Lowe TC, Valiev RZ, Stolyarov VV, Latysh VV, Raab GI. USA Patent #6,399,215 "Ultrafine-grained Titanium for Medical Implants", published on July 4, 2002.
[441] Latysh VV, Semenova IP, Salimgareeva GH, Kandarov IV, Zhu YT, Lowe TC, et al. Mater Sci Forum 2006;503–504:763.
[442] Lowe TC, Valiev RZ. JOM 2004;56 (10):64.
[443] Stolyarov VV, Zhu YT, Raab GI, Zharikov AI, Valiev RZ. Mater Sci Eng 2004;A385:309.
[444] Horita Z, Fujinami T, Langdon TG. Mater Sci Eng 2001;A318:34.
[445] Srinivasan R, Cherukuri B, Chaudhury PK. Mater Sci Forum 2006;503–504:371.